Benha University
Benha Faculty of Engineering
Civil Engineering Department

Behaviour of flanged reinforced concrete beams subjected to shear force

A Thesis Submitted in Partial Fulfillment of the Requirements of the Ph.D. in Engineering Sciences in Civil Engineering

By
Ibrahim Ali Ibrahim El-Eazab
Assistant Lecturer, Civil Engineering Department.
M.Sc of Engineering and technology in civil engineering technology
Benha University (2013)

Supervised by

Prof. Dr. Osman Mohamed Osman Ramadan
Department of structural Engineering, Cairo University, Cairo, Egypt. Dean, Higher Technological Institute HTI at 10th of Ramadan City, Egypt.

Prof. Dr. Ahmed Hassan Abdel-kareem
Department of civil Engineering, Benha University, Benha, Egypt. Vice Dean for Environmental Community Service Affairs at Benha Faculty of Engineering.

Assoc. Prof. Dr. Hala Mohamed Refaat Abu Safa
Assoc. Professor, Civil Engineering Department, Benha Faculty of Engineering, Benha University.

Benha 2022

Statement

This thesis is submitted to the Department of Civil Engineering, Faculty of Engineering, Benha University, for awarding the Degree of Ph. D. in civil engineering.

Thesis Title

Behaviour of flanged reinforced concrete beams subjected to shear force

The work included in this thesis has been carried out by the author in the Department of Civil Engineering, Benha Faculty of Engineering, Benha University.

The contents of this thesis are not submitted to any University or Engineering Institute, and it is not copied from any qualification.

Author's name: - Ibrahim Ali Ibrahim Ahmad El Azab

Signature :- ( )

Date :- 18 / 7 / 2022

The above statement has been signed by the author.

Supervisors

Prof.Dr. Osman Mohamed Osman Ramadan ----------

Prof.Dr. Ahmed Hassan Abdel-Kareem ----------

Assoc. Prof. Dr. Hala Mohamed Refaat Abu Safa ----------

Head of the Department

Benha 2022

ABSTRACT

This research presents the test results of a special designed and a conducted experimental study. The aim of the thesis is to evaluate the performance of T-beams with thick and wide flanges in compression for instance the cap beam. Most of the present design codes as ACI 318-14 and ECP-203 ignore the contribution of the flanged part on RC flanged beams in shear resistance. The studied variables were about flange dimensions (thickness and width) and reinforcement (longitudinal and/or vertical). Nineteen simply supported beam specimens were tested to failure under a load configuration made of two concentrated loads. Eighteen specimens had T-shaped cross sections, while one specimen had rectangular cross section for comparison purposes. The items monitored during testing included the development of diagonal cracks, concrete strains, reinforcement strains, maximum loads, and deflections. Test results showed that the shear capacity of T-beams was with a notable increase compared to that of rectangular beams with the same web size. For T-beam specimens without transverse reinforcement in their webs, the flange increased the shear strength by up to 160% to 330% of the shear strength of the web alone.

The percentage increased in the shear strength due to flange existence which varied depending on flange dimensions and amount of longitudinal reinforcement in flange. In addition, test results were compared to the prediction of a simple model that included the contribution of flange to shear capacity in T-beams [2], where good agreement was observed. A simplified method to include the flange contribution in evaluating the shear strength of flanged beams is proposed and verified by numerous comparisons with test results and finite element predictions. Moreover, statistical analysis for comparison of the proposed method with the code formulation and F.E. results.

Benha 2022

Nonlinear constitutive models are proposed for reinforced concrete T-beam for shear strength prediction. The models were implemented in the finite element computer program ANSYS V-19.2 for 3-D nonlinear analysis of flanged specimens under concentrated two-points static loading. Several validation studies have been per-formed for flanged beams with variable flange dimensions. Good agreement is generally achieved between experimental and numerical results for the load-deflection curves and crack patterns. Additionally, parametric studies have been performed in order to investigate the effect of structural parameters on the performance of T-section against shear straining action. Four design parameters were considered, including flange dimensions (width and depth), longitudinal reinforcement in flange, concrete compressive strength “fc’” and shear span to depth ratio. Ninety-six models of simply supported reinforced concrete T-beams were loaded monotonically with two incremental concentrated loads. Beams were simulated to obtain the load-deflection relationships, ultimate loads and crack patterns and compared them with the solid reference one. Three experimental T-beams were considered in this study and verified to ensure the validity of models.

Supervisors:

Prof. Dr. Osman Mohamed Osman Ramadan
Department of structural Engineering, Cairo University, Cairo, Egypt. Dean, Higher Technological Institute HTI at 10th of Ramadan City, Egypt.

Prof. Dr. Ahmed Hassan Abdel-kareem
Department of civil Engineering, Benha University, Benha, Egypt. Vice Dean for Environmental Community Service Affairs at Benha Faculty of Eng.

Assoc. Prof. Dr. Hala Mohamed Refaat Abu Safa
Assoc. Professor, Civil Engineering Department, Benha Faculty of Engineering, Benha University.

Benha 2022

ACKNOWLEDGEMENT

First and foremost, praise and thanks be to Almighty Allah for his limitless help and guidance, and peace is upon his last messenger Mohamed.

I would like to express my sincere thanks and profound gratitude to, Prof.Dr. Osman Mohamed Ramadan Professor of Structural Analysis, Civil engineering department, Cairo University for his supervision.

The author wishes to express his deep gratitude to Prof. Dr.Ahmed Hassan Abdel-Kareem and Assoc. Prof. Dr. Hala Mohamed Refaat, Civil engineering department, Benha University for their valuable supervision, continuous encouragement, valuable discussions, and sincere help.

I was really honored to be one of their undergraduate students and would really appreciate their support and encouragement throughout the undergraduate curriculum.

Appreciation goes to Benha Faculty of Engineering Benha University for rendering the necessary support to carry out this research. The technical staffs of the Structural Engineering Laboratory of the Faculty deserve special thanks form for their assistance in the experimental works of this study. The friendly cooperation received from the fellow researchers is also highly appreciated, the author expresses his heartiest appreciation to his wife for, patience and continuous support throughout this study.

The author expresses his heartiest appreciation to his mother, his wife and his brother Mohamed El-Azab, for their understanding, patience, and continuous support throughout this study.

Finally, I dedicate the reward for this work to my dear mother, may God have mercy on her.

Author: - **Ibrahim Ali Ibrahim El Azab**

Signature: - ( )

Benha 2022

Table of Contents

LIST OF TABLES

LIST OF FIGURES

NOMENCLATURE

LIST OF SYMBOLS

l	effective span
h	overall depth of beam section
d	effective depth of beam section
b_w	web width
b_f	flange width
t_f	flange thickness
a	*shear span*
l/h	span-to-depth ratio
ρ_t	flange thickness "depth ratio" t_f/h
ρ_b	flange width "width ratio" b_f/b_w
Es	elastic modulus of reinforcement
$f_{c'}$	cylinder compressive strength of concrete
f_{cu}	cube compressive strength of concrete
fy	yield strength of reinforcement
A_s	area of main reinforcement
$A_{s'}$	area of top reinforcement
ζ	longitudinal reinforcement ratio in flange
P_u	ultimate load capacity
$P_{u.c}$	ultimate load capacity of control specimen
V_s	shear resisted by concrete and by the transverse reinforcement
V_c	shear resisted in the uncrack compression head
V_l	contribution of the longitudinal reinforcement
V_w	shear transfer across web cracks
v_c, v_w, v_l and v_s	*dimensionless values of the shear transfer action.*
f_{ct}	tensile concrete strength
α_e	$= E_s/E_c$ *is the modular ratio between steel and concrete*
ρ	$=A_s/(b.d)$ *is the longitudinal reinforcement ratio.*
η	$= b_f/b_w$ *width ratio according to ref. (30).*

LIST OF ABBREVIATIONS

G1	group of specimens without longitudinal reinforcement in flange
G2	group of specimens with longitudinal reinforcement in flange
G3	group of specimens with longitudinal and stirrups in flange

CHAPTER (1)

INTRODUCTION

CHAPTER (1)

INTRODUCTION

1.1- General

Reinforced Concrete T-beams are frequently used in industrial construction, especially in building floors, retaining walls, bridge decks, and more generally in all reinforced concrete construction projects where an appropriate portion of the slab is associated to the resisting section of the supporting beam.

Most of the previous experimental studies were focused on reinforced (RC) beams under flexure, shear and torsion. The behavior of T shaped beams with both web and flange are not fully explored. In this research, an innovative test setup capable of simulating the behavior of T-shaped beams under shear was developed and implemented. Reinforced concrete (RC) flanged beams are being used as the main girders that support the lateral secondary precast beams or slabs which is one of the popular structural systems for many existing bridges and parking garages. The behavior of T-shaped beams is more complicated “specially in shear analysis” than that of conventional rectangular RC beams.

The performance of T-beams with thick and wide flanges in compression was investigated in this thesis. The major goal of this study is to evaluate the shear behaviour of RC thick flanges with rectangular and T cross sections, as well as the effect of the flange and its

contribution to shear strength, both experimentally and analytically. The results of this study help in saving construction costs by utilizing the flange's contribution to shear strength for flanged beams with thick flanges in the compression side such as the case of double-cantilevered cap beams with inverted T sections.

The thesis consists of seven chapters as follows:

Ch.-1: Contains an introduction and definition of the problem, the objectives of the research work, and the thesis outlines.

Ch.-2: Presents a literature review for the previous investigations carried out on the torsion and shear behaviour of RC girders with rectangular and T cross sections.

Ch.-3: Presents a description of experimental program carried out in this study, which includes detailing, fabrication, instrumentation and test set up of the specimens.

Ch.-4: Includes the analysis and discussion of the experimental results obtained from the tested beams. Results were analyzed and compared under the effect of the parameters investigated.

Ch.-5: Analytical analysis by using model for shear capacity of T-beam.

Ch.-6: Finite Element (FE) analysis Method for test specimens were carried out. This chapter also includes the general comparative study between experimental and analytical result and proposed simplified model.

Ch.-7: Includes the summary and conclusions obtained from this research.

CHAPTER (2)

LITERATURE REVIEW

CHAPTER [2]

LITERATURE REVIEW

2.1 Introduction

RC beams with T-cross sections are frequently used in construction especially in building floors, bridge decks, and other reinforced concrete construction projects. An important application of RC, flanged beams is their use as the main girders that support precast beams or slabs. Examples of such applications are present in the structural systems of many bridges and multi-story parking buildings.

2.2 Review of T-beam

RC beams with T-cross sections are frequently used in construction especially in building floors, bridge decks, and other reinforced concrete construction projects. An important application of RC flanged beams was used as the main girders that supported precast beams or slabs. Examples of such applications were presented in the structural systems of many bridges and multi-story parking buildings.

Thamrin et al. [1] investigated the shear strength of RC T-beams without stirrups. Test results showed that the shear strength of T-beams is affected by both flange size and the main longitudinal reinforcement in the web. They found that the shear capacity of T-beams was 5% to 20% higher than that of rectangular beams with same web dimensions. It was also stated in the research that the angle of the diagonal crack was significantly influenced by the web longitudinal reinforcement ratio in the shear span. Generally, the angle of diagonal cracks decreased when the longitudinal reinforcement in the beam web increased for both rectangular and T-sections.

Cladera et al. [2] provided an analytical model for the ultimate shear capacity prediction of slender RC beams with rectangular section and T-section, they concluded the contribution of the compression flanges to the shear strength which was extremely relevant and couldn’t be neglected. When the neutral axis lied in the flanges, both the global inclination and the horizontal projection of the critical crack increased. As a result, the contribution of concrete and the web transverse reinforcement have increased, resulting in higher ultimate shear capacity resistance.

Elgohary et al. [3] studied the influence of flange dimensions on shear capacity of RC T-beams. six of RC beams without stirrups were tested: one with R-sec and five with T-sec, and these have variable flange width to web width ratio. Test results showed that an increase in shear strength ranging from 10% to 30% occurred due to the flange contribution.

Deifalla et al. [4] studied the action of the T-shaped beams. They were tested and influenced by the torque-to-shear ratio rating. Reducing the applied torque to the sum of shear force applied was resulting in the following: (1) Significant decrease in the spacing among diagonal cracks, angle of strut for inclination, cracking and ultimate torque, flange and web stirrup strain ; (2) Significant increase in failure, cracking and ultimate shear, cracking load, and torsional rigidity after cracking,; (3) The efficiency of the stirrups has been reduced and therefore beams have failed due to concrete diagonal failure rather than the yield of stirrups. The flange's presence revealed a section's shear strength increased by 29 % relative to the rectangular beam.

Etman [5] showed that strengthening RC beams in shear zone using carbon fiber-reinforced polymer (CFRP) enhanced the shear capacity of existing RC beams. The main objective was to obtain a good understanding and enhance

the experimental database of shear behavior of RC T-beams strengthened by externally bonded reinforcement (EBR) systems. The existence of the flange showed a 29 % increase in the shear capacity of the section compared with the rectangular section. The use of CFRP sheet reflected higher specimen stiffness, compared to steel.

Amna et al. [6] studied the shear behavior of lightweight reinforced concrete T-beam by experimental and FE model. This study showed that T-beams with different flange widths decreased vertical deflection, longitudinal steel strain, stirrup steel strain, and the compressive concrete strain. In the event of failure, the shear stresses tended to concentrate in flexure around the neutral axis in the compressed concrete area. It leads to an obvious contribution of the flanges to the shear capacity. The maximum percentage of shear force taken by the entire compressed concrete area in flexure exceeded 51.8%, whereas the total percentage of shear taken by the flanges for the cases analyzed was 31.3%. This total percentage can be considered a highly significant quality as the shear force generated by the flanges increases with the increase in width and depth. Since shear stresses are concentrated around the web, their distribution in the flanges is minimal, so their contribution shows an asymptotic tendency towards 25% of the total shear resisted. This trend was not observed as the depth of the flange increased.

Ayensa et al. [7] showed that the contribution of flanges may lead to significant cost savings in new structures and might be decisive in assessing the shear capacity of existing structures. Analytical model was used to analyze the shear response of beams with different geometry and main longitudinal reinforcement in the web. It has been found that, to a certain extent, the contribution of flanges to the shear capacity increased as the

amount of web longitudinal reinforcement decreased. Increasing the width and thickness of flange led to increasing the contribution of the flanges to the shear capacity. Moreover, the maximum contribution of flanges found in the study was 31.3% of the total shear resisted.

Eswaramoorthi et al. [8] investigated two RC T-beams and one rectangular beam both experimentally and analytically. The study found that the beams were strengthened by Glass Fiber Reinforced Polymer (GFRP). T-beam's total load carrying capacity was 23% higher than that of the rectangular specimen. Also, shear capacity of the tested T-beams was significantly influenced by the flange presence and the ratio of main beam web longitudinal reinforcement. The deflection of the strengthened flanged beam was reduced by 5% in all the load cases compared to the rectangular beam.

Other studies [9-12] showed that shear strength of T-beams was much higher than the shear strength of their corresponding rectangular beams. This is solely due to the compression zone increase.

Most experimental studies on the subject focused on RC beams under shear strength. In this research, a test was set up to detect the capability of simulating the behavior of flanged beams under shear force, the saying of “without transverse reinforcement within shear zone” was developed and implemented. The study variables were embodied in flange dimensions (thickness and width) and in the existence of reinforcement in flange.

Flanged reinforced concrete beams have been widely used in many applications in the civil engineering field. The behavior of this kind of structural members was investigated experimentally as well as analytically. Numerical analysis technique based on the finite element method has been used in this research work to investigate the effect of the flange on the

reinforced concrete T-beam in the pre. and post-cracking stages of loading and up to ultimate load. The extensive research in the field of numerical modeling of reinforced concrete members and structures has led to the development and formulation of many models which are capable of predicting their behavior under various conditions. These models are put to real use when implemented in a suitable computer code. Then they can be used for both practical and research purposes. Many computer codes exist and are used daily in the construction industry, research activities and engineering education.

Flanged reinforced concrete beams have been widely used in many applications in the field of civil engineering. The attitude of this kind of structural members was discussed experimentally as well as analytically. Numerical analysis technique that is based on the finite element method has been checked in this research to detect the effect of the flange on the reinforced concrete T-beam in both pre- and post-cracking stages of loading and up to ultimate load.

ANSYS [13] is one of the most exceedingly famous computer programs which used structural analysis through the finite element method. The overall study in the area of numerical modeling and finite element support the engineers and researchers with many applications not only in construction on but also in other industries and scientific aspects. One of the characteristics of ANSYS, which was appealing to researchers, is the possibility of specification through adding extra features and qualities. This simplified the research process by contributing in the production of new material models or finite elements and anticipated to the spread of understanding knowledge in all scientific realms.

According to Hesham et al. [14] a numerical experimental study was fulfilled to check the validity of using lightweight concrete beams. It observed the shear behavior of lightweight concrete; six lightweight concrete beams were tested in two-point bending to urge the effect of flange width and shear span on depth ratio. In the experimental and FE studies, the failure load of the T-beams with different flange widths (320, 520, and 720 mm) were increased in proportion to the flange width. During the experimental and FE studies, the failure load noticed to be inversely proportional to all the shear span to depth ratio, vertical deflection, longitudinal steel strain, stirrup steel strain, and compressive concrete strain of the T-beams with various flange widths (320, 520, and 720 mm) respectively.

As Balamuralikrishnan et al. [15] mentioned, the main objective of this work is to evaluate the static load trend of RC T-beams reinforced internally with GFRP reinforcements using finite element analysis software ANSYS. Totally twelve numbers of specimens were completely Pm outlined in this study in a way of varying parameters such as the type of reinforcements, reinforcements ratio, and concrete grade. Modeling of the T- beams was done with ANSYS by using solid 65 and link 8 element and the same was tested under static loading atmospheres. The experimental outcomes of the flanged beams met perfectly that of the analytical results that were gathered from the flanged beams reinforced with steel and GFRP reinforcements. The accomplishment of the flanged beam resulted from the analytical tool ANSYS was approximately equal to the experimental values.

El-din et al. [16] showed that Finite Element Modeling FEM which used ANSYS program was done to explore the efficiency of strengthening. Here carbon Fiber Reinforced Polymer CFRP and basalt Fiber Reinforced Polymer BFRP sheets for RC T-beams were used to achieve shear zone large

rectangular opening. A combination of the RC shallow T-beams and openings could react as solid beams when only they were properly strengthened. Finite element modeling could expect reasonably the final load and mode of failure for the analyzed beams. It could be substituted by the highly cost experimental work.

Biscaia et al. [17] put in his consideration that the serviceability circumstances of the T-beams can be improved step by step due to an increase of the concrete strengths. It reflected that concrete had an essential influence on the de- bonding phenomenon. Still, the FEA with interface finite elements and the rotated crack approach could check together the displacement at mid-span, then they could calculate precisely the deformation of the T-beams.

Pansuk et al. [18] also reached the result that, an increase in the flange width of a T-beam gave higher shear capacity with a nonlinear relationship for the T-beam with shear reinforcement. In the case of a T-beam without shear reinforcement, however, the width of the flange has almost no effect on shear capacity.

Pansuk et al. [19] proved that Existing of concrete top flange had significant effects on shear behavior of RC T-beams as in shear strength stress, in shear reinforcement and in crack propagation. Concrete top flange could reduce the strain of concrete in the web. For original shear resisting mechanism of T-beam, concrete top flange near compression zone should be considered with average stress on the appropriate flange area.

Giaccio et al. [20] fifteen flanged specimens were tested, each specimen had a constant amount of shear, web longitudinal reinforcing, and a constant web width. There was an effect of the ratio of flange width to web width

(b_f/b_w) on the shear strength of a point-loaded reinforced concrete T-beam which depended on the ratio of flange depth to effective depth for shear (d_f/d_o). It is suggested for the geometric ratios used in the research experiments that as long as the ratio d_f/d_o is above a certain minimum value ($d_f/d_o \geq 0.25$ for the experiments in this study), then the increase in shear resistance for a given increase in b_f/b_w is independent of d_f/d_o, would provide the beam with shear failure mechanism appeared on the specimen.

2.3 Research Significance.

T-beams are widely used in many structures. In precast structures, the flange thickness is relative to the web depth and is much larger than of beams in ordinary buildings that is cast in situ. Thus, it does not seem wised to ignore the flange contribution in resisting shear as it is currently done by various design codes [21-24]. For example, ACI 318-19: Building Code Requirements for Structural Concrete and the Egyptian Code of Practice ECP-203 do not utilize any contribution of the flange in resisting shear. Therefore, experimental, and theoretical studies on this subject shall be of great benefits to structural engineers, construction companies, and other involved bodies.

CHAPTER (3)

EXPERIMENTAL STUDY

CHAPTER [3]

EXPERIMENTAL STUDY

3.1 Introduction

This research presents the test results of an experimental study on shear strength of reinforced concrete (RC) flanged beams. The studied variables are flange dimensions (thickness and width) and reinforcement in flange. Nineteen simply supported specimens (the first has rectangular cross-section while the remaining have T-shaped sections) were subjected to two-point loads and tested until failure. During the tests, development of diagonal cracks, crack width, reinforcement strains, maximum loads, as well as the deflections were monitored. In addition, a simple model for predicting the contribution of flange to shear capacity in T-beam was presented.

3.2 Experimental Test Program

3.2.1 Details of Test Specimens.

The test specimens consisted of nineteen simply supported beams, one with rectangular section "control specimen", and remaining specimens with flanged section (T-Section), which consists of 6-Groups and each group contains 3-specimens with variable depth ratio of flange ($\rho_t = t_f /h$), three groups with width ratio ($\rho_b = b_f /b_w$) equal 3 and the remaining three groups with width ratio (ρ_b) equal 5, from each three groups one of them without longitudinal reinforcement in flange (G1), the second with longitudinal reinforcement (G2) and the third with longitudinal and stirrups in flange (G3). The total length of the tested specimen was 1400 mm with overall depth equal to 300 mm, web width 100 mm and the effective span of 1300 mm giving an *l//h* ratio (span-

to-depth ratio) > 4. To prevent the failure of the bearings at supports, increasing the web width over supports to equal the flange width. The end supports were reinforced with two vertical bars U-shape Ø10 and three horizontal stirrups Ø6. The beams were monotonically loaded until failure with two-point loads" with shear span to depth ratio equal 1.5" using a 1000 kN capacity hydraulic jack and all specimens were designed in such a way to induce shear failure prior to any flexural distress, the typical details of tested specimens are shown in Fig. 3.1. Each specimen has a main bottom reinforcement consists of four steel bars Ø16 (diameter of 16 mm, area of 201 mm^2) laid in two layers at the bottom of the beam cross section and two Ø10 bars (diameter of 10 mm, area of 78.54 mm^2) laid in one layer at the top. The bottom and top bars are anchored at the support with 90-degree hooks to prevent premature anchorage failure, The web reinforcement was Ø 8 @ 100 mm spacing in the middle part between two applied loads, for flanged beams with longitudinal reinforcement, the ratio of longitudinal reinforcement in the flange nearly1%, of flange concrete area, and the stirrups Ø8 steel bars with a distance a part 75 mm with branch distance 100 mm as shown in Fig.3.2.

The nomenclature of tested specimens given in Table3.1 includes three parts. The first Part refers to reinforcement in the flange (G1 without reinforcement, G2 with longitudinal reinforcement and G3 with longitudinal and flange stirrups within the two shear zones). The second Part refers to the flange thickness "depth ratio" (ρ_t = 0.3, 0.4 and 0.5). The third Part refers to the flange width "width ratio" (ρ_b = 3 for flange width equal 300mm and 5 for flange width equal 500mm).

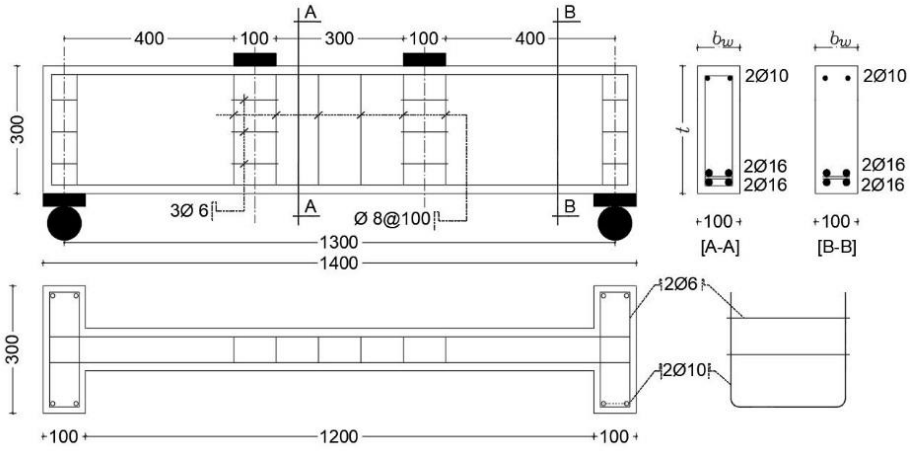

Fig. 3.1.a Specimen with rectangular cross section (control)

Fig. 3.1 Specimen details and arrangement of reinforcement

(All dimensions in mm)

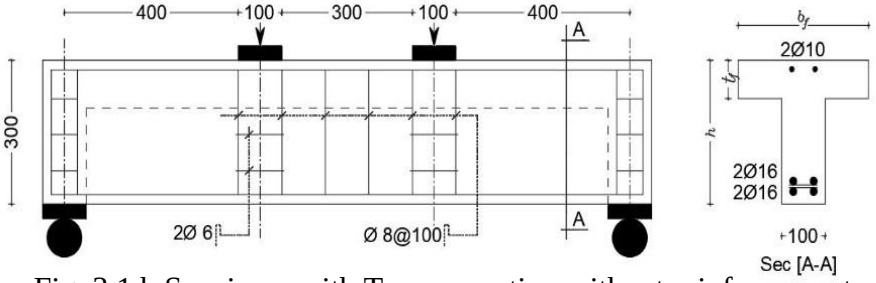

Fig. 3.1.b Specimen with T-cross section without reinforcement in flange (G1)

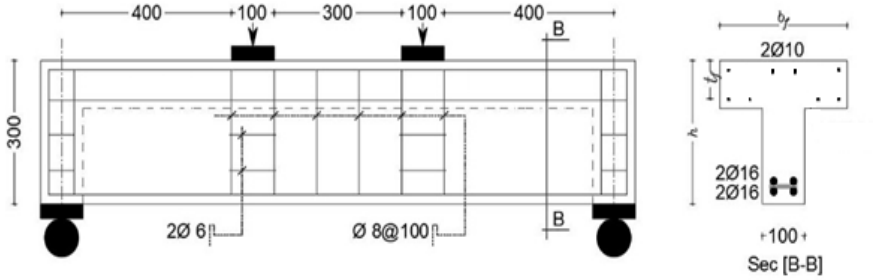

Fig. 3.1.c Specimen with T-cross section with longitudinal steel and without stirrups in flange within shear zone (G2)

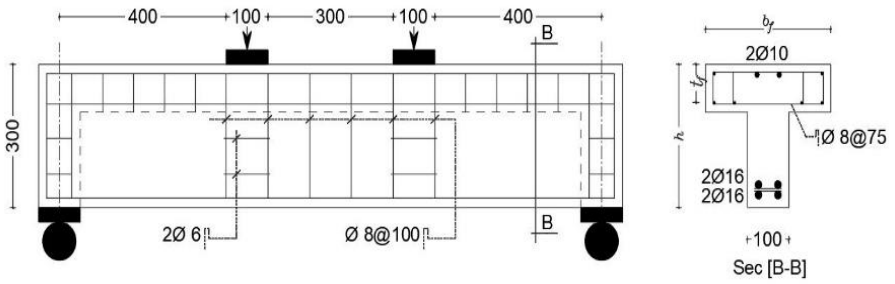

Fig.3.1 (*cont.*)

Fig. 3.1.d Specimen with T-cross section with longitudinal steel and with stirrups in flange (G3)

3.3 Characteristics of Reinforced Concrete Materials.

The test specimens in this investigation were made from normal-strength concrete using local materials. The production of normal-strength concrete according to the standard specifications met the requirements for workability and strength. Fine and coarse aggregates were composed of ordinary siliceous sand and Dolomite of good quality, respectively and clean from impurity materials. Cement used was Ordinary Portland Cement. High and normal strength reinforcement bars locally produced were used. The properties of these materials were determined from tests carried out according to the standard specifications, the obtained results were compared with the limits given in these specifications.

3.3.1 Fine Aggregates

Natural siliceous sand was used as fine aggregate in the concrete mix. It was clean from impurities, silt, loam, and clay. It was free from organic materials. The Fineness modulus of the used sand was 2.75. Table (3. 1) lists the physical and the mechanical properties of fine aggregates.

Table 3.1 Physical and mechanical properties of fine aggregates

Property	Test Result
Specific gravity	2.61
Volumetric weight (t/m^3)	1.75
Void ratio	35%
Fineness modulus	2.75
Clay, silt, and fine dust (by weight)	1.85%
Chloride % (by weight)	0.02

3.3.2 Coarse Aggregates

Crushed hard Dolomite with maximum grade size of 10 mm was used in the concrete mix and had well-graded gravel. Moreover, their general particular shape was round and sub-angular, and the surface textures were more or less smooth and uniform and free from any undesired impurities.

3.3.3 Cement

Ordinary Portland cement used in all experimental work was provided from Suez-factory, Egypt. The usual chemical and physical properties are in compliance with the Egyptian Standard Specification ESS 373/2007. Table 3.2 gives the test results.

Table 3.2 Physical properties of ordinary Portland cement

Test Description	ESS 373 / 2007 Specification Limits	Test Results
Fineness of cement percentage retained on the standard 0.09 mm sieve by weight	Not more than 10 %	6.80%
Soundness of cement (Le Chatelier test)	Not more than 10 mm	3.5 mm

Table 3.2 (*cont.*)

Percentage of water to give a paste of standard consistency, w/c %	----------	30%
Setting Time (Vicat test):		hr.: min.
Initial	Not less than 45 min.	1: 45
Final	Not more than 10 hr.	6: 50
Compressive strength of mortar 7×7cm cubes		
after 3 days	Not less than 160 kg / cm^2	215
after 7 days	Not less than 240 kg / cm^2	290

3.3.4 Water

Clean drinking fresh water free from impurities was used for mixing and curing the tasted beams.

3.3.5 Steel Reinforcement

Normal mild steel bars grade 24 / 36 were used for horizontal and vertical stirrups 6 mm diameter and top reinforcement 8 mm diameter. High tensile steel bars grade 36 / 52 were used for all other reinforcement. Tests were performed to evaluate yield stress, ultimate strength, and elongation for the steel used. The reinforcing steel used in this research was obtained from El-Ezz steel company, Egypt. The results are given in Table 3.3.

Table 3.3 Mechanical properties of steel reinforcement

Steel Type	**Yield Stress (MPa)**	**Tensile Strength (MPa)**	**Elongation %**	**Modulus of Elasticity (MPa)**
High Tensile	366.5	536.1	16.12	205940
Normal Mild	254.0	374.2	24.21	200056

3.4 Concrete Mix Design

The method used for the concrete mix design was the absolute volume method. Four trail mixes have been designed using this method. The following equation was applied:

$$\frac{C}{p_c} + \frac{F.A}{p_{FA}} + \frac{C.A}{p_{CA}} + \frac{W}{p_W} = 1\ m^3 \quad \text{..... (3-1)}$$

Where

C : Cement weight.

F.A: Fine aggregate weight.

C.A: Coarse aggregates weight.

W : Water weight.

P_c : Specific gravity of cement.

$P_{F.A}$: Specific gravity of the fine aggregate (natural sand).

$P_{C.A}$: Specific gravity of the coarse aggregates (gravel).

P_w : Specific gravity of water.

The main variables considered in mix proportioning were the cement content, water/cement ratio (w/c) and the ratio of coarse aggregate to the fine aggregate. The obtained average compressive concrete cube strength was 33 MPa at 28 days age (based on 15 cm cubic specimens). The concrete mixes proportions, and compressive strength at 28 days are presented in Table (3.4).

Table 3.4 Concrete mix proportions and compressive strength

Mix No	Mix proportions				Unit Weight	C. A/ F.A.	W/C%	Cube Compressive Strength
	Kg/m^3							MPa
	C	W	F.A	C.A				28 days
								MPa
1	350	175	602	1204	2331	2	50	33

where,

C= Cement, W = Water**,** F.A = Fine aggregate and C.A.=Coarse aggregate

3.5 Casting and Curing Procedures.

3.5.1 Moulds

The mould for beams were made of 25 mm thick plywood sheets with very smooth faces and having the dimensions the same as that of the tested beam, as shown in Fig. (3-2). Along with each beam, three cubes of 15 cm size were cast to determine the compressive strength of the concrete used in tested beams. Standard steel moulds were used for casting of these control specimens.

Fig. 3.2 wooden forms prepared to cast specimens

3.5.2 Casting

Before casting, the beam moulds were tightly assembled and checked for dimensional accuracy. The moulds were cleaned well. Required cover was ensured by placing cover blocks made of cement mortar placed between the stirrups and the mould, and the thick plywood sheets were used to create the open.

A 360-liter capacity mixer was used with a speed of about 50 revolutions per minute. Materials were added in the following sequence: coarse aggregate, sand, cement. The dry constituents were mixed without water for two minutes, then the water was added, and the operation continued for

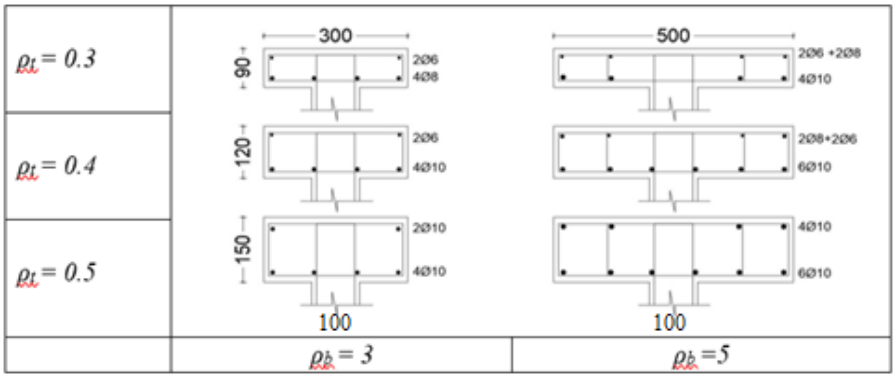

Fig. 3.3 Arrangement of longitudinal reinforcement and stirrups in flange

additional three minutes to ensure adequate mixing. The forms were coated with oil before casting. The reinforcement was then placed in their right position in the forms. A batch size of about 120 liter was required to cast two specimens and six control test cubes. Pouring concrete in the forms took place immediately after mixing. After filling the mould to about half depth of the specimen, the concrete was vibrated by a mechanical vibrator. Later the top half of the mould was filled with the concrete and vibrated.

After vibration, the excess concrete at the top of the moulds was struck off with a straight edge and the top surface was finished smooth by trawling. Fig. 3.3 shows the arrangement of longitudinal reinforcement in flange, Fig 3.4 shows the steel reinforcement details.

Fig. 3.4.a Details of reinforcement for control beam

Fig. 3.4 Details of reinforcement for tested specimens

Fig. 3.4.b Details of reinforcement for flanged beams

3.5.3 Curing

The beams were left in the forms for 24 hours, after that the sides of the forms were stripped away. The specimen was cured by water sprinkling twice a day for 28 days as shown in Fig. 3.5. Then they were left in the lab atmosphere until testing day. Generally, the concrete standard test cubes were also removed from the molds after 24 hours from casting and then cured by submerging them in a tank filled with water until the testing day.

Fig. 3.5 Specimens curing

3.6 Test Setup and Testing Procedure

3.6.1 Test Setup and Preparation of Specimens for Test

The test set-up used in this study consisted of rigid steel frames supported by the laboratory rigid floor in Reinforced Concrete laboratory at faculty of engineering-Benha University. All the beams were tested under pure shear. Schematic arrangement of loading for the tested beams is shown in Fig. 3-5.

3.6.2 Loading system and instrumentation

The test set-up used in this study consisted of rigid steel frames supported by the laboratory rigid floor in reinforced concrete laboratory at faculty of engineering-Benha University. All beams were tested over a simple

span of 1300 mm, and the load was applied through two symmetrical points of 400 mm apart. Schematic arrangement of loading for the tested beams refer to Fig. 3-6. The load was applied using a hydraulic jack of 1000 KN capacity and measured by using load cell connected to Data Acquisition System. To monitor the deflection, three of Linear Variable Differential Transformer (LVDT) were placed beneath the center of the specimen and under the two load points. The applied load was equally distributed on two concentrated points. The specimens were prepared for testing in a simply supported condition under two symmetrically placed concentrated loads and testing procedure for the all the specimen is same as mentioned above.

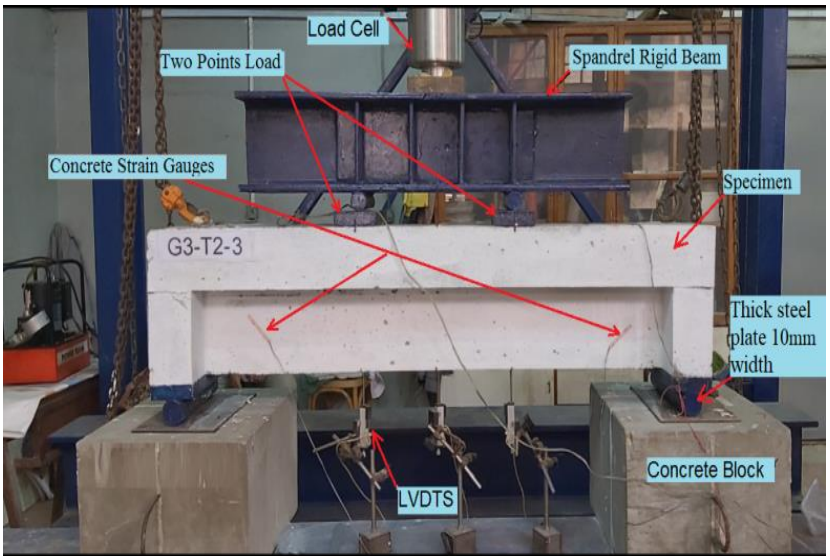

Fig. 3.6 Preparation of Test Specimens

Strain gauges were used to measure the strain in the longitudinal reinforcement in flange and in the concrete within shear zone.

3.6.3 Test Procedure

After the specimen aligned within the testing frame, all the initial reading of all instruments was noted down. A load increment was applied, noting down

all the reading at the end of each load step. Load was applied at a regular load interval (10 kN), before the formation of first crack. After the formation of first crack, the load was applied at a regular load interval (5 kN), the load was kept constant while cracks were marked and photographed and recording the reading of all dial gauges for deflection.

Table 3.5 Experimental Program

Specimen	Cross Sectional Area (cm^2)	Cross Sec. Area Increasing (%)	Flange Dim.		Stirrups in flange	Longitudinal reinforcement		Longitudinal reinforcement %
			ρ_t	ρ_b		Bottom	Top	
C0	300	------	------		------	------		------
G1-0.3-3	480	60%	90/h= 0.3	3	------	------		------
G2-0.3-3					------	4 Ø 8	3 Ø 6	1.055 %
G3-0.3-3					Ø8@75			
G1-0.4-3	540	80%	120/h=0.4		------	------		------
G2-0.4-3					------	4 Ø 10	2 Ø 6	1.029%
G3-0.4-3					Ø8@75			
G1-0.5-3	600	100%	150/h=0.5		------	------		------
G2-0.5-3					------	4 Ø 10	2 Ø 10	1.047%
G3-0.5-3					Ø8@75			
G1-0.3-5	660	120%	90/h= 0.3	5	------	------		------
G2-0.3-5					------	4 Ø 10	2 Ø 6+2 Ø 8	1.046%
G3-0.3-5					Ø8@75			
G1-0.4-5	780	160%	120/h=0.4		------	------		------
G2-0.4-5					------	6 Ø 10	2 Ø 8 + 2 Ø 6	1.046%
G3-0.4-5					Ø8@75			
G1-0.5-5	900	200%	150/h=0.5		------	------		------
G2-0.5-5					------	6 Ø 10	4 Ø 10	1.046%
G3-0.5-5					Ø8@75			

Finally, we would like to focus attention on, a test set-up and program were developed to investigate the performance of T-beams with thick and wide flanges in compression.

CHAPTER (4)

ANALYSIS AND DISCUSSION OF EXPERIMENTAL RESULTS

CHAPTER (4)

ANALYSIS AND DISCUSSION OF EXPERIMENTAL RESULTS

4.1. Introduction

This chapter presents the experimental results of reinforced concrete (RC) thick and wide flanges in compression. The studied variables are flange dimensions (thickness and width) and reinforcement. Nineteen simply supported specimens (the first has a rectangular cross-section while the remaining have T-shaped sections) were subjected to two-point loads and tested until failure. During the tests, development of diagonal cracks, crack width, reinforcement strains, maximum loads, as well as the deflection was monitored. The experimental results, for all specimens were presented and discussed for all tested variables.

4.1.1. The Effect of Web Reinforcement (By Ansys)

One factor that affects the design of test specimens is the capacity of the test frame. In this study, the tests were conducted at the reinforced concrete laboratory of the Faculty of Engineering, Benha University, which has a test frame with a capacity of approximately 60 tons. Since our initial calculations of the specimen capacity were close to this maximum value, few options were considered to reduce the maximum required load. As the study focuses on the flange contribution to shear strength, one choice was to use specimens without stirrups in the web (within the test shear zone). This way the maximum shear capacity of specimens was marginally reduced to below 60 tons. To verify that the use of such specimens will not affect the experimental evaluation of

flange contribution to shear strength, we first analyzed FE models of all test specimens for the two cases of with and without web stirrups. The following section presents an assessment of the error in the FE estimates of the flange contribution to shear strength when no stirrups are used in the web.

4.1.2. Model Validation

Thirty-eight FE models (19 without and 19 with stirrups in the web) that are exactly similar-to the test specimens are analyzed. The objective is to evaluate the relative error in using beams without stirrups in the web to estimate the flange contribution to shear strength. The details of models (specimens) are shown in Fig. [4.1-a& b].

4.1.3. Discussion of results

Table 4.1 shows the FE results of all 38 models, also includes the difference (error) in flange contribution to shear strength calculated using models without stirrups in the web compared to the standard case of models with stirrups. Also, Fig.4.2 presents the estimated error in relative flange contribution. It is seen from Fig.4.2 that the error in relative flange contribution does not exceed ±5% for $t_f/h=0.3$ and does not exceed ±7% for $t_f/h=0.4$ *and* ranges from +10% to +15% for $t_f/h=0.5$. Thus, using test specimen without stirrups in web is justified for thin flanges ($t_f/h \leq 0.4$) as the error is marginal. For thicker flanges ($t_f/h = 0.5$), however, the error is always positive and amounts to 15%. So, the flange contribution obtained from beams without stirrups in the web may be conservatively estimated by reducing it by a factor of $\frac{1}{1.15} \approx (0.87)$.

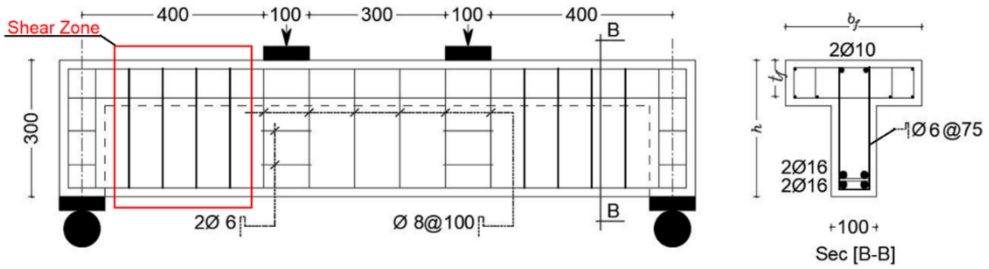

Fig. 4.1.a Specimen with web stirrups within shear zone

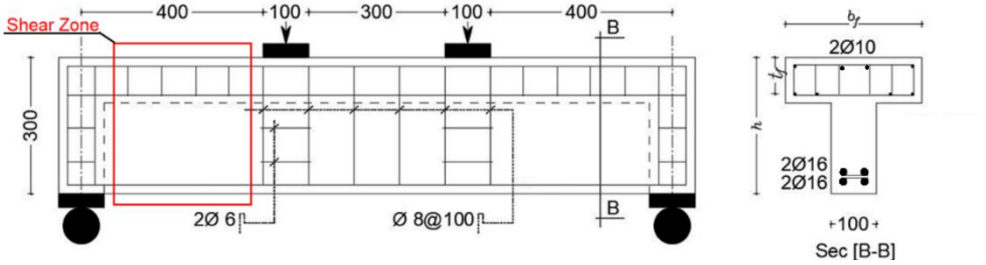

Fig. 4.1.b Specimen without web stirrups within shear zone

Fig. 4.1 Specimen details and arrangement of reinforcement
(All dimensions in mm)

Table 4.1 The output results for the analyzed specimens. (By Ansys)

Specimens	**Pu(kN) Ansys**	Without Stirrups (Δw) kN	With Stirrups (Δs) kN	$\frac{\Delta w - \Delta s}{\Delta w}$ %
		$\Delta w = Pu_T - Pu_{C0}$	$\Delta s = Pu_T - Pu_{C0}$	
C0	113.40			
with stir.	232.90			
G1-0.3-3	275.00	161.60		-2.17
with stir.	398.00		165.10	
G2-0.3-3	304.00	190.60		-3.50
with stir.	430.16		197.26	
G3-0.3-3	346.70	233.30		-3.81
with stir.	475.08		242.18	
G1-0.3-5	301.77	188.37		2.21
with stir.	417.11		184.21	

Table 4.1 (*cont.*)

G2-0.3-5	364.38	250.99		-3.05
with stir.	491.53		258.64	
G3-0.3-5	423.32	309.92		4.28
with stir.	529.56		296.66	
G1-0.4-3	358.46	245.06		-3.58
with stir.	486.73		253.83	
G2-0.4-3	368.78	255.38		-3.46
with stir.	497.12		264.22	
G3-0.4-3	375.70	262.30		-6.65
with stir.	512.64		279.74	
G1-0.4-5	401.11	287.71		2.53
with stir.	513.32		280.42	
G2-0.4-5	382.55	269.15		-4.86
with stir.	515.13		282.23	
G3-0.4-5	431.55	318.15		4.76
with stir.	535.52		302.62	
G1-0.5-3	434.9	321.50		10.22
with stir.	521.54		288.64	
G2-0.5-3	437.392	323.99		9.42
with stir.	526.356		293.46	
G3-0.5-3	452.94	339.54		9.41
with stir.	540.478		307.58	
G1-0.5-5	420.36	306.96		14.01
with stir.	496.87		263.97	
G2-0.5-5	445.85	332.45		9.91
with stir.	532.39		299.49	
G3-0.5-5	474.9	361.50		14.39
with stir.	542.39		309.49	

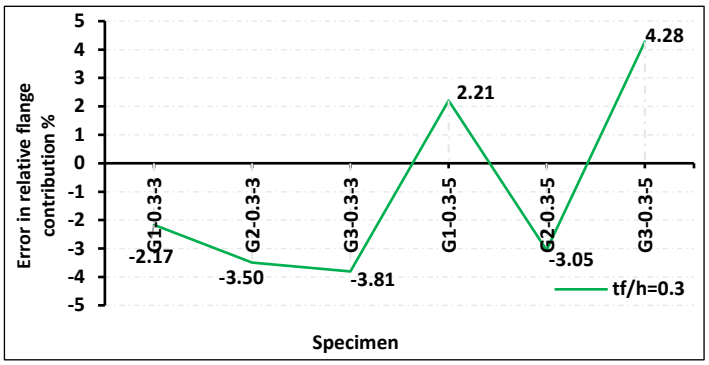

Fig. 4.2.a Specimens with $t_f/h = 0.3$

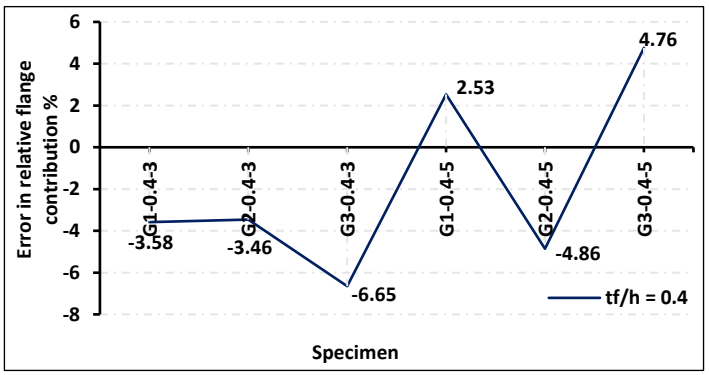

Fig. 4.2.b Specimens with $t_f/h = 0.4$

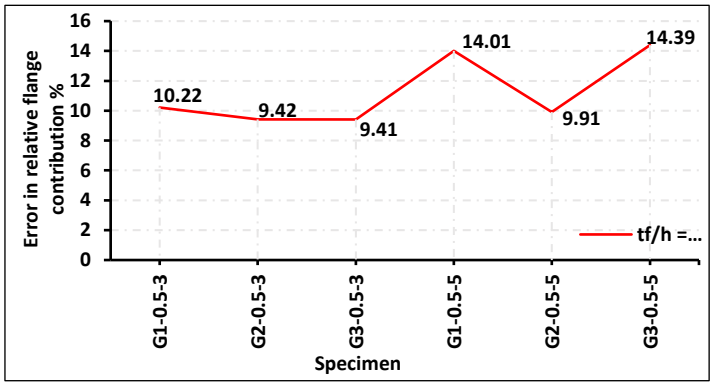

Fig. 4.2.c Specimens with $t_f/h = 0.5$

Fig. 4.2 Error percentage in relative flange contribution between all tested specimens with and without web stirrups by FE model.

What has been described above supports and clarifies the tested results that will be explained in this chapter, Where the dispensing of web stirrups in the nerve in all tested specimens, as was previously indicated, in order to maintain the error rate of all specimens.

4.2. Ultimate Load

Fig.4.3 shows a comparison of ultimate load (P_u) for all tested specimens. It is obvious that increasing the dimensions of flange, either the width or the depth, generally increased P_u "for tested ratio". Increasing width ratio ρ_b = 3& 5, the ultimate load P_u increases from 6% to 8% for the first group that (without any reinforcement in flange). But, when comparing to rectangular specimen "control", we find that the P_u increasing from 165 % to 307%. The increasing of depth ratio ρ_t leads to enhancement of the ultimate load for flanged specimens, for increasing of ρ_t from 0.3 to 0.5, leads to increasing of P_u from 29% to 53% for specimens having ρ_b =3, and 31% to 44% for specimens having ρ_b =5. But when compared to rectangular specimen, we find that improving in P_u in the range, from 165% to 307%. The adding of longitudinal reinforcement to flange increases the ultimate load in the range, from 207% to 320% when compared with control specimen.

Table 4.2 Experimental Results specimens.

Specimen	f_{cu}, (Mpa)	ρ_t	ρ_b	ζ	Cracking Load "P_{cr}" (kN)	Ultimate Load "P_u" (kN)	$\frac{P_u - P_{u.c}}{P_{u.c}}\%$	Max. Recorded Deflection (mm)	Mode of Failure
C0	36.4	---	---	---	95	106	0	2.33	
G1-0.3-3	36.4	0.3	3	---	100	282	165	4.74	
G1-0.4-3	36.4	0.4		---	105	363	241	5.97	

Table 4.2 (*cont.*)

G1-0.5-3	36.4	0.5		---	110	431	305	5.98	
G2-0.3-3	34.2	0.3		1.055	90	326	207	5.80	Shear
G2-0.4-3	34.2	0.4		1.029	105	377	255	5.87	
G2-0.5-3	34.2	0.5		1.047	115	439	312	4.43	
G3-0.3-3	34.2	0.3		1.055	110	358	237	5.89	
G3-0.4-3	36.8	0.4		1.029	100	384	261	7.07	
G3-0.5-3	36.8	0.5		1.047	115	454	327	6.22	
G1-0.3-5	36.8	0.3	5	---	115	299	181	4.49	
G1-0.4-5	35.6	0.4		---	120	392	268	4.79	
G1-0.5-5	35.6	0.5		---	115	432	307	6.59	
G2-0.3-5	35.6	0.3		1.046	110	342	221	5.11	
G2-0.4-5	35.6	0.4		1.046	120	383	260	6.51	Shear
G2-0.5-5	35.6	0.5		1.046	115	446	320	9.11	
G3-0.3-5	34.8	0.3		1.046	95	429	304	8.05	
G3-0.4-5	34.8	0.4		1.046	85	437	311	9.56	
G3-0.5-5	34.8	0.5		1.046	125	474	346	10.13	

ζ **:** Longitudinal reinforcement ratio in flange, ρ_t **:** depth ratio (t_f/h), ρ_b **:** width ratio (b_f/b_w), $P_{u.c}$: ultimate load of control specimen

While when compared with the first group, we find enhancement in P_u from 2% to 16%. The existing of stirrups with longitudinal reinforcement in flange induces to increase in the ultimate load in the range of 5% to 43% when compared with the first group that without any reinforcement in the flange.

4.3. Load Deflection relationship.

It is very clear from Fig.4.4, that the load-deformation relationship of RC T-beam is changed because of the existing of the concrete top flange. Also, the shear strength of flanged beam is higher than that of the rectangular

specimen. After the first diagonal crack appeared a larger deflection was observed with increasing load, especially for specimens that without longitudinal reinforcement in the flange. Reinforcement decreased by 30%-80% with respect to the deflection of control specimen, which means that there is a very good control on mid-span deflection when adding longitudinal reinforcement in flange, where a large reduction in the deflection at the same load.

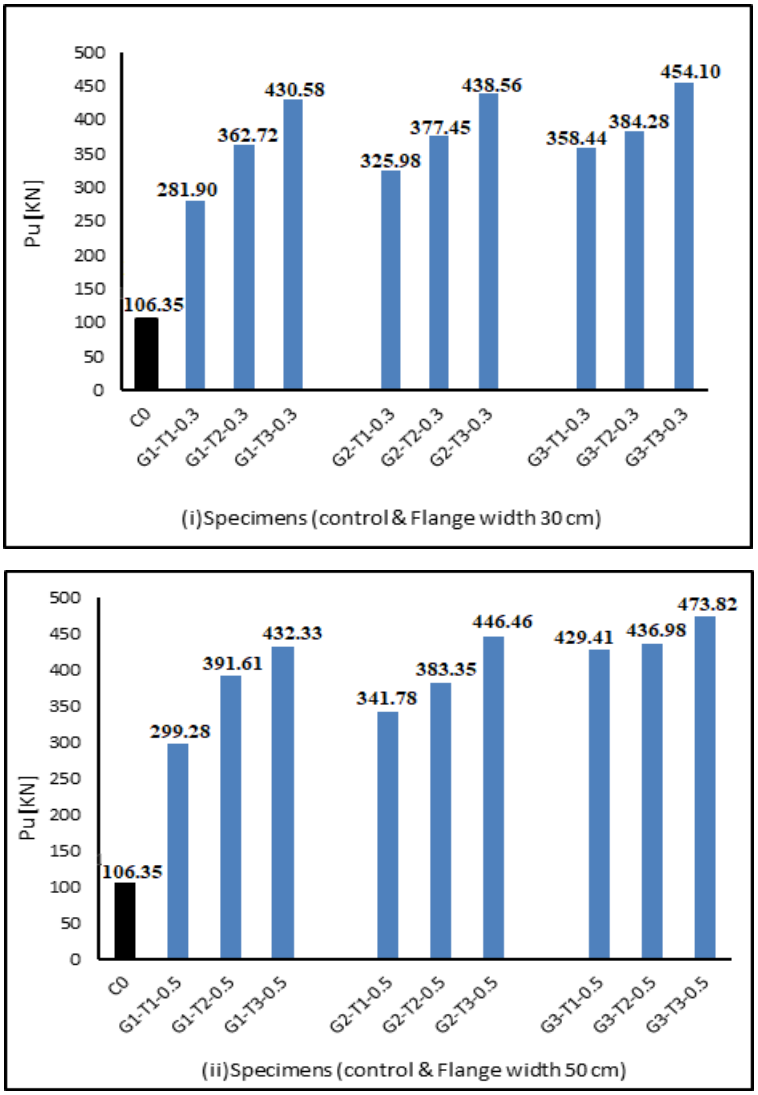

Fig. 4.3 Max. ultimate load for all specimens

Specimens with different flange dimensions and without reinforcement provided for the study of the flange dimensions effect, during a comparison between them and another rectangular one" control specimen". At 25% P_u of control specimen, the deflection of specimens with longitudinal Fig.4.4- (a-c) and (d-f) show load-deflection curves of the tested specimens. Comparison between load-deflection curves for individual group with rectangular and T sections are shown in Fig.4.4. It is shown from these figures that beam capacity increases as the depth ratio (ρ_t) and width ratio (ρ_b) of flange increase, also the shear capacity "strength" improves with the existing of longitudinal reinforcement within the flange. In addition, it is confirmed from Fig.4.4-f that beam G3-0.4-5 and G3-0.5-5 failed in shear after longitudinal reinforcement yielded. This is indicated by the flat region in the end part of load-deflection curve "*improvement the ductility*". However, the reinforcement in beams G3-0.3-3 and G3-0.3-5 did not reach the yield strength up to the occurrence of shear failure.

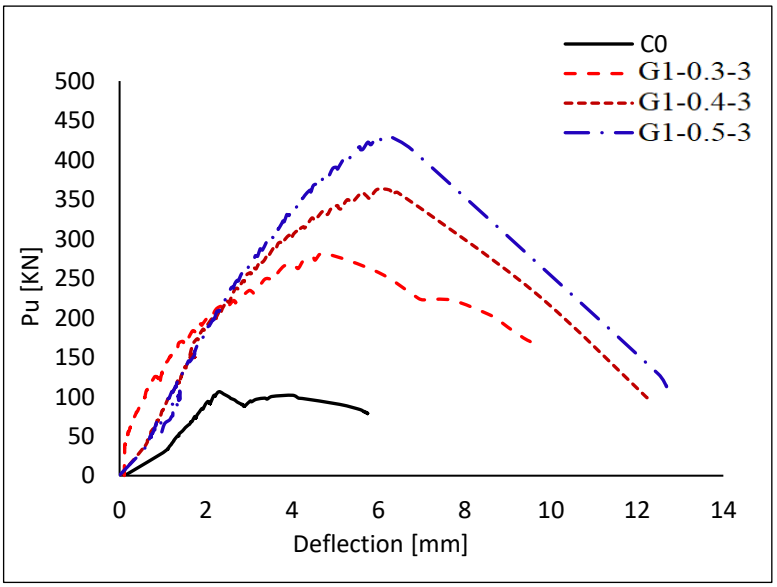

Fig. 4.4 Load deflection relationship
Fig. 4.4.a *G1*, ρ_b *=3*

Due to the contribution of flange in the compression zone of the section, it is revealed that the capacity and stiffness of beams with T sections are higher than that of beams with rectangular sections and lead to improvement in the shear strength significantly.

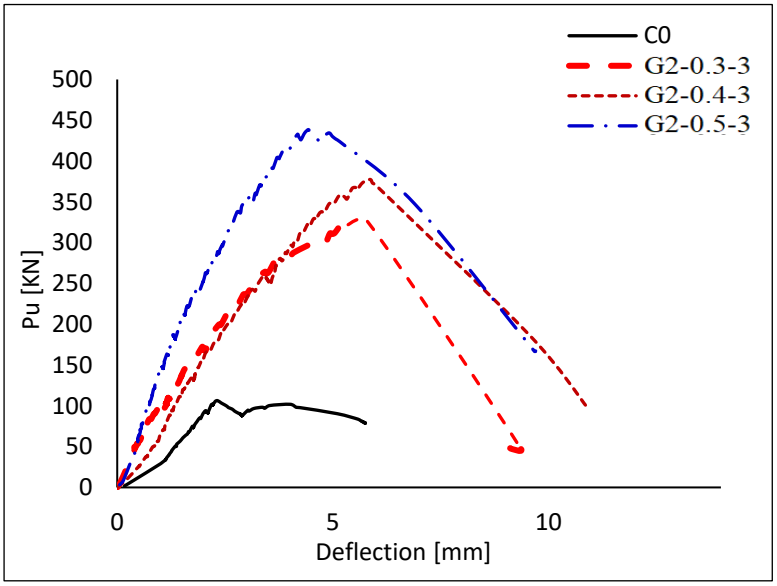

Fig. 4.4.b *G2*, ρ_b *=3*

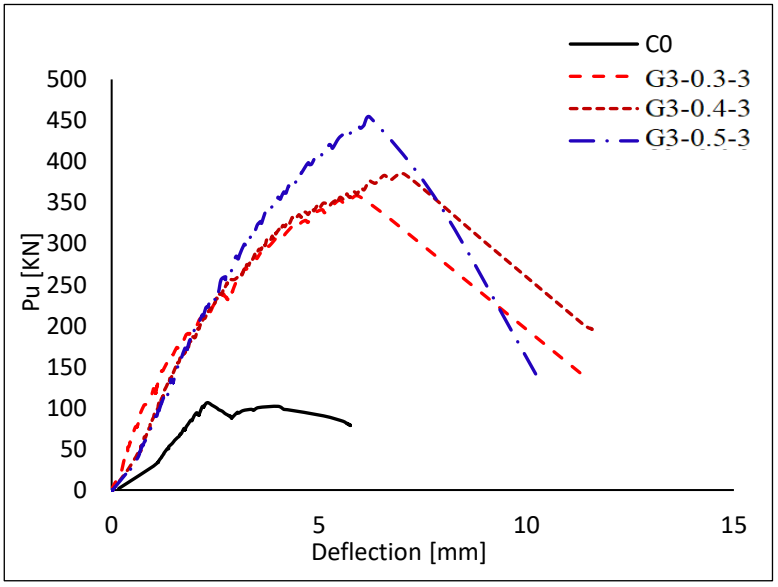

Fig. 4.4 (*cont.*)

Fig. 4.4.c *G3*, ρ_b *=3*

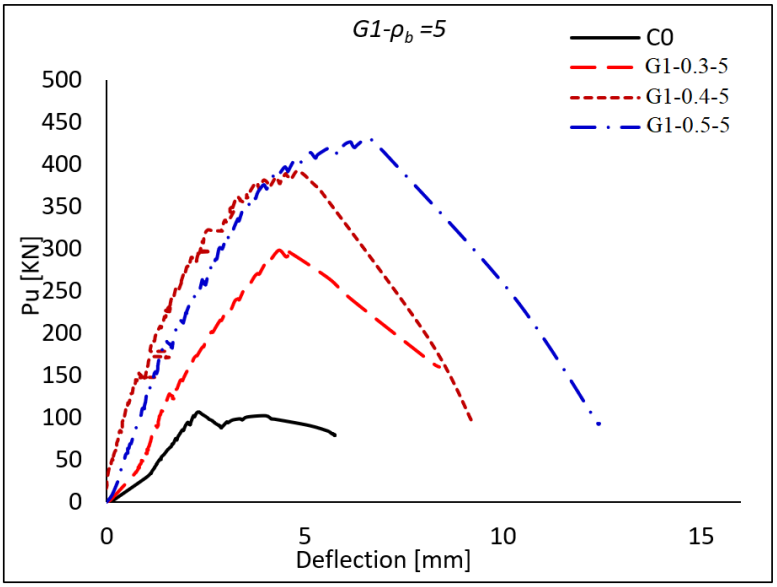

Fig. 4.4.d *G1*, ρ_b =5

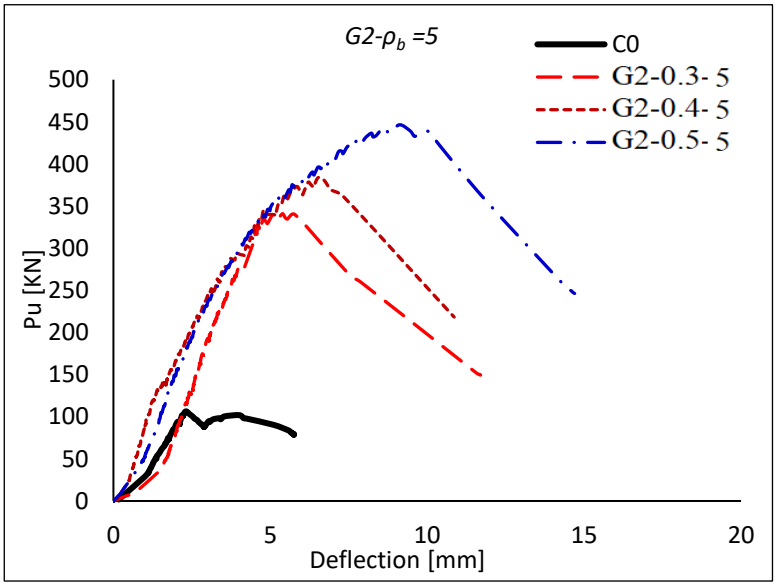

Fig. 4.4 (*cont.*)
Fig. 4.4.e *G2*, ρ_b =5

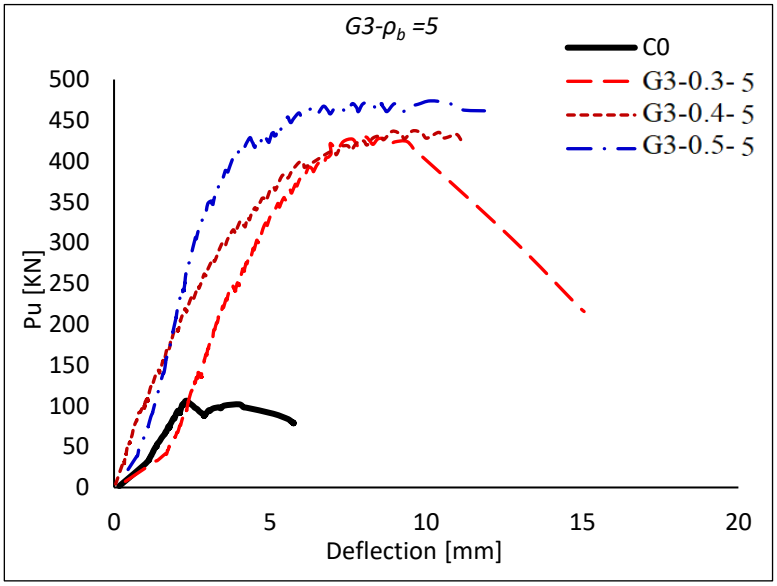

Fig. 4.4 (*cont.*)
Fig. 4.4.f *G3, ρ_b =5*

4.4. Cracking pattern and failure mode

The cracking pattern and modes of failure of all specimens with flange are as shown in Fig.4.5. For the rectangular specimen, the diagonal cracks were initiated at the shear zone about 89% of maximum load, and these are followed by diagonal cracks on both sides. With load increasing more inclined cracks appeared in the compression path joining the end load plate and end support plate, while for flanged specimens, the diagonal shear cracks appear at a load of 19-30% of maximum load, in addition, the failure modes are listed in table 4.2.

The cracks started at the center of both shear zones. As shown in Fig.4.5 the load increases, the crack widened and propagates towards the support and loading plates. For the flanged specimens leading to diagonal shear cracks at a load form 104-125 kN “19-30% of maximum load” and a horizontal crack

appeared at the flange but late, depending on the thickness, width of the flange, and the presence of reinforcement in it. The inclined cracks followed a much shallower path (approximately 15-25°) in the flange according to the flange thickness and longitudinal reinforcement in flange.

Fig. 4.5 Experimental Crack Pattern
Fig. 4.5.a *Control specimen*

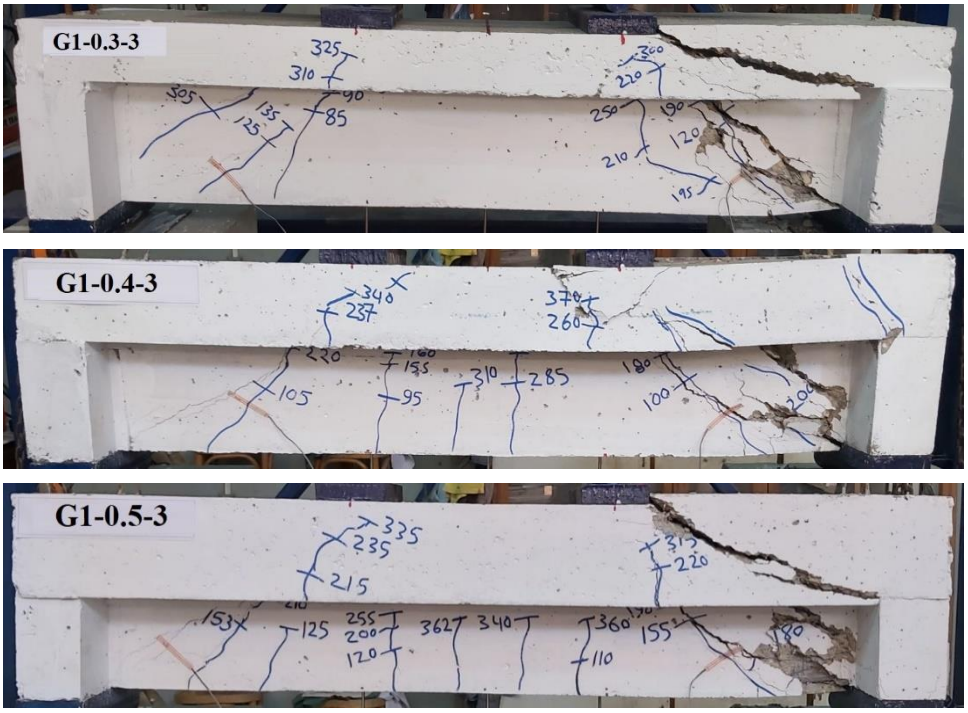

Fig. 4.5.b Specimens without reinforcement (ρ_b =3)

Visual inspection of control specimen C0 at failure revealed that it had a wider main inclined crack compared with the corresponding cracks in flanged specimens. Afterwards, more diagonal cracks were initiated within both the web and the flange, which were uniformly distributed, as shown in

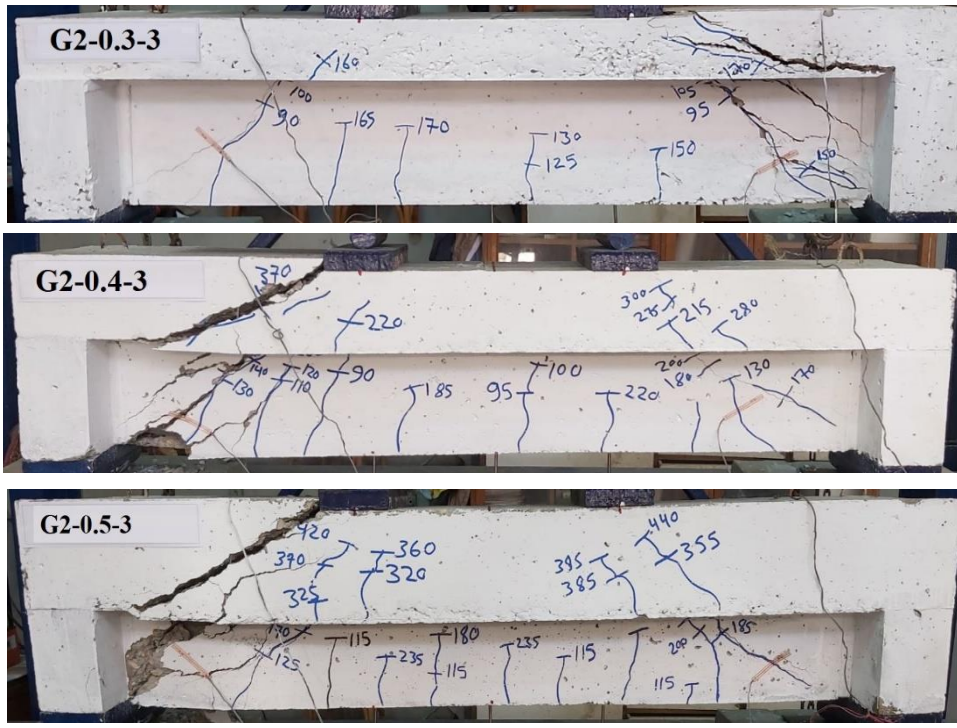

Fig. 4.5 (*cont.*)

Fig. 4.5.c Specimens with longitudinal reinforcement (ρ_b =3)

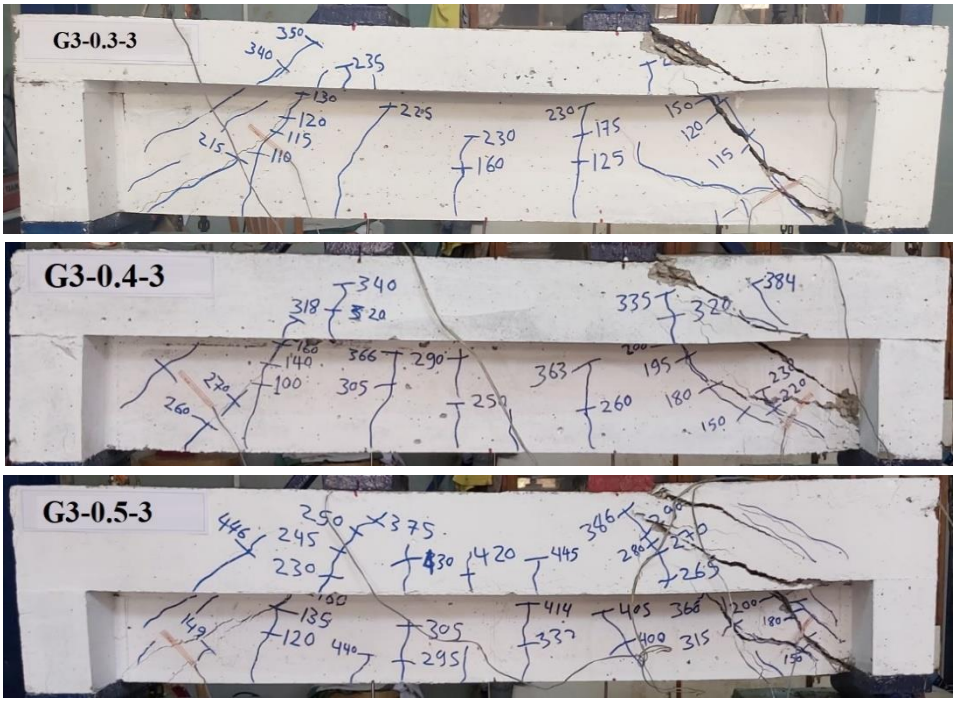

Fig. 4.5.d Specimens with longitudinal and shear reinforcement (ρ_b =3)

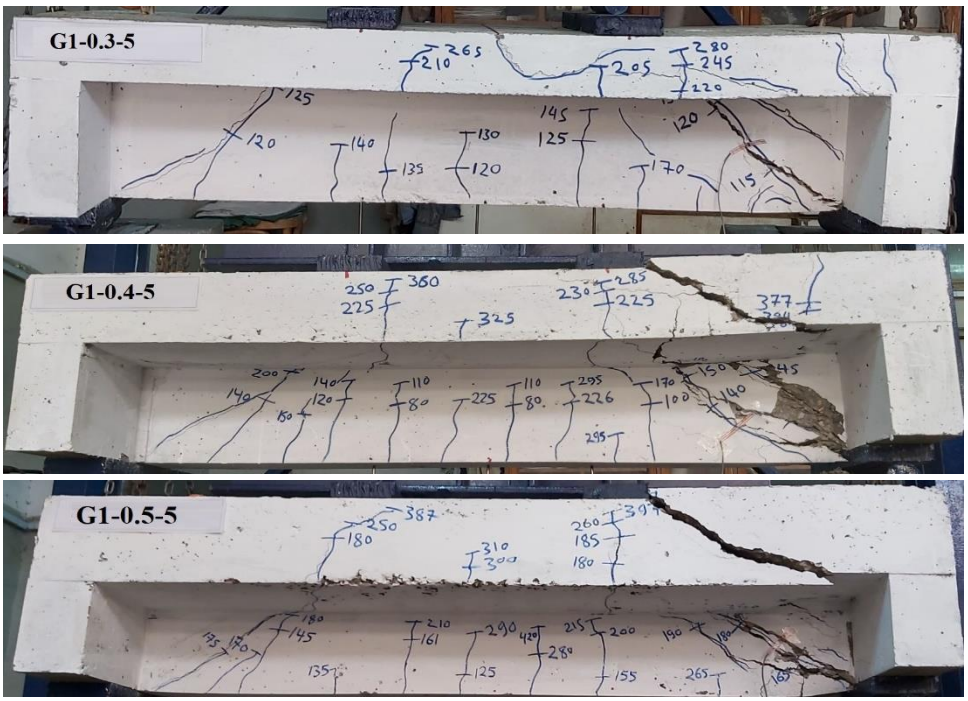

Fig. 4.5 (*cont.*)

Fig. 4.5.e Specimens without reinforcement (ρ_b =5)

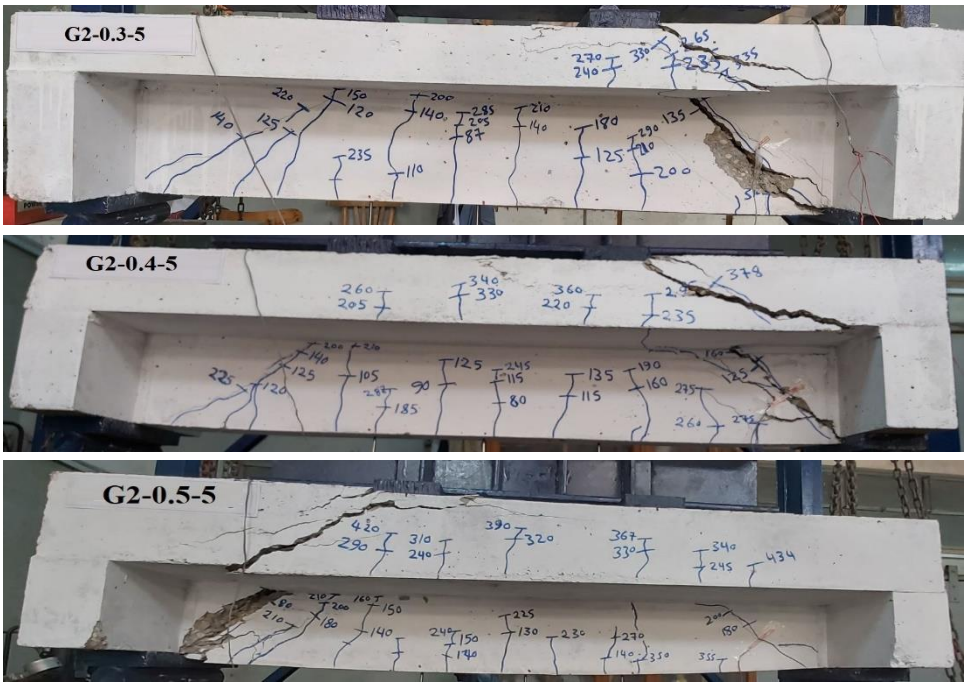

Fig. 4.5.f Specimens with longitudinal reinforcement (ρ_b =5)

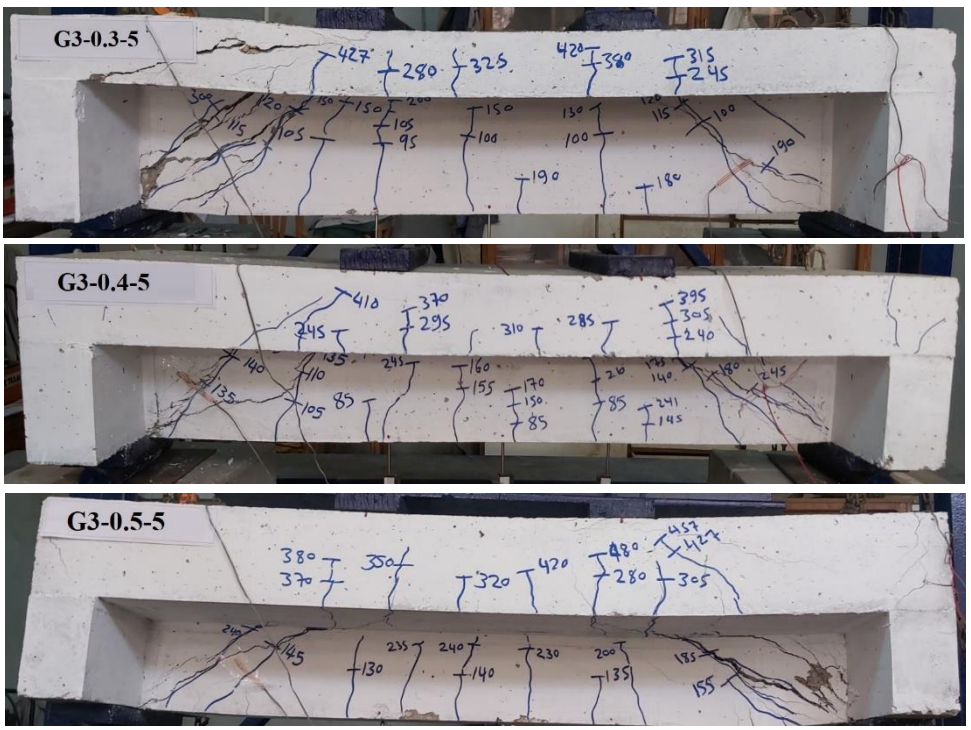

Fig. 4.5 (*cont.*)

Fig. 4.5.g Specimens with longitudinal and shear reinforcement (ρ_b =5)

4.5. Strain analysis

This part of the study investigates the behavior of the longitudinal steel and the concrete element. The extensive instrumentation for strain monitoring was carefully engineered to provide the information and data much needed for the understanding of the shear resistance mechanisms of flanged reinforced concrete beams.

4.5.1. Strain in longitudinal reinforcement

Fig.4.6 presents a variation in the strains in the flange longitudinal steel with the applied shear force for different flange thicknesses at flange width ratios of 3 and 5, respectively. These curves indicated that the behavior of the longitudinal steel went through three phases during loading. In the first initial phase, no noticeable contribution of the steel to the resistance was observed. In the second phase, the first diagonal cracks initiated, and the longitudinal steel started to strain. In the flanged specimens, for instance, this phase started at an average applied load of approximately 95-125 kN “26-29%” for G2& G3 specimens.

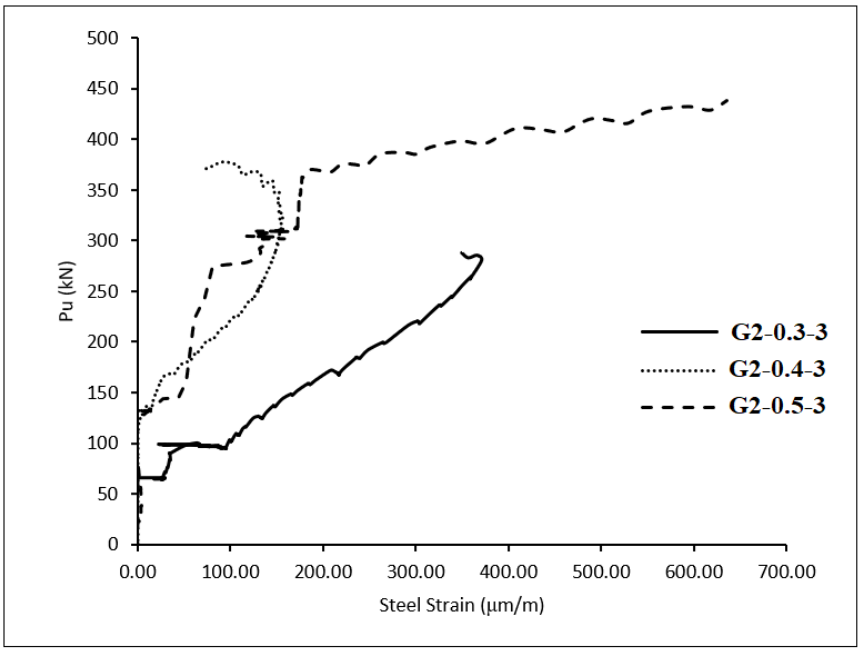

Fig. 4.6 Steel Strain
Fig. 4.6.a Specimens with ρ_b=*3*

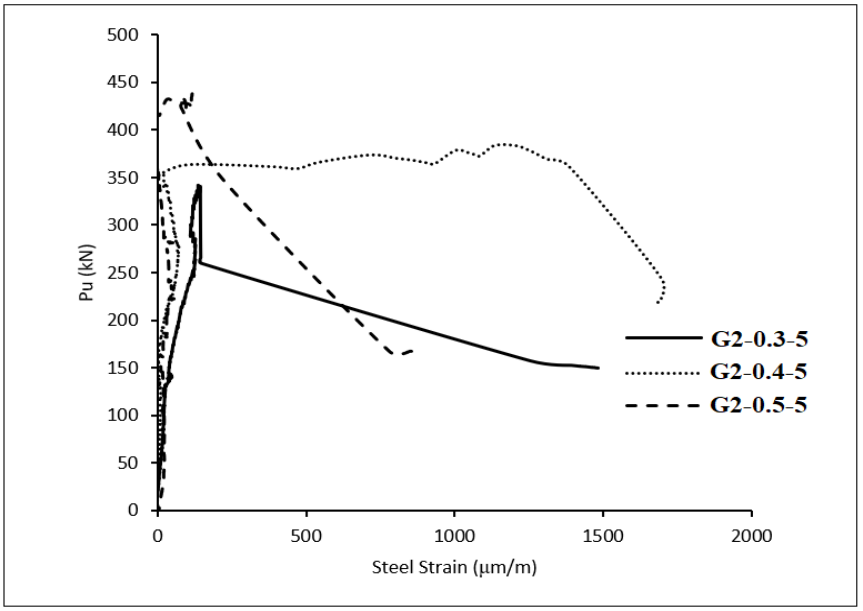

Fig. 4.6 (*cont.*)
Fig. 4.6.b Specimens with ρ_b =5

The longitudinal steel strain continued to increase with increasing load until the steel yielded and at that time the failure occurred easily by flexure in flange. Given the applied load, the strain in the longitudinal steel was substantially greater in specimens with $\rho_t = 0.5$. It must be noted, however, that yielding of longitudinal steel wasn't achieved in most cases, this is due to smallness of flange thickness.

4.5.2. Concrete strain

The curves representing the shear force versus the concrete strain measured on the concrete are presented in Fig.4.7. For all specimens, these curves which featured similar pattern, indicated that in the initial phase of loading, the compression concrete struts were not strained practically. This held true up to an applied shear force of approximately "80% of P_u" for specimens with rectangular section "control specimen" and "22%-33% of P_u" for specimens retrofitted with flange. In other words, the contributions of both the concrete struts and the flange engage only after the diagonal cracks have developed. Consequently, the truss mechanism became effective only after the formation of the diagonal cracks. Since then, it has been observed that the strut strain increased almost linearly with increasing loads until it reached approximately 800 micro-strains on average. Beyond that point, the curves featured a somewhat plastic response. Physically, this corresponded to the propagation of cracks towards the compression zone. The strut strain at failure attained 1000 to 1800 micro-strains on average.

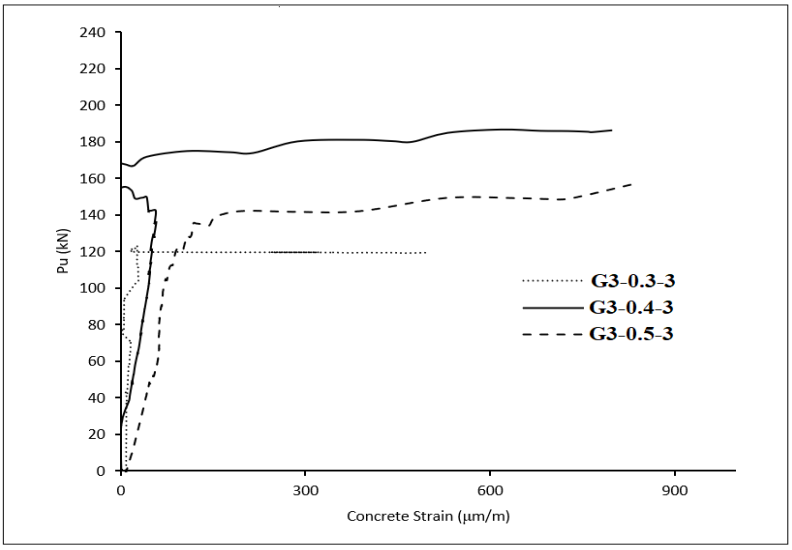

Fig. 4.7 Concrete Strain

Fig. 4.7.a Specimens with ρ_b =3

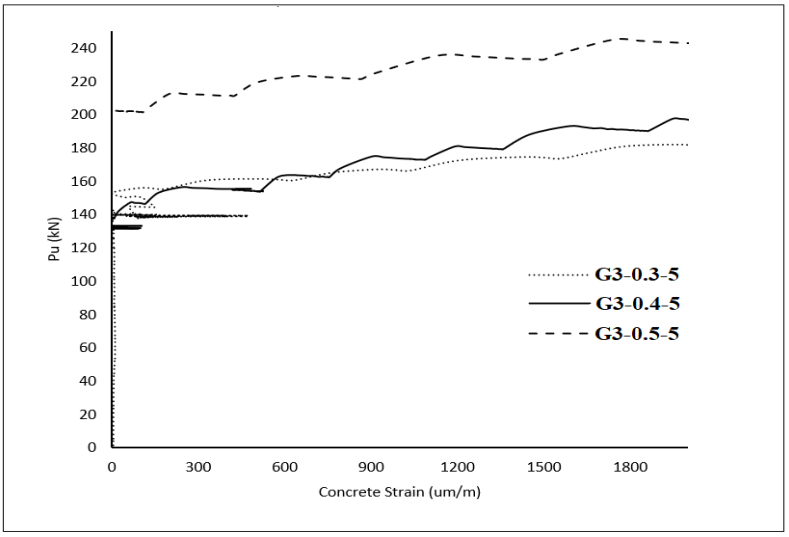

Fig. 4.7.b Specimens with ρ_b =5

CHAPTER (5)

ANALYTICAL STUDY

CHAPTER (5)

ANALYTICAL STUDY

5.1. Introduction

The shear strength was assumed to be the sum of the shear transferred by a chord of the concrete compression, along the crack which happened due to residual tensile stress, frictional stress, the stirrups and the longitudinal reinforcement where available. As generally accepted, the total shear resistance, Eq. (1), was the combination of the shear resisted by concrete and by the transverse reinforcement (*Vs*). However, the shear resistant contribution of concrete was explicitly divided into the following components, the importance of which is considered to be variable as damage propagates**:** shear resisted in the uncrack compression head (V_c), Transfer of shear across web cracks (V_w) and the contribution of the longitudinal reinforcement (V_l).

$$V = V_c + V_w + V_l + V_s$$

$$= f_{ct} \cdot b \cdot d \cdot (v_c + v_w + v_l + v_s) \qquad [1]$$

Where v_c, v_w, v_l and v_s are the dimensionless values of the shear transfer action.

f_{ct} *:* tensile concrete strength

5.2. Model for shear capacity of rectangular beams.

5.2.1. Compression head contribution (v_c)

The shear capacity of the compression chord was evaluated assuming that failure occurred when the first fiber in the compression chord reached the Kupfer's failure envelope. It is considered that failure occurred when the principal stresses reached the Kupfer's compression-tension branch of the failure surface [25].

Table 5.1 simplified expressions of dimensionless shear contributing components. [25]

Contributing component	Final simplified dimensionless expressions	
Cracked concrete web	$v_w = 167\frac{f_{ct}}{E_c}\left(1+\frac{2E_cG_f}{f_{ct}^2 d}\right)$	[2]
Longitudinal reinforcement	if $v_s > 0 \rightarrow v_l = 0.23\frac{\alpha_e\cdot\rho}{1-x/d} \approx 0.25\frac{x}{d} - 0.05 \geqslant 0$	[3a]
	if $v_s = 0 \rightarrow v_l = 0$	[3b]
Transversal reinforcement	$v_s = 0.85\rho_w\frac{f_{yw}}{f_{ct}}$	[4]
Compression chord	$v_c = \zeta\left[(0.88+0.70v_s)\frac{x}{d}+0.02\right]$	[5]
	$\zeta = 1.2 - 0.2\cdot a \geqslant 0.65$ (a in meters)	[6]

Where, f_{ct} *:* tensile concrete strength,

G_f *:* fracture energy, = $0.028\cdot f_c^{0.18}\cdot d_{max}^{0.32}$

E_c : concrete modulus of elasticity = $22\cdot(0.1f_c)^{0.3}$ (Mpa)

f_{yw} : yield strength of the transverse reinforcement

5.2.2. Cracked concrete web contribution (v_w)

Shear resistance of cracked concrete in the web is considered as the residual tensile stress of cracked concrete. The mean tensile stress of the softening curve is considered distributed in a depth x_w of the cracked zone of the cross-section where the tensile σ–ε curve reached zero tension, see Fig.5.1. A linear softening branch of the σ–ε curve has been assumed which was consistently dependent on the fracture energy. The derivation of the equation was carried out in Ref. [26] and the resulting equation is presented in Eq. (2) of Table5.1.

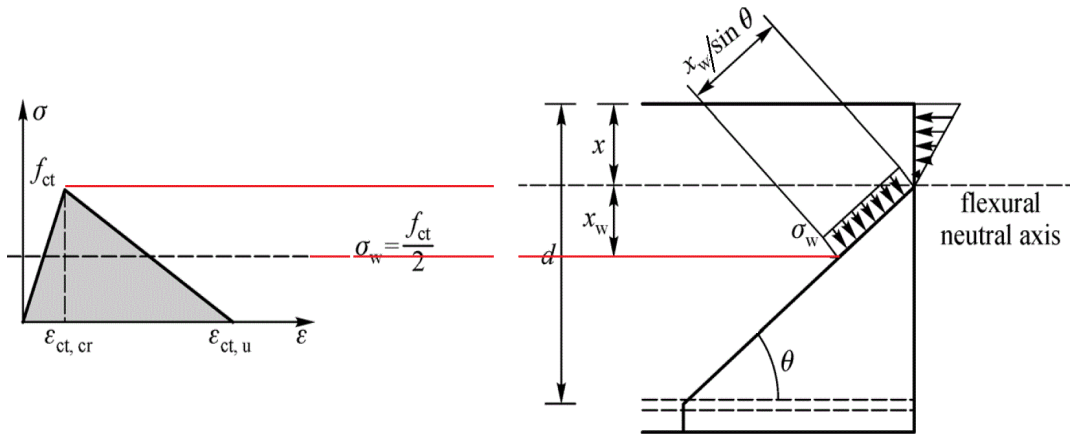

Where, x is the depth of neutral axis and d is the effective depth.

Fig. 5.1 Contribution of cracked concrete to shear resistance. [25]

5.2.3. Transversal reinforcement contribution (v_s)

Transversal reinforcement contribution, Eq. (4) of Table5.1, is taken as the integration of the stresses cut by the inclined crack up to a height of (d-x), see Fig. 5.2, and assuming that transversal reinforcement **was** yielded along the total crack height.

5.2.4. Longitudinal reinforcement contribution (v_l)

Contribution of longitudinal reinforcement, or dowel action, is considered only when transversal reinforcement exists, Eq. (**3a**), became negligibly when there are no stirrups, Eq. (**3b**). Stirrups provided a constraint to the vertical movement of the longitudinal bar enabling them to transfer a certain shear. To evaluate such shear force, it is considered that the longitudinal bars were doubly fixed at the two stirrups adjacent to the crack initiation and subjected to bending due to a relative imposed displacement between those points. This vertical relative displacement was caused by the critical crack opening and the shear deformation of the compression chord. This

contributing component clearly depended on the tensile steel ratio which was implicitly represented by means of the x/d parameter. The simplified expression is presented in Eq. (3a) of Table5.1.

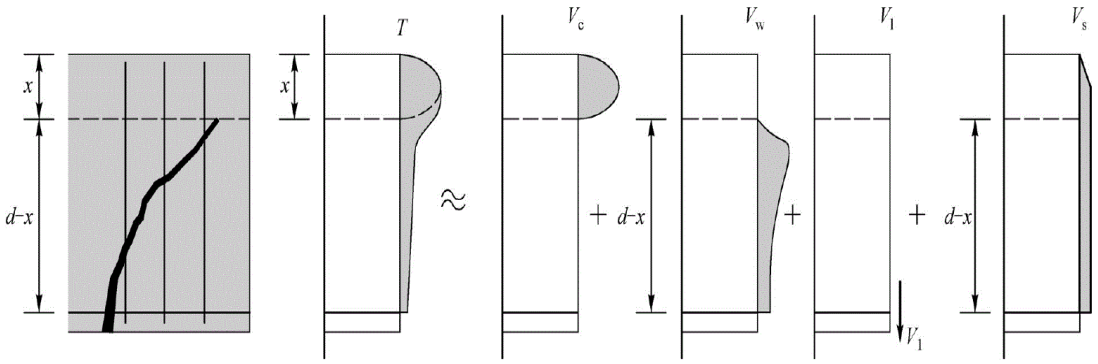

Fig. 5.2 Shear stresses distribution in the imminent failure situation and qualitative distribution of the different contributing actions. [25]

5.3. Model for shear capacity of T-beams

According to numerical analyses performed [26,27,28] only a portion of the flanges closer to the web contributed to resist shear, this portion was approximately equal to h_f at each side of the web. Similar analyses have been performed to other T-shaped beams, arriving to similar results. Consequently, in this work a shear effective flange width b_v was defined as indicated in Eq. (7) and in Fig.5.3.

$$b_v = b_w + 2h_f \leq b \qquad [7]$$

Eq. (**7**) is coincident with that proposed by Placas and Regan [**29**] and Zsutty [**30**]. However, Paulay and Taylor [**31**] reduced the influence of the flanges considering an effective width equal to b_w +1.5h_f, Moayer and Regan considered the influence of all the flange depth, h_f, and not only until the

neutral axis depth, *x*, as in the model utilised. Wolf and Frosch [**32**] proposed an effective flange width equal to $b_w + h_f$.

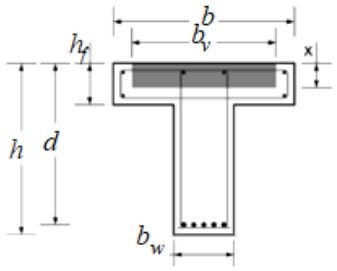

Fig. 5.3 Effective width in a T-shaped section.

The cracking moment of a T section is different to that of a rectangular section. This fact affects the position where the critical crack initiated, the position of the critical section and the level of normal stresses at the compression concrete chord. The ratio between the cracking moments of the T section ($M_{cr,T}$) and that of a rectangular reference section of the same height and b = b_w, ($M_{cr,R}$), is called K_{cr}, and could be obtained analytically. A very good approximation could be also obtained by Eq. (8).

$$K_{cr}=\frac{M_{cr,T}}{M_{cr,R}} \quad \textbf{[8]}$$

It is also possible to define a coefficient K_T as a product of K_{cr} by the ratio b_w/b. This coefficient will be useful in the derivation of the contribution of the compression concrete chord for T-shaped beams, and it is given by Eq. (9).

$$K_T = \frac{M_{cr,T}}{M_{cr,R}} \frac{b_w}{b} \quad \textbf{[9]}$$

The uncracked concrete zone and a neutral axis depth (*x*) were treated as equivalent. It is assumed that it can be obtained by standard analysis of cracked reinforced concrete sections under pure flexure Eq. (10). In a cracked T beam, in the case that the neutral axis depth, *x*, was placed inside

the concrete chord ($x \leq h_f$), the width of the concrete compression block was equal to the flexural effective width of the flanges, b. The neutral axis depth became, therefore, smaller than that of the reference rectangular section of $b = b_w$. The following equation provides the limit condition for the location of the neutral axis depth with respect to the flange's depth, h_f:

$$\frac{x}{d} = \alpha_e \rho \left(-1 + \sqrt{1 + \frac{2}{\alpha_e \rho}} \right) \qquad \textbf{[10]}$$

where $\alpha_e = E_s/E_c$ is the modular ratio between steel and concrete

and $\rho = A_s/(b.d)$ is the longitudinal reinforcement ratio.

$$x \leq h_f \quad \text{if } \alpha_e \rho \leq \frac{1}{2} \frac{\delta^2}{1-\delta} \; ; \qquad \delta = \frac{h_f}{d} \; ; \qquad \rho = \frac{A_s}{b.d} \qquad \textbf{[11]}$$

In that case, Eq. (10) which corresponded to a rectangular section of effective depth, d, and width, b, might be used to obtain the neutral axis depth (see Figs.5.4 and 5.5a). Therefore, in a T-beam the neutral axis depth will be lower than that of a similar rectangular beam with a constant width equal to that of the web of the T beam, b_w, and the cracks will be more vertical.

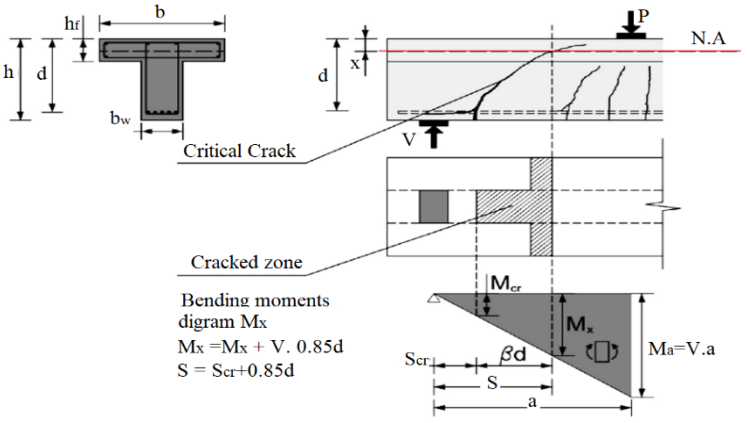

Fig. 5.4 Scheme of cracking in a beam with T section ($x \leq h_f$). [2].

At Eq. (11) not satisfied; the neutral axis depth will be $x > h_f$ and it could be calculated by solving Eq. (12), which is derived by setting the equilibrium of horizontal forces in the section, accounted for the two different widths of the section as shown in Fig.5.5b.

$$\xi^2 + 2\xi\,[\delta(\eta\text{-}1) + \alpha_e\rho\,\eta] - [\delta^2(\eta\text{ -}1) + 2\alpha_e\rho\,\eta] \qquad [12]$$

where $\eta = b/b_w$ and the rest of parameters have been previously defined.

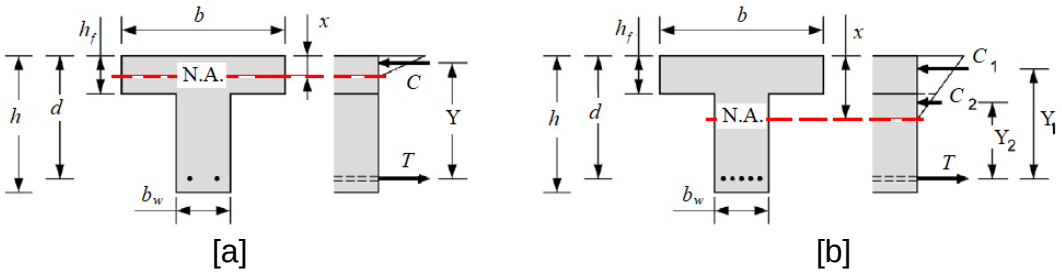

Fig. 5.5 Neutral axis depth in a T section. (a) $x \leq h_f$. (b) $x > h_f$.

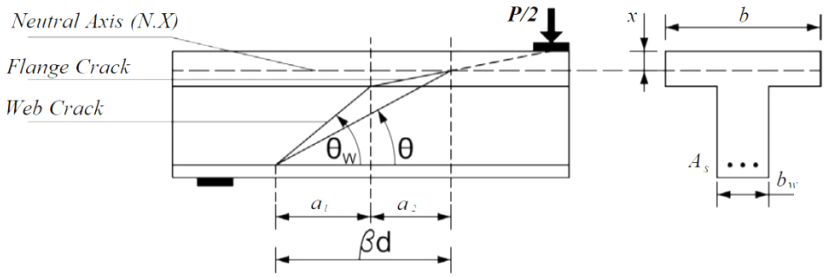

Fig. 5.6 Inclined crack with two branches in beams with T section.

When $x < h_f$, the crack might penetrate into the flanges assuming a more horizontal path than in the web. This could be due to the difference in the ratio between the normal and the shear stresses generated by the change of width as shown in Fig.5.6. Therefore, the horizontal projection of the critical crack, βd, was higher than the reference of the rectangular section.

To evaluate the effect in V_s, it was essential to obtain the inclination of the crack in the flanges and the global angle of inclination. From Fig.5.6, the following ratio between the global crack angle, Θ, the inclinations of the web crack, Θ_w, and the flange crack, Θ_f, was obtained from geometrical considerations Eq. (14).

$$Cot\theta = Cot\theta_w \frac{(d-h_f)+(h_f-x)\frac{b_v}{b_w}}{d-x} = \frac{0.85}{1-\frac{x}{d}} K_\theta \quad \textbf{[13]}$$

Where K_Θ

$$K_\theta = \frac{d-h_f)+(h_f-x)\frac{b_v}{b_w}}{d-x} \quad \textbf{[14]}$$

and the horizontal projection of the crack will be:

$$\beta.d = 0.85 \,.\, K_{\theta.}\, d \quad \textbf{[15]}$$

In order to obtain the beam shear capacity V_c for T-beam, the non-dimensional compression chord contribution to the shear strength had to be modified to take into account the influence of the T-shape, according to the above considerations. Related to the position of the neutral axis depth, the following situations should take place:

5.3.1. Neutral axis inside the compression flange ($x \leq h_f$)

The formulation developed for rectangular sections was still valid for this case, with small modifications. When calculating the normal stresses due to bending, the neutral axis depth had to be obtained with a reinforcement ratio $\rho = A_s/(b.d)$ relative to the compression flange flexural effective width, b. In addition, the cracking moment of the T section, $M_{cr,T}$, had to be used. Further, by relating the vertical confining stress (σ_y) with the capacity of the

transversal reinforcement (v_s), Eq. (16) is derived for the shear capacity of the compression chord, where $R_t = \sigma_1/f_{ct}$, was a reduction factor of the tensile stress due to the biaxial stress state.

$$v_c = R_t K_\lambda \zeta \xi \frac{b_v}{b} . \sqrt{1 - \frac{2.\lambda(0.2K_T + \beta v_c + v_w z_w + 0.5.\beta\, v_s)}{\xi\left(1-\frac{\xi}{3}\right)R_t}\left(\frac{v_s}{\beta R_t} - 1\right) - \frac{v_s}{\beta R_t}} \qquad [16]$$

where ζ is the size effect parameter for the compression chord = 1.2-0.2a ≥ 0.65 (a: shear span in meter)

$$z_w = \frac{0.85.d - 0.5.x_w .\cot\theta}{\cos^2\theta} \qquad [17]$$

z_w is the lever arm.

The position of the critical fiber could be reasonably considered constant, for reinforced elements, and approximately equal to λ = 0.425. And K_λ was a parameter relating the mean shear stress in the compression chord with stress in the critical fiber. Therefore, it depended on the shape of the distribution of shear stresses in the compression chord and the critical fiber.

5.3.2. Neutral axis in the web ($x > h_f$)

In order to obtain V_c, it must be integrated in two domain**s:** corresponding to the flanges ($x < h_f$, $b = b_v$) and to the compressed part of the web ($x > h_f$, $b = b_w$), and becomes:

$$Vc = \int_0^{h_f} \tau(y).b_v.dy + \int_{h_f}^{x} \tau(y).b_w.dy = \frac{\tau_\lambda .b_{v,eff} . x}{6.\lambda.(1-\lambda)} \qquad [18]$$

Where;

$$b_{v,eff} = b_v\left[\nu^2(3-2\nu) + \frac{b_w}{b_v}(1 - 3\nu^2 + 2\nu^3\right]; \qquad \nu = \frac{h_f}{x} \qquad [19]$$

Eq. (20) can be used, that conservatively fits quite well the actual results, that valid for any value of the neutral axis depth:

$$v_c = \zeta\left[\left(0.70 + 0.18K_T + \left(0.20 + 0.50\,\frac{b}{b_w}\right) v_s\right)\frac{x}{d}\;0.02\,K_T\right]\frac{b_{v,eff}}{b} \qquad [20]$$

The effective width for shear strength calculation, $b_{v,eff}$, was calculated as follows:

i. *If* $x \le h_f$, $b_{v,eff} = b_v = b_w + 2h_f \le b$ [21]

ii. *If* $x > h_f$, $b_{v,eff}$ *use eq. (19)* [22]

Finally, the shear strength of T-beams was given by substituting from (Eq. 23-26) in the equation Eq. (1)

Table 5.2 simplified expressions for rectangular or T beams of dimensionless shear contributing components. Adapted from Ref. [2]

Contributing component	Final simplified dimensionless expressions	
Cracked concrete web	$v_w = 167\frac{f_{ct}}{E_c}\left(1 + \frac{2E_cG_f}{f_{ct}^2 d}\right)\frac{b_w}{b}$	[23]
Longitudinal reinforcement	if $v_s > 0 \rightarrow v_l = 0.23\frac{\alpha_e \cdot \rho}{1 - x/d}$	[24.a]
	if $v_s = 0 \rightarrow v_l = 0$	[24.b]
Transversal reinforcement	$v_s = 0.85K_\theta\rho_w\frac{f_{yw}}{f_{ct}}$	[25]
Compression chord	$v_c = \zeta\left[\left(0.70 + 0.18K_T + \left(0.20 + 0.50\frac{b}{b_w}\right)v_s\right)\frac{x}{d} + 0.02K_T\right]\frac{b_{v,eff}}{b}$	[26]

5.4. Experimental verification

The simple model published in [2] was applied to predict the ultimate shear strength of reinforced concrete T-beams. Table 5.3 shows comparison of the theoretical results according to the model with 19 test results of T-beams. The model underestimated the flange contribution for short and/or thick flange without transverse reinforcement.

The experimental and the theoretical model results were in good agreement for all tests with a mean deviation less than 1.06 and a standard deviation of 0.21.

Table 5.3 Verification of experimental results for rectangular and T specimens.

Specimen	P_u(exp.)	P_u(cal.)	P_u(exp./cal.)
C0	106.35	105.80	1.01
G1-T1-0.3	281.9	261.40	1.08
G1-T2-0.3	362.72	288.38	1.26
G1-T3-0.3	430.58	294.15	1.46
G2-T1-0.3	325.98	271.67	1.20
G2-T2-0.3	377.45	297.55	1.27
G2-T3-0.3	438.56	303.09	1.45
G3-T1-0.3	358.44	385.98	0.93
G3-T2-0.3	384.28	443.95	0.87
G3-T3-0.3	454.10	470.88	0.96
G1-T1-0.5	299.28	311.88	0.96
G1-T2-0.5	391.61	375.37	1.04
G1-T3-0.5	432.33	462.15	0.94
G2-T1-0.5	341.78	305.16	1.12
G2-T2-0.5	383.35	375.37	1.02
G2-T3-0.5	446.46	453.54	0.98
G3-T1-0.5	429.41	438.52	0.98
G3-T2-0.5	436.98	541.40	0.81
G3-T3-0.5	473.82	679.50	0.70
mean			1.06
Standard deviation			0.21

CHAPTER (6)

SHEAR STRENGTH PREDICTION OF RC T-BEAMS BY NONLINEAR FE

CHAPTER (6)

Shear Strength Prediction of RC T-Beams by Nonlinear FE

6.1 Introduction

Flanged reinforced concrete beams have been widely used in many applications in the civil engineering field. The behavior of this kind of structural members was investigated experimentally as well as analytically. Numerical analysis technique based on the finite element method has been used in this research work to investigate the effect of the flange on the reinforced concrete T-beam in the pre- and post-cracking stages of loading and up to ultimate load. The extensive research in the field of numerical modeling of reinforced concrete members and structures has led to the development and formulation of many models which are capable of predicting their behavior under various conditions. These models are put to real use when implemented in a suitable computer code. Then they can be used for both practical and research purposes. Many computer codes exist and are used daily in the construction industry, research activities and engineering education.

6.2 Finite Element Modeling Using ANSYS

6.2.1 Geometric

Finite element modeling and nonlinear analysis are performed by using ANSYS software. The structural element types which helped for geometric idealization of the different materials are SOLID 65 for concrete, LINK 8 for steel bars and stirrups. In order to avoid stress concentration problems such as localized crushing of concrete elements near the bearing and loading

plates, steel plates with 30 mm thickness are modeled by SOLID 45 at the location of supports and loading places in specimen. The structural element types functioned to simulate the different materials which are presented in Fig.6.1. For solving the nonlinear analysis equations of specimen, Newton-Raphson equilibrium iteration technique is used in the ANSYS software. This technique relayed on a series of successive linear approximations with corrections. According to this study, the convergence criterion relies on a displacement control. The infinite norm of displacement and the convergence precision is 0.05 [33,34,35]. Thus, to improve the convergence of nonlinear analysis, adaptive descend gene, linear searching, fore-casting, and dichotomy were applied at the same time. The displacement boundary conditions are necessary to protect the models. To show the cut off support boundary condition of the specimen, the translations at the nodes (UX, UY and UZ) were specified as a constant value of zero, whereas the other support was displayed as roller by indicating the translations at the nodes (UY) equal zero value. The force (P) at two points was placed at the top of specimen in the gravity direction to reveal the experimentally tested. The applicable load was known as incremental loads. There was an adjustment for every increase in the result at certain specific load level. Fig.6.2 shows the occurred load and the supports conditions. The maximum number of iterations in each load step is set as program default.

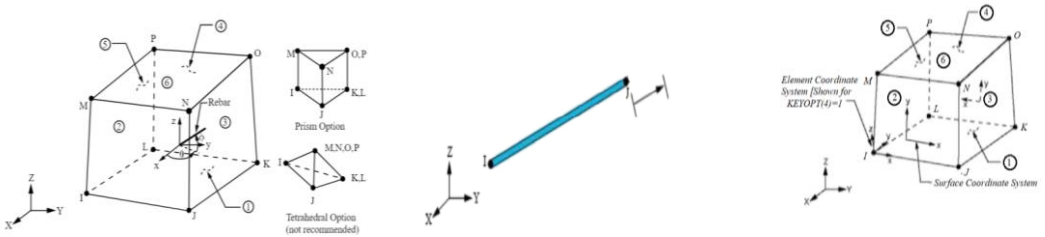

(a) Solid 65 (b) Link 8 (c) Solid 45

Fig. 6.1 Structural elements idealization for the numerical models [34].

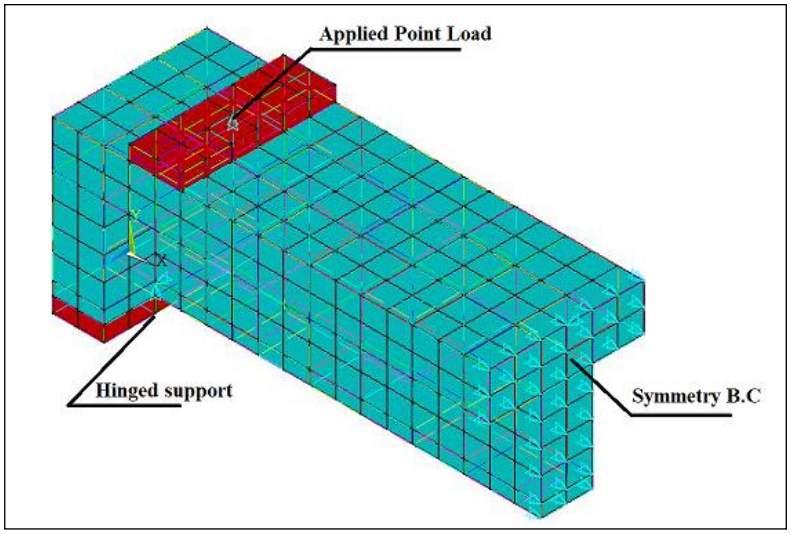

Fig. 6.2 Applied Load and Support Conditions.

6.2.2 Constitutive Relations

Constitutive relationships were desired to connect average stresses to average strains for both the reinforcement as well as the concrete. These relations may deviate much from the usual local stress-local strain relations which are specified by the standard materials tests.

6.2.2.1 Constitutive relation for concrete

To develop a model for the attitude of concrete, it was a difficult activity. Concrete is a quasi-brittle material and has different reaction in compression and tension. The tensile strength of concrete is typically 8-15% of the compressive strength [36](*Shah, et al. 1995*). Fig.6.3 shows a typical stress-strain curve for normal weight concrete [37](*Bangash 1989*).

To cover a descriptive analysis, the stress-strain curve expressed for concrete is linearly elastic up to about 30 percent of the maximum

compressive strength. Above this point, an increase of stress is shown gradually up to the maximum compressive strength. After it reaches the maximum compressive strength f_{cu}, the curve begins to decline into a softening region. finally, crushing failure happens at an ultimate strain ε_{cu} . In tension, the stress-strain curve for concrete is almost linearly elastic up to the maximum tensile strength. After this point, the concrete cracks and the strength rises down gradually to zero [38].

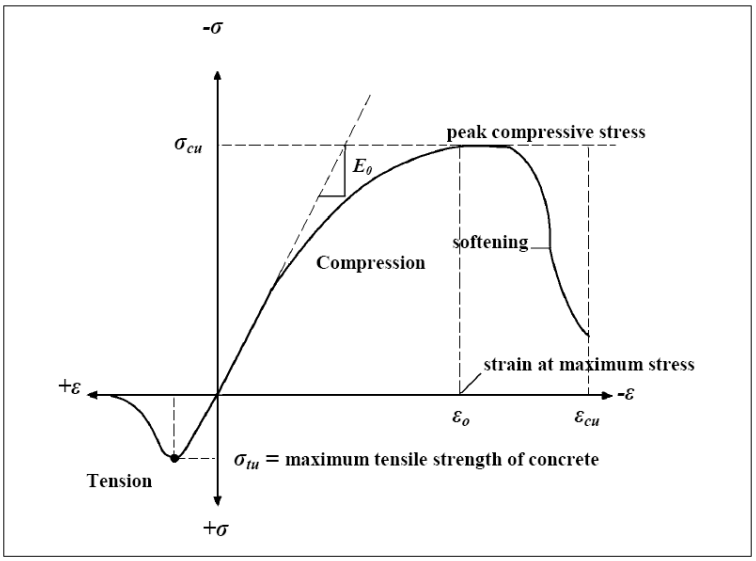

Fig. 6.3 Typical uniaxial compressive and tensile stress-strain curve for concrete (*Bangash 1989*) [37]

For concrete, ANSYS requires input data for material properties as follows:

Elastic modulus (E_c).

Ultimate uniaxial compressive strength (f'_c).

Ultimate uniaxial tensile strength (modulus of rupture, f_r).

Poisson's ratio (v).

Shear transfer coefficient (β_t).

i. Compressive Uniaxial Stress-Strain Relationship for Concrete

The ANSYS program requires the uniaxial stress-strain relationship for concrete in compression. Numerical expressions, Eq. 1 &2, were used along with Eq.3 (*Gere and Timoshenko 1997*) to construct the uniaxial compressive stress-strain curve for concrete [**38**].

$$f = \frac{E_c \varepsilon}{1 + \left(\frac{\varepsilon}{\varepsilon_0}\right)^2} \quad (1)$$

$$\varepsilon_0 = \frac{2 f'_c}{E_c} \quad (2)$$

$$E_c = \frac{f}{\varepsilon} \quad (3)$$

Where:

f = stress at any strain ε, psi

ε = strain at stress f

ε_o= strain at the ultimate compressive strength f_c'

E_c = the initial tangent modulus for concrete in MPa and is defined according to ACI-318 14 [**39**] by the following equations:

$$E_c = 4700\sqrt{f_c'}$$

Fig.6.4 shows the simplified compressive uniaxial stress-strain relationship that was used in this study.

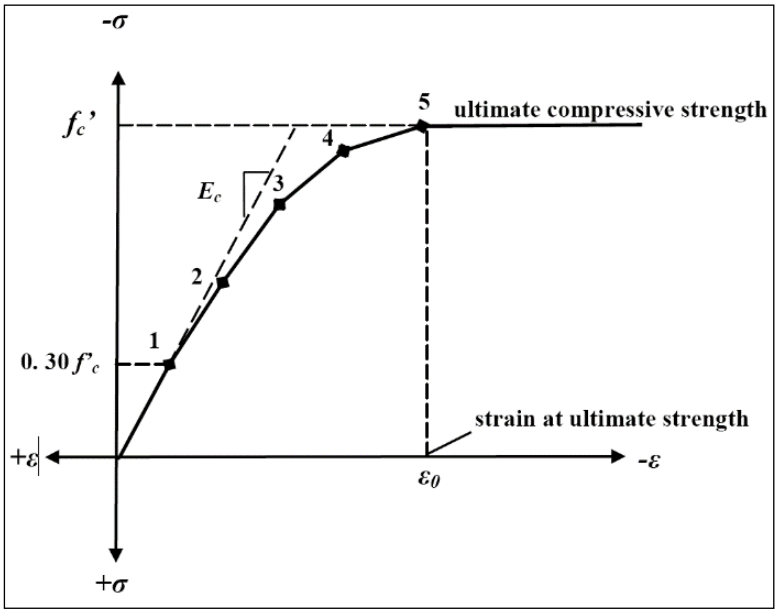

Fig. 6.4 Simplified compressive uniaxial stress-strain curve for concrete

The simplified stress-strain curve for each beam model is constructed from six points connected by straight lines. The curve starts at zero stress and strain. Point No. 1, at $0.30f'_c$, is calculated for the stress-strain relationship of the concrete in the linear range (Eq.3). Point Nos. 2, 3, and 4 are obtained from (Eq.1), in which ε_0 is calculated from (Eq.2). Point No. 5 is at ε_0 and f_c'.

ii. Failure Criteria for Concrete

The model gives an expect failure for concrete materials. The cause for this return to both cracking and crushing failure modes. The two input strength

parameters *i.e.*, ultimate uniaxial tensile and compressive strengths are important to define a failure surface for the concrete. Then, the standard of concrete failure DC which is caused by a multi-axial stress state can be calculated (*William and Warnke 1975*). A three-dimensional failure surface for concrete is described in Fig.6.5. The most considerable nonzero principal stresses found in the x and y directions, are symbolized by σ_{xp} and σ_{yp}, respectively.

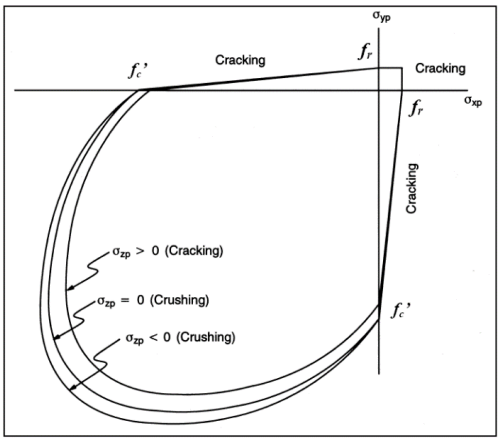

Fig. 6.5 3-D failure surface for concrete (*ANSYS*)

Three failures in the surfaces are exhibited as projections on the σ_{xp}-σ_{yp} plane. The mode of failure is a function of the sign of σ_{zp} (principal stress in the z direction). For example, if σ_{xp} and σ_{yp} are both negative (compressive) and σ_{zp} is slightly positive (tensile), cracking would be revealed in a direction perpendicular to σ_{zp} Although, if σ_{zp} is zero or slightly negative, it is supposed that the material will crush.

6.2.2.2 Constitutive *relation for steel*

The experimental beams originated steel reinforcement with typical Grade 60 steel reinforcing bars. In this FEM discussion, steel reinforcement had certain qualities, i.e., elastic modulus and yield stress, it follows the design material properties shown in the experimental investigation (*Kachlakev and McCurry 2000*) [**40**]. The steel for the finite element models was assumed to be an elastic-typical plastic material and identical in tension and compression. Poisson's ratio of 0.3 was applied for the steel reinforcement in this study (*Gere and Timoshenko 1997*). Fig.6.6 shows the idealized stress-strain relationship mentioned in this research.

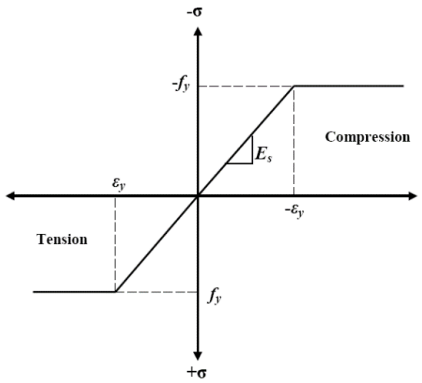

Fig. 6.6 Idealized stress-strain curve for reinforcing steel

Material properties for the steel reinforcement are stated as follows:

Elastic modulus, E_s = 200,000 MPa

Yield stress, f_y = 420 MPa (Lab test)

Poisson's ratio, v = 0.3

6.2.3 Model Validation studies

Validation studies were discussed on several T-beams. Table 6.1 introduces a summary for the geometrical and mechanical properties of the available specimens. FE model offers an alternative tool that is used in the analysis process, and also for getting different results with the previously done experiments, Hesham et al. [14]. The details and set-up of tested specimens are shown in shape. 7& 8 respectively. Also, the finite element simulation models are shown in Fig.6.9.

Fig. 6.7.a Specimen with Rectangular cross section (control)

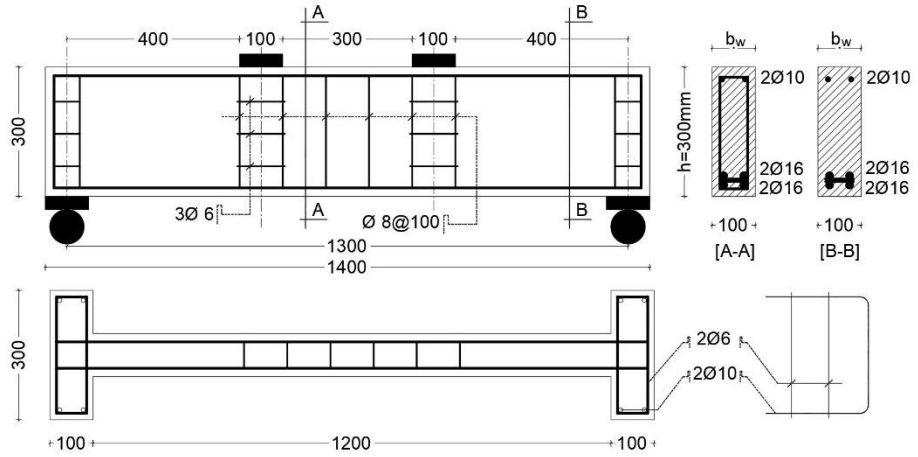

Fig. 6.7 Specimen details and arrangement of reinforcement

(All dimensions in mm)

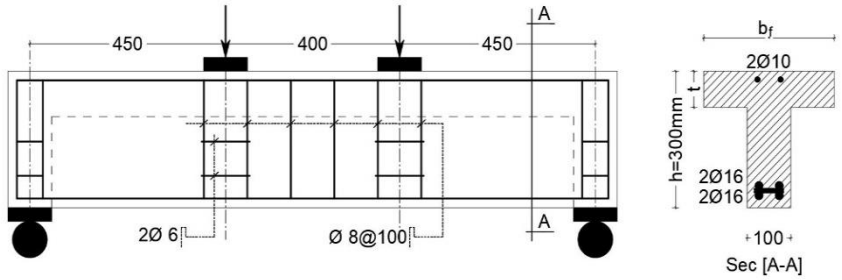

Fig. 6.7 (*cont.*)

Fig. 6.7.b T-cross section without stirrups

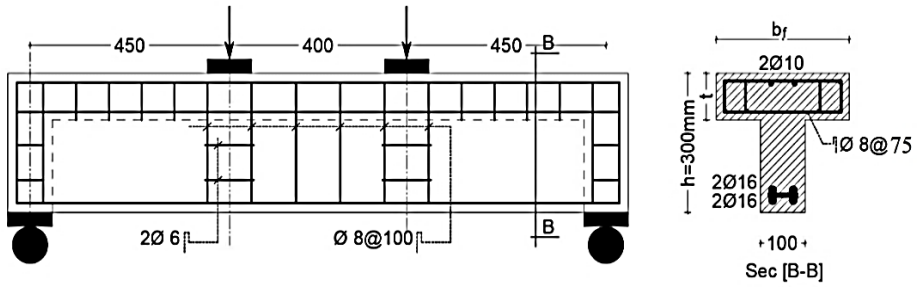

Fig. 6.7.c T- cross section with stirrups

Table 6.1 Experimental Program

Specimen	Cross Sectional Area (cm^2)	Cross Sectional Area Increasing (%)	Flange Dim.			Stirrups in flange within shear zone (mm)	Longitudinal reinforcement in Flange		Longitudinal reinforcement in Flange [%]
			t_f (cm)	b_f (cm)	A_f (cm^2)		Bottom Steel	Top Steel	
C0	300	------		------		------	------		------
G1-0.3-3	480	60%	0.3h=9	30	270	------	------		------
G3-0.5-5	900	200%	0.5h=15	50	750	Ø8@75	6 Ø 10 + 1Ø10/side	2 Ø 8+ 2 Ø 6	1.046%

G = Reinforcement group, "G1" without reinforcement, "G3" with longitudinal and stirrups in shear zone. Total depth 300 mm, web width (bw) 100 mm. 0.3 = Flange thickness, "0.3=0.3h" 90 mm, "0.4=0.4h" 120mm& "0.5=0.5h" 150mm. 3& 5 = Flange width; "3b"= 300 mm& "5b"= 500mm.

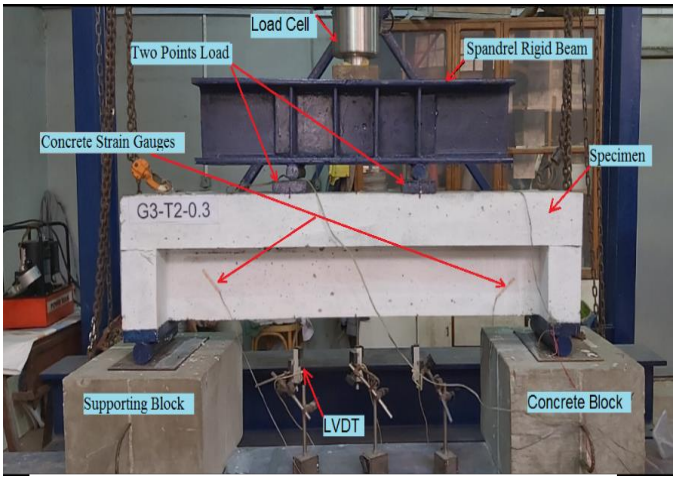

Fig. 6.8 Preparation of Test set-up

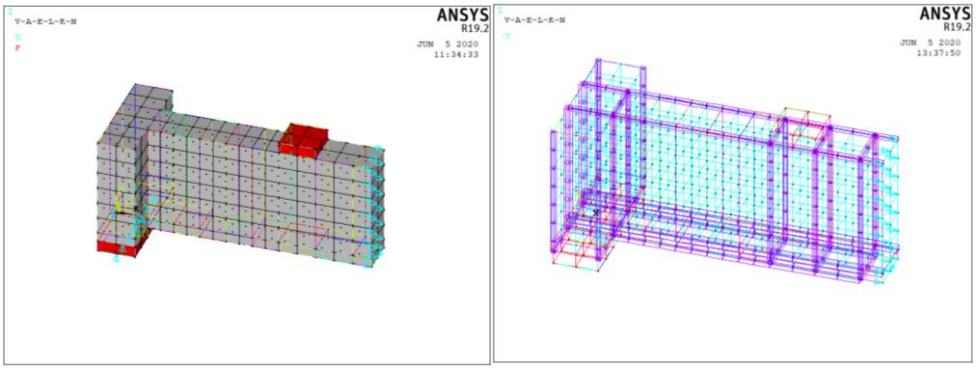

Fig. 6.9.a Finite Element Model for C0 (control)

Fig. 6.9 Finite Element Simulation Models for specimens

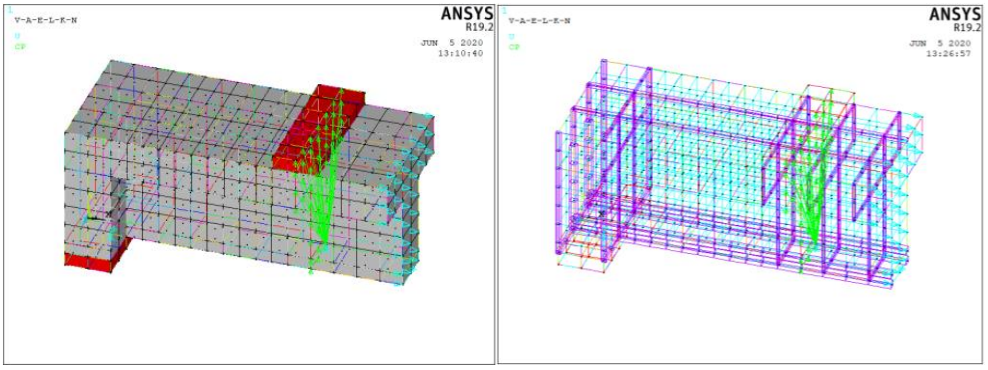

Fig. 6.9.b Finite Element Model for G1-0.3-3

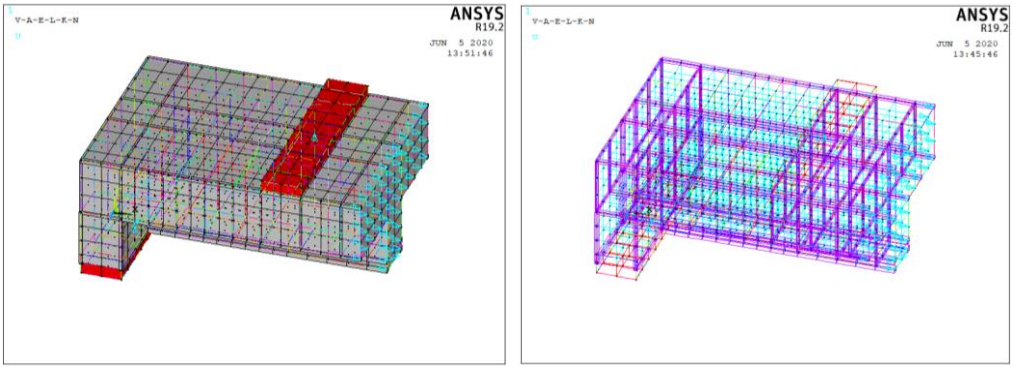

Fig. 6.9 (*cont.*)

Fig. 6.9.c Finite Element Model for G3-0.5-5

6.2.3.1 Load deflection curves

The load-deflection curve achieved outlined results such as the ultimate load capacity (P_u) and the corresponding ultimate deflection (Δ_u). The area under the load-deflection curve which represents the toughness (I) is also calculated. Fig.6.10 introduces the obtained numerical results altogether with the experimental results for definite specimens. The figure is reflecting a good agreement between the experimental results and the desired results at different levels of response, the load-deflection plot from the finite element analysis matches well the experimental data for C0, G1-T1-0.3& G3-T3-0.5. In the linear range, the load-deflection which is derived from the finite element analysis is stiffer than that from the experimental results by about 10.7, 8.8& 16.1% respectively.

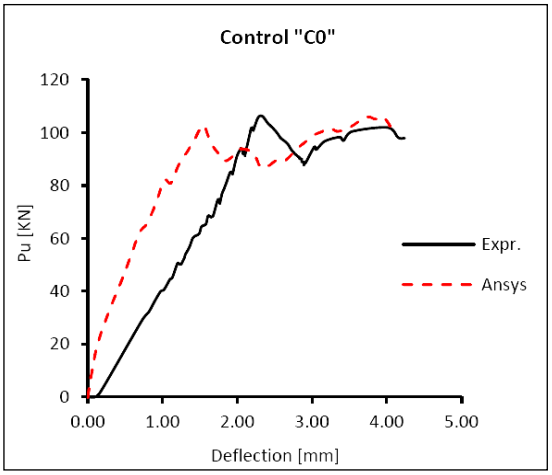

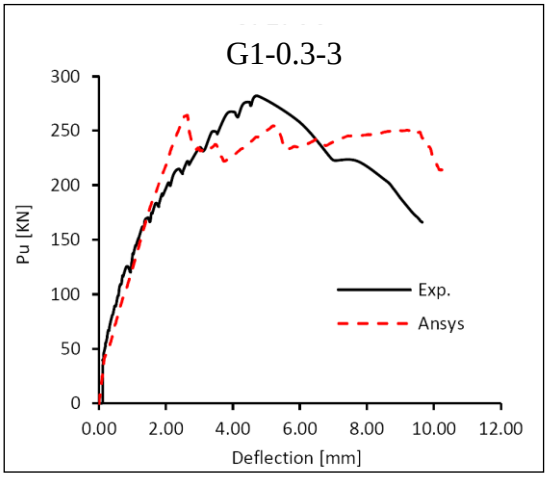

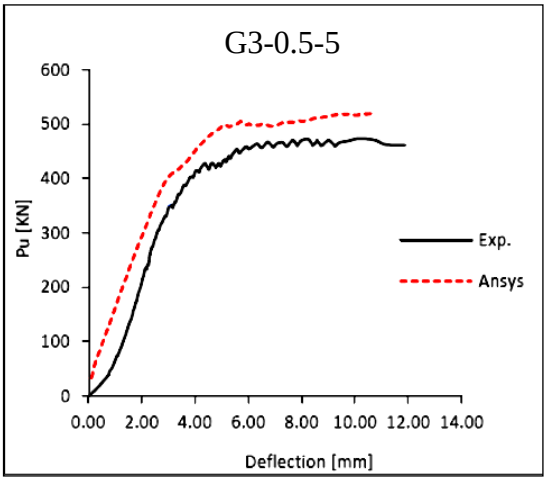

Fig. 6.10 Predicted and Measured Load-Deflections curves

6.2.3.2 Ultimate load comparison

The ultimate load had the test for C0, G1-T1-0.3& G3-T3-0.5 was 106.4, 281.9& 473.8 kN respectively, while on the other hand the ultimate load obtained from ANSYS analysis was 113.4, 264.1& 516.2 kN. So, the difference is about ± 6% and this assures that ANSYS program is an appropriate method to know the behavior of reinforced concrete T-beams.

6.2.3.3 Crack pattern and failure mode

A comparison between the predicted crack patterns against the experimental crack patterns for tested beams is shown in Fig.6.11. As cleared in the shape, there is an outstanding harmonization noticed between the experimental and the numerical crack patterns. For all specimens suggested, the expected failure mode becomes shear mode. The failure mode is distinguished by wide shear diagonal cracks which occurs so close to the support column intersection with loading steel plate at the top. In addition, the figure describes that the spreading of cracks is changing in relation to the flange dimensions.

(a) Experimental crack pattern for C0 (b) Predicted crack pattern for C0

Fig. 6.11 Predicted & observed cracking patterns for specimens

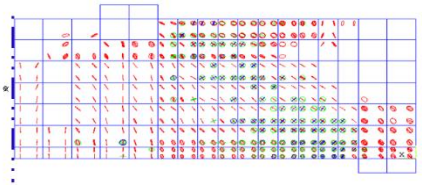

(c) Experimental crack pattern for G1-0.3-3 (d) Predicted crack pattern for G1-0.3-3

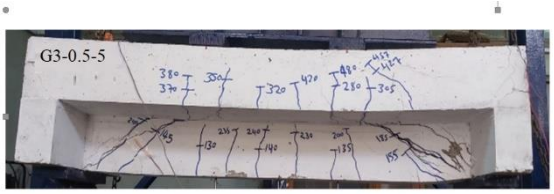

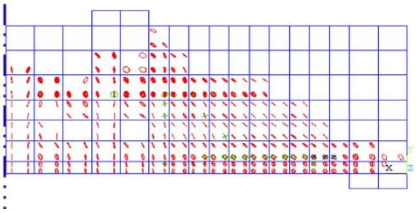

(e) Experimental crack pattern for G3-0.5-5 (f) Predicted crack pattern for G3-0.5-5

Fig. 6.11 (*cont.*)

6.3 Concluding remarks

For all discussed cases, a good agreement was observed when comparing between the experimental and the predicted results by finite element (FE) which involved the load-deflection curves and crack patterns. At the final level, the total average value for [$Pu_{(FE)}$ / $Pu_{(EXP)}$] ratio and [$\Delta u_{(FE)}$ /$\Delta u_{(EXP)}$] ratio for all specimens were 1.03 and 0.87 respectively. Hence, ANSYS computer program which was applied to joint with the offered constitutive models was a good tool for modeling. This program was mainly designed to study the flange effect on the shear strength of flanged reinforced concrete beam with or without longitudinal reinforcement in flange and with different material parameters.

6.4 Parametric study

6.4.1 General

In order to discuss the effect of different parameters on the structural response; groups of reinforced concrete T-beam, which labeled as (S1, S2... S96) are analyzed. As given in Table 6.2, the main parameters studied here include: (1) the concrete strength (*fc'*), (2) width ratio (ρ_b), (3) depth ratio (ρ_t), (4) ratio of longitudinal steel in flange (ρ), and (5) shear span to depth ratio (*a/d*). For each parameter, the predicted response curve is personalized by the load-deflection curve. The control used specimen in this paper is the rectangular beam S plus the geometry given in Table 6.2.

Table 6.2 Parametric Study

Specimen	width ratio (ρ_b)	depth ratio (ρ_t)	*a/d*	$f_{c'}$	*Longitudinal steel in flange* ρ %	*No of Runs*
S	------	------	2.0	30	-----	1
S 01:12	3	0.10, 0.3, 0.5& 0.7	0.5, 1.0, and 2.0	30	0.5	12
S 13:24	5	0.10, 0.3, 0.5& 0.7	0.5, 1.0, and 2.0	30	0.5	12
S 25:48	7	0.10, 0.3, 0.5& 0.7	0.5, 1.0, and 2.0	30 and 60	0.5	24
S 49:84	7	0.10, 0.3, 0.5& 0.7	0.5, 1.0, and 2.0	30	0.0, 1.0, and 2.0	36
S 85:96	9	0.10, 0.3, 0.5& 0.7	0.5, 1.0, and 2.0	30	0.5	12
					Total	97

Width ratio ($\rho_b = b_f/b_w$) is the ratio of flange width "b_f "and web width "b_w", depth ratio ($\rho_t = t/h$) is the ratio of flange thickness "*t*" and total web depth "*h*". Control specimen S is rectangular section, with total depth 300 mm and width 100 mm.

6.4.2 Evaluation criteria of the parametric studies

From the predicted load-deflection curve, the effects of the analyzed parameters have been studied using the following measures:

- Loads at the yield level (P_y) and at the ultimate level (P_u).
- Deflection at the yield level (Δ_y) and at the ultimate level (Δ_u).
- Displacement ductility (μ_Δ) = (Δ_u/Δ_y).
- Toughness (I) = the area under the load-deflection curve.

For the given parameters, the results of a specified specimen (S) are considered as reference values to calculate the following relative measures:

$$Q_{uR}=P_u / P_{ur} \quad (5)$$

$$\alpha_{uR}=\Delta_u / \Delta_{ur} \quad (7)$$

$$I_{uR}=I / I_{ur} \quad (8)$$

Table 6.3 The output results for the analyzed specimens of parametric studies.

Specimen	P_u (kN)	P_y (kN)	P_{cr} (kN)	Δ_u (mm)	Δ_y (mm)	Δ_{cr} (mm)	Q_{uR}	α_{uR}	I	I_{uR}
S	141.61	------	33.47	2.81	------	0.34	1	1	1089	1.0
S1	559.50	356.40	140.44	2.86	3.03	0.36	3.95	1.02	2907	2.7
S2	516.96	437.77	142.56	2.04	2.51	0.33	3.65	0.73	3846	3.5
S3	692.85	430.30	150.87	2.91	3.18	0.38	4.89	1.04	3673	3.4
S4	714.67	N.Y*	178.62	2.43	N.Y*	0.38	5.05	0.86	4364	4.0
S5	300.22	210.57	72.36	2.53	2.82	0.38	2.12	0.90	1717	1.6
S6	328.58	271.78	72.66	2.67	3.53	0.33	2.32	0.95	2715	2.5
S7	440.19	427.09	73.28	3.92	4.21	0.34	3.11	1.40	3104	2.9
S8	500.99	N.Y	86.67	3.65	N.Y	0.33	3.54	1.30	3119	2.9
S9	156.09	100.52	38.30	2.69	7.35	0.32	1.10	0.96	1022	0.9
S10	198.57	147.53	35.73	3.57	5.05	0.27	1.40	1.27	1446	1.3
S11	270.99	195.03	37.47	4.50	5.37	0.27	1.91	1.60	1674	1.5

Table 6.3 (*cont.*)

S12	354.17	N.Y	45.78	5.13	N.Y	0.29	2.50	1.83	2127	2.0
S13	572.64	560.06	148.62	2.54	2.56	0.38	4.04	0.90	3088	2.8
S14	623.87	621.41	157.71	2.93	2.90	0.37	4.41	1.04	4861	4.5
S15	769.96	756.27	168.70	2.75	3.50	0.40	5.44	0.98	6633	6.1
S16	882.42	N.Y	218.41	2.86	N.Y	0.34	6.23	1.02	6909	6.3
S17	284.25	193.88	71.34	2.35	4.11	0.33	2.01	0.84	1883	1.7
S18	361.60	282.53	73.14	2.70	3.72	0.32	2.55	0.96	2871	2.6
S19	520.52	492.87	80.92	4.67	5.07	0.33	3.68	1.66	4373	4.0
S20	651.44	N.Y	110.52	4.23	N.Y	0.33	4.60	1.51	4493	4.1
S21	155.06	98.58	34.58	4.24	6.02	0.23	1.09	1.51	1087	1.0
S22	205.31	172.54	38.04	3.23	6.78	0.30	1.45	1.15	1540	1.4
S23	291.47	253.38	43.59	4.14	5.38	0.23	2.06	1.47	2194	2.0
S24	437.37	422.75	59.74	5.62	5.01	0.29	3.09	2.00	3605	3.3
S25	539.03	450.27	147.13	2.50	1.55	0.36	3.81	0.89	4428	4.1
S26	601.13	555.55	155.19	2.03	2.28	0.36	4.24	0.72	5587	5.1
S27	813.05	598.64	186.74	2.41	4.57	0.37	5.74	0.86	6426	5.9
S28	955.33	N.Y	266.28	2.51	N.Y	0.35	6.75	0.89	6911	6.3
S29	291.17	206.89	75.67	2.16	3.73	0.32	2.06	0.77	2055	1.9
S30	370.20	340.28	76.91	2.53	4.11	0.31	2.61	0.90	3413	3.1
S31	583.19	432.66	89.37	3.64	4.33	0.31	4.12	1.29	4434	4.1
S32	683.84	N.Y	140.99	3.85	N.Y	0.33	4.97	1.37	5042	4.6
S33	155.33	142.38	40.71	2.58	5.27	0.28	1.10	0.92	1172	1.1
S34	216.92	162.65	43.43	3.07	6.90	0.23	1.53	1.09	1683	1.5
S35	345.30	N.Y	48.58	4.41	N.Y	0.26	2.44	1.57	2678	2.5
S36	468.64	N.Y	73.43	4.76	N.Y	0.28	3.31	1.69	3403	3.1
S37	966.03	780.48	184.95	3.21	3.44	0.29	6.82	1.14	8841	8.1

Table 6.3 (*cont.*)

S38	1160.45	1091.52	190.97	4.03	3.66	0.30	8.19	1.43	10419	9.6
S39	1616.71	1488.36	225.87	11.42	5.14	0.33	11.42	4.06	16049	14.7
S40	1575.32	1409.87	337.32	4.47	8.56	0.33	11.12	1.59	12934	11.9
S41	537.98	457.99	88.35	3.81	5.05	0.33	3.80	1.35	4829	4.4
S42	729.11	674.25	94.84	15.30	7.70	0.31	5.15	5.44	9242	8.5
S43	899.35	830.58	113.21	17.34	6.49	0.31	6.35	6.17	13217	12.1
S44	1089.80	1010.36	178.46	12.49	5.27	0.33	7.70	4.44	14311	13.1
S45	291.42	258.80	43.89	5.41	7.07	0.27	2.06	1.93	2239	2.1
S46	387.44	362.88	46.12	11.57	6.76	0.26	2.74	4.12	3544	3.3
S47	471.56	420.76	57.63	11.46	5.11	0.26	3.33	4.08	4526	4.2
S48	594.53	515.21	93.98	12.00	4.23	0.28	4.20	4.27	5637	5.2
S49	552.96	N.Y	141.13	2.34	N.Y	0.33	3.90	0.83	4069	3.7
S50	618.56		155.58	2.23		0.29	4.37	0.80	5694	5.2
S51	772.52		157.25	2.73		0.25	5.46	0.97	5932	5.4
S52	831.80		184.54	2.95		0.24	5.87	1.05	7118	6.5
S53	305.85		102.28	2.40		0.60	2.16	0.85	2832	2.6
S54	340.13		76.79	2.35		0.31	2.40	0.84	1628	1.5
S55	456.24		87.24	3.21		0.30	3.22	1.14	3252	3.0
S56	648.25		135.01	5.25		0.35	4.58	1.87	5316	4.9
S57	161.20		37.59	2.66		0.27	1.14	0.95	1086	1.0
S58	229.81		39.64	3.93		0.27	1.62	1.40	1591	1.5
S59	310.08		46.74	5.56		0.27	2.19	1.98	2277	2.1
S60	336.09		65.19	6.74		0.26	2.37	2.40	3019	2.8
S61	545.20	435.37	146.33	2.21	9.09	0.36	3.85	0.79	4563	4.2
S62	673.43	N.Y	159.83	2.25	N.Y	0.39	4.76	0.80	5696	5.2
S63	839.89		188.97	2.51		0.33	5.93	0.89	6190	5.7
S64	972.73		254.32	2.45		0.31	6.94	0.87	8186	7.5
S65	319.21	216.90	78.21	2.47	9.33	0.37	2.25	0.88	2430	2.2
S66	418.11	N.Y	83.40	3.02	N.Y	0.37	2.95	1.07	3392	3.1
S67	610.65		91.59	4.44		0.30	4.31	1.58	5294	4.9
S68	703.74		151.69	3.51		0.34	4.83	1.25	5627	5.2
S69	155.78		40.91	2.50		0.28	1.10	0.89	1139	1.0
S70	246.86		38.21	3.84		0.25	1.74	1.37	2008	1.8
S71	433.35		49.18	6.42		0.26	3.06	2.28	3222	3.0

Table 6.3 (*cont.*)

S72	460.77		82.91	4.61		0.30	3.25	1.64	3440	3.2
S73	564.70		147.63	2.55		0.36	3.99	0.91	4697	4.3
S74	744.36		153.98	2.94		0.31	5.26	1.05	5158	4.7
S75	853.55		196.26	2.37		0.32	6.03	0.84	6025	5.5
S76	982.97		295.72	4.54		0.35	6.87	1.62	8148	7.5
S77	325.30		72.43	2.63		0.32	2.30	0.94	2289	2.1
S78	396.49		77.21	2.70		0.31	2.80	0.96	3879	3.6
S79	574.60		99.76	3.09		0.32	4.06	1.10	4708	4.3
S80	690.89		160.98	3.47		0.34	4.88	1.24	5451	5.0
S81	169.86		38.23	3.02		0.27	1.20	1.07	1317	1.2
S82	260.72		39.36	4.61		0.27	1.84	1.64	2169	2.0
S83	401.81		51.43	4.20		0.26	2.84	1.50	2647	2.4
S84	473.23		87.67	4.94		0.29	3.34	1.76	3589	3.3
S85	552.58		143.38	2.30		0.32	3.90	0.82	3252	3.0
S86	657.33		159.68	6.30		0.29	4.64	2.24	5226	4.8
S87	855.04		211.25	5.43		0.36	6.04	1.93	4052	3.7
S88	1091.01		262.26	3.22		0.29	7.70	1.15	4738	4.4
S89	307.32	192.59	76.99	2.40	4.66	0.32	2.17	0.85	2017	1.9
S90	406.85	381.67	84.37	2.75	4.01	0.31	2.87	0.98	3574	3.3
S91	613.52	462.25	102.29	3.70	4.40	0.32	4.33	1.32	4266	3.9
S92	690.99	N.Y	164.68	3.37	N.Y	0.33	4.88	1.20	6088	5.6
S93	159.26	129.55	37.48	2.73	7.28	0.27	1.12	0.97	1203	1.1
S94	247.99	192.69	41.81	3.78	6.50	0.27	1.75	1.34	1920	1.8
S95	389.48	302.82	53.68	5.79	8.00	0.26	2.75	2.06	2914	2.7
S96	512.85	N.Y	85.62	5.08	N.Y	0.28	3.62	1.81	2074	1.9

: The longitudinal steel in flange **Not **Y**ield*

Where:

P_u : Ultimate load (kN).

P_y : Load at yielding of longitudinal steel reinforcement in flange (kN).

P_{cr} : Cracked load (kN).

Δ_u : The deflection at the ultimate (mm).

Δ_y : The deflection at the yielding (mm).

Δ_{cr} : The deflection at the first crack (mm).

I : The toughness (the area under the load-deflection curve).

Where:

Q_{uR} : Shear capacity ratio at the ultimate load level.

P_{ur} : Shear capacity at the ultimate load level for the control specimen (S).

α_{uR} : Deflection ratio at the ultimate load level.

Δ_{ur} : Deflection at the ultimate level for the control specimen.

I_{uR} : Toughness ratio.

I_{ur} : Toughness of the control specimen.

6.4.2.1 Effect of flange dimensions: width ratio ($\rho_b=b_f / b_w$) and depth ratio ($\rho_t = t/h$)

Fig. 12 presents the variation of beam ultimate shear strength, P_u, with the flange width ratio (ρ_b) for T-beams with variable flange thickness ratio (ρ_t). In addition, Fig. 13 presents the variation of beam ultimate shear strength, P_u, with the flange thickness ratio (ρ_t) for T-beams with variable flange width ratio (ρ_b). The data in Figs. 12 and 13 corresponds to beams with ρ= 0.5, fc'= 30, and a/h= 2. Compared to control beam S (with P_u= 141.61 kN), presence of flange with a width of triple times web width (ρ_b= 3) and with thickness of 0.1, 0.3, 0.5, and 0.7 of beam depth; increased beam shear strength P_u by 10%, 40%, 90%, and 150%; respectively. Besides, for flange width of nine times web width (ρ_b= 9), the corresponding increases in beam shear strength become 12%, 75%, 175%, and 260%; respectively. Both flange width and thickness affect the shear strength of T-beams while the effect of flange thickness is more pronounced. For thin flanges (ρ_t= *0.10*), increasing flange width does not help.

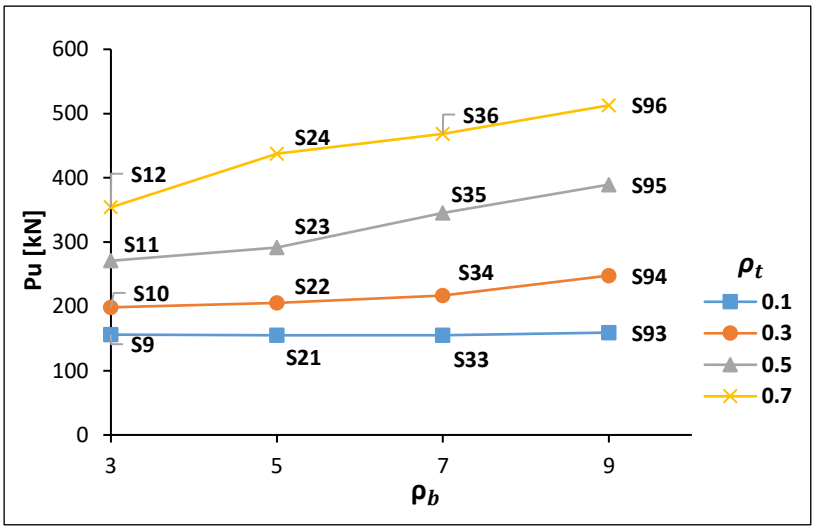

Fig. 6.12 Variation of ultimate load P_u with flange width ratio (ρ_b) at different flange thickness ratios (ρ_t) for ρ= *0.5, fc'= 30* MPa & a/h= 2.

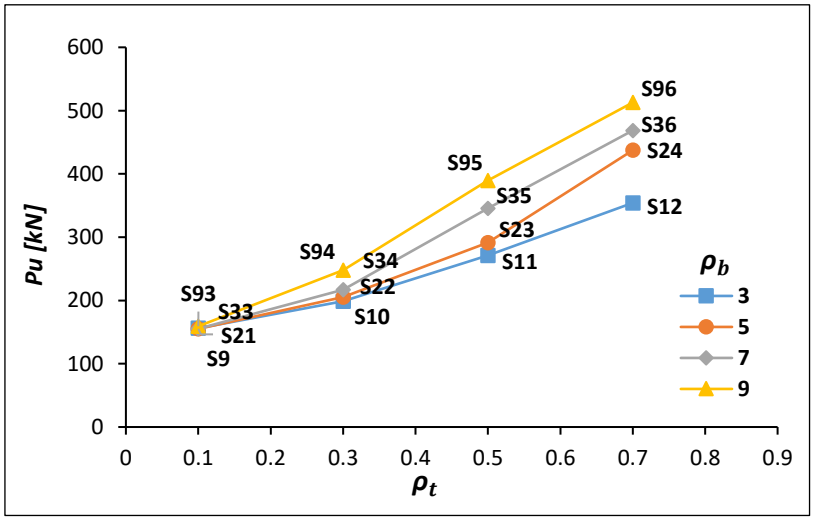

Fig. 6.13 Variation of ultimate load P_u with flange thickness ratio (ρ_t) at different flange width ratios (ρ_b) for ρ= *0.5, fc'= 30* MPa & a/h= 2.

6.4.2.2 Effect of longitudinal steel in flange

The ultimate load predicted for T-beams with variable flange longitudinal reinforcement percentile ratios (0, 0.5, 1.0, and 2) is shown in Fig.14 for three cases of shear span to depth ratio (*a/h*= 0.5, 1.0, and 2.0). This figure shows that increasing flange longitudinal reinforcement, ρ, from 0% to 2% increases the beam ultimate load by an average of 8%, 29%, and 27% for *a/h*= 0.5, 1.0, and 2; respectively.

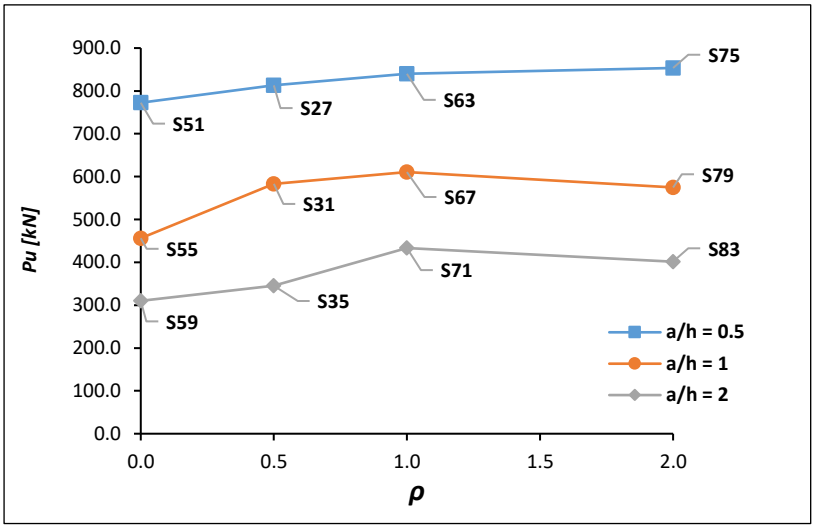

Fig. 6.14 Effect of flange longitudinal reinforcement on Ultimate load for different shear span to depth ratios for ρ_b =7, ρ_t =0.5 & *fc'* =30 MPa.

6.4.2.3 Effect of shear span to depth ratio

Results for T-beams with different shear span to depth ratios (*a/h*= 0.5, 1, and 2) are shown in Figs. 14 and 15 for ρ_t *=0.3* and ρ *=0.5*. Fig.15 presents variations of the ultimate shear strength with the shear span-to-depth ratio for ρ_b *=7* and two values of concrete characteristic strength (f_c*'= 30* MPa *and 60* MPa), ρ_t *=0.3,* ρ *=0.5)* and ρ_b *=7*. For *fc' =30* MPa, Fig. 16 depicts variations of the ultimate shear strength with the shear span-to-depth ratio at various flange widths (ρ_b *=3, 5, 7, & 9)*. The increase in (*a/h*) obviously reduced the shear capacity of flanged beams. Decreasing the shear span to depth ratio from 2.0 to 1.0, and then to 0.5 increased the ultimate shear strength by an average of 49% and 120%, respectively. This trend is repeated for all flange widths and concrete strengths. The load deflection curves for three T-beams that are identical but have different shear span to depth ratios (*a/h= 0.5, 1.0, and 2.0*) are presented in Fig.17. The curve indicates that the beam toughness (I) is reduced as the shear span increases. Numerical values revealed that the toughness of beams having *a/h* of 1.0 and 2.0 were less than that of the similar beam with *a/h* of 0.5 by about 28% and 49%, respectively.

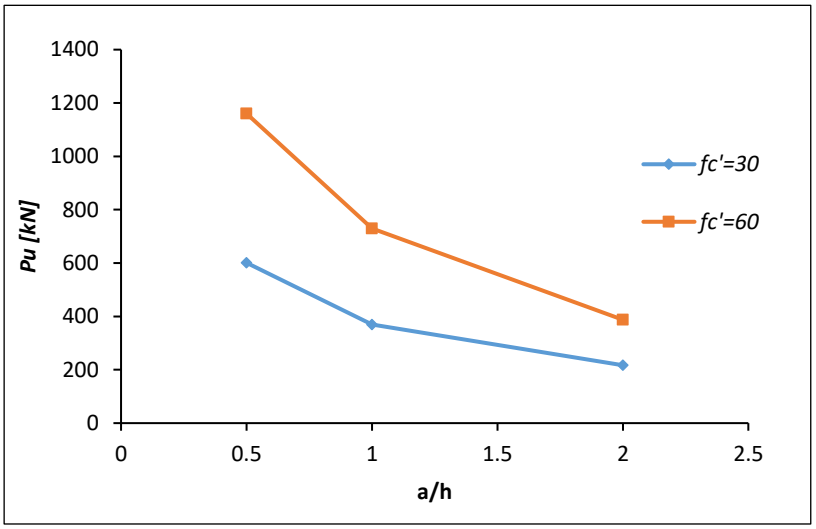

Fig. 6.15 Effect of shear span-to-depth ratio on ultimate shear strength of T-beams for two values of concrete characteristic strength *(ρ_b =7, ρ_t =0.3, ρ =0.5).*

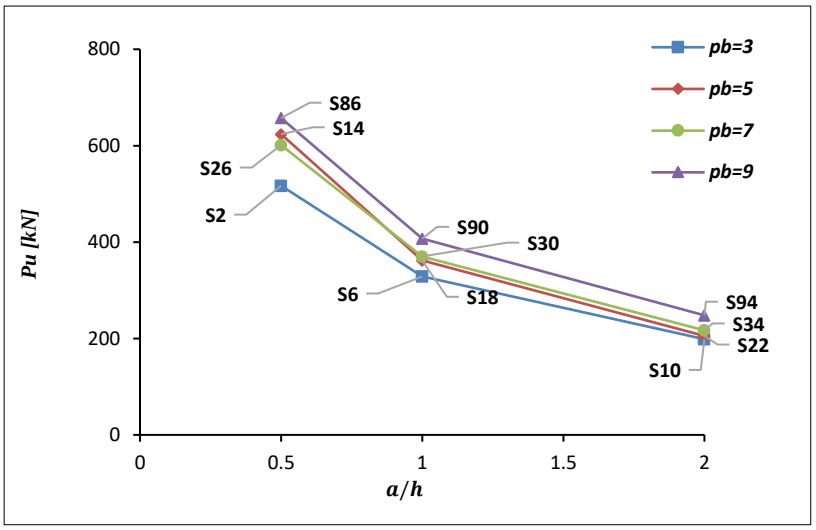

Fig. 6.16 Effect of shear span-to-depth ratio on ultimate shear strength of beams with various flange widths (*ρ_t =0.3, ρ =0.5& fc' =30* MPa*).*

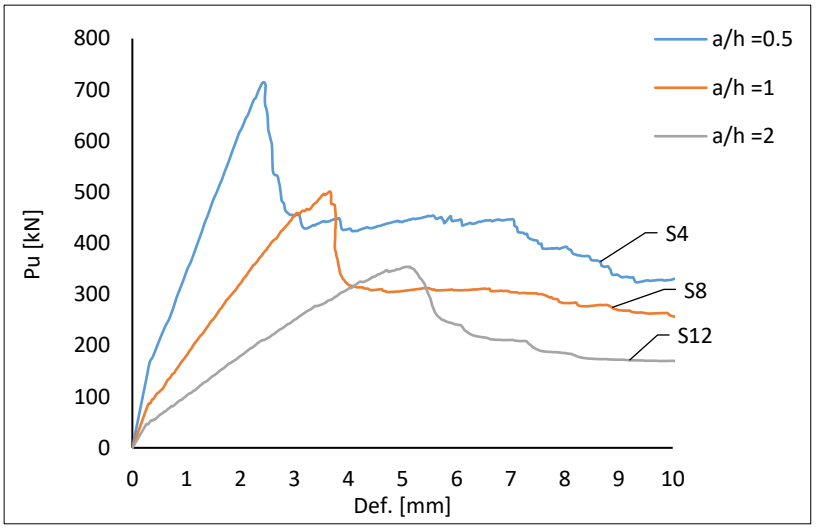

Fig. 6.17 Effect of shear span-to-depth ratio on load-deflection curves of flanged beams (ρ_b=3, ρ_t=0.7, *fc'*=30 MPa & ρ=0.5.)

6.4.2.4 Effect of concrete characteristic strength.

Values of the ultimate shear strengths calculated for 24 T-beams are displayed in Fig. 18. These values correspond to T-beams with one flange width ρ_b=7; four values of flange thickness ρ_t=0.1, 0.3, 0.5 & 0.7; and two values of concrete characteristic strengths (*fc'*= 30 and 60MPa). Study of data in Fig.18 and Table 3 showed that- on average- doubling concrete strength of beams results in doubling the first-yield load and increases the first-crack load by about 20%. The increase in beam ultimate shear capacity varies with both shear span and flange thickness. Numerically, doubling *fc'* lead to shear capacity increases of 65%:99% for *a/h* =0.5; 54%:97% for *a/h*=1; and 27%:88% for *a/h*=2. It is also noted that the increase in shear

capacity with increasing concrete strength becomes less pronounced as the span length or the flange thickness increases.

To examine the effect of concrete characteristic strength on beam toughness, the load-deflection relationship for beams with *fc'*= 30 and 60MPa are presented in Fig. 18 for three flange thickness ratios ρ_t= 0.1, 0.3 &0.7 (other variables are ρ_b=7, *a/h*= 0.5). Considerable increase with an average of 74% in beam toughness, *I*, is observed with the increase in *fc'* from 30 to 60 MPa. Finally, Fig.19 shows that the flexural crack pattern at failure is similar for beams with concrete strength of 30 to 60 MPa, while the use of higher concrete strength delayed the premature shear failure.

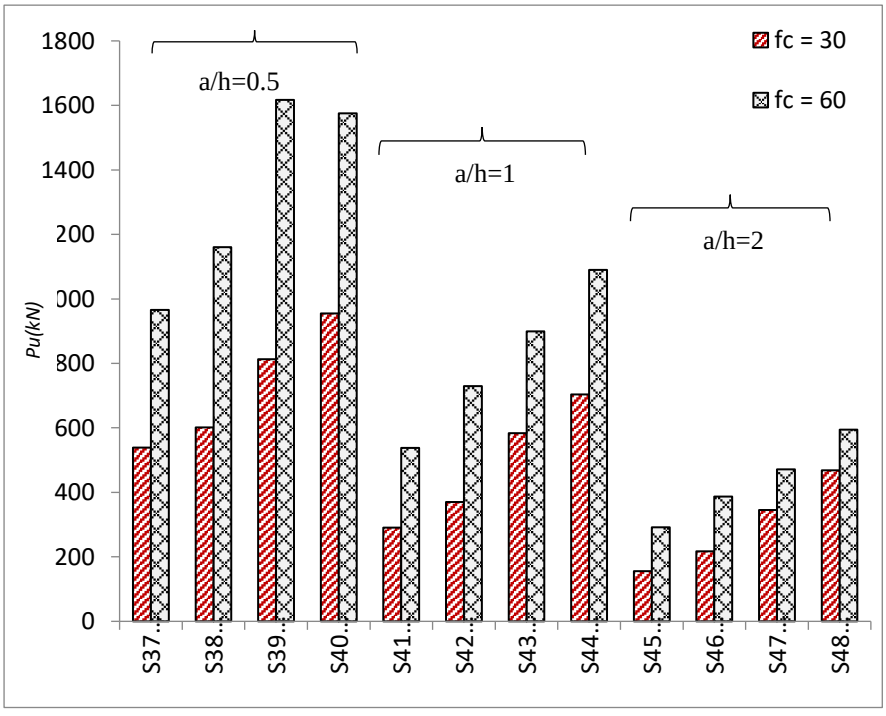

Fig. 18 Effect of concrete characteristic strength on shear capacity for beams with variable shear span to depth ratios (ρ_b=7, ρ_t= 0.1, 0.3, 0.5& 0.7).

$\rho_t = 0.1$

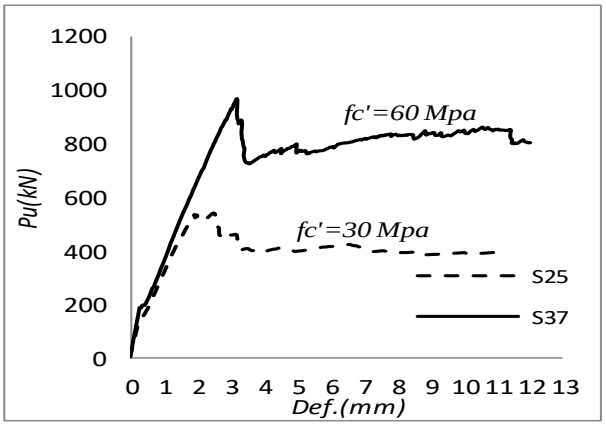

$\rho_t = 0.3$

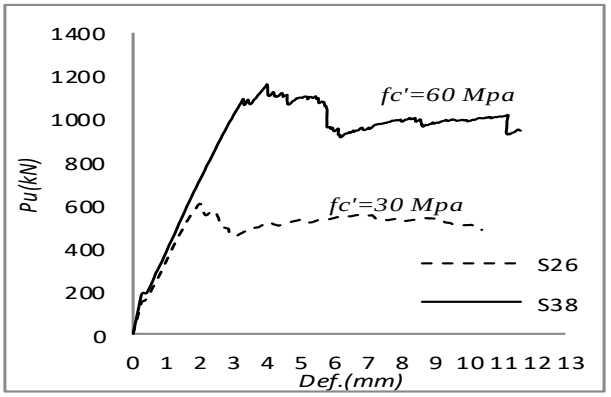

$\rho_t = 0.7$

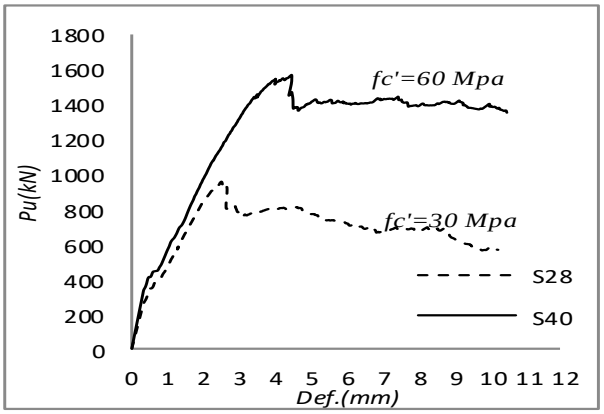

Fig. 6.19 Effect of concrete characteristic strength on Deflection

S38	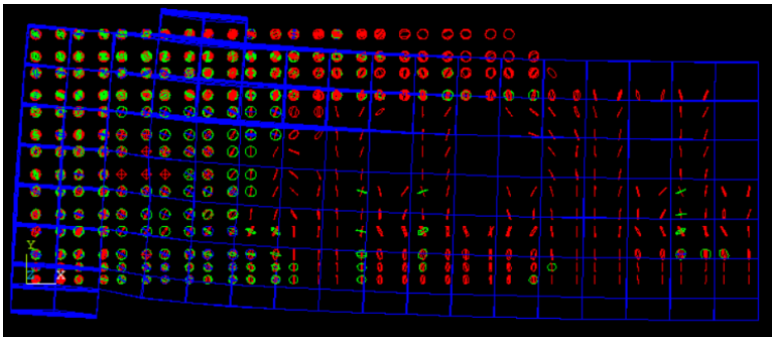
S46	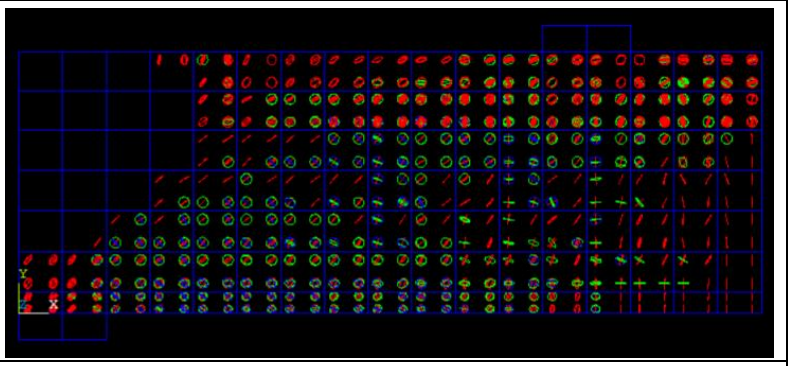
S3	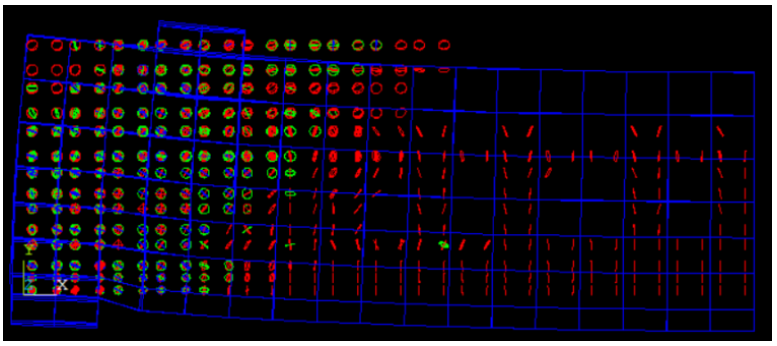

Fig. 6.20 Crack patterns

S6	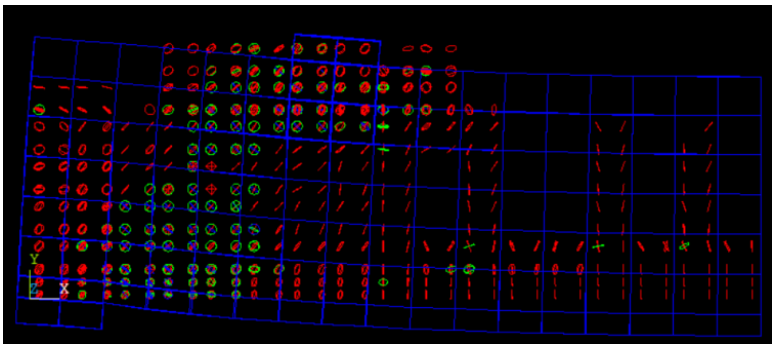

S8	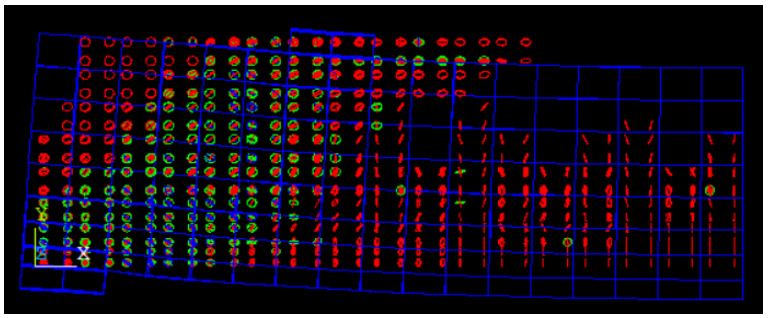
S9	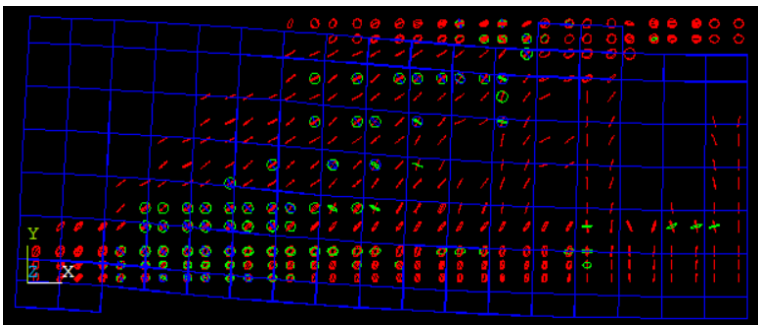
S29	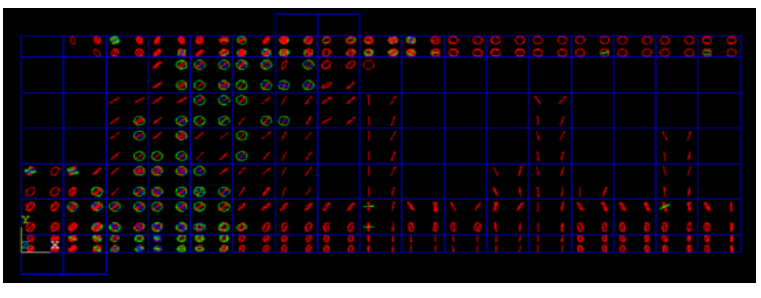

Fig. 6.20 (*cont.*)

S94	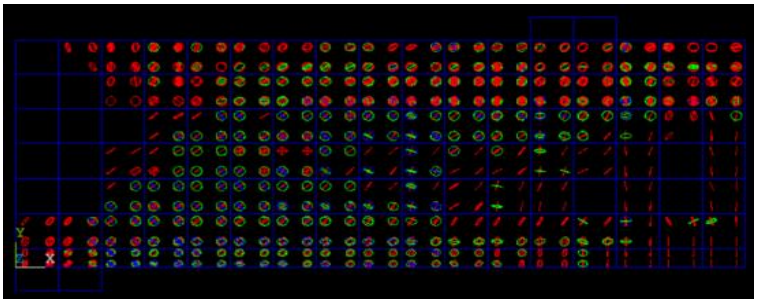

Fig. 6.20 (*cont.*)

6.5 Proposed simplified calculations.

In international codes, such as the ACI Building Code Equation (1), and the Euro code, the shear force in a T-beam is assumed to be carried only by its web. This simplified assumption, which has prevailed in the shear design practice, is not correct for T-beams with a thick flange in the compression side. Experimental measurements as well as results of the finite element made it clear that the enhancement of shear strength due to beam flanges (when subject to compressive stresses) cannot be neglected. Analysis of all results showed that, limited to the range of parameters considered, we can conservatively assume that the total area of the flange is effective in resisting shear. Then, the shear strength of T-beams with the flange in the compression side is calculated using Figure 6.21 and Equations (1 and 2) as follows:

a) Width ratio

($\rho_b = b_f/b_w$) ≤ 5

b) Depth ratio

($\rho_t = t_f/h$) up to 1

c) $L' \leq 2b_w$

where L' is the left and right part of flange.

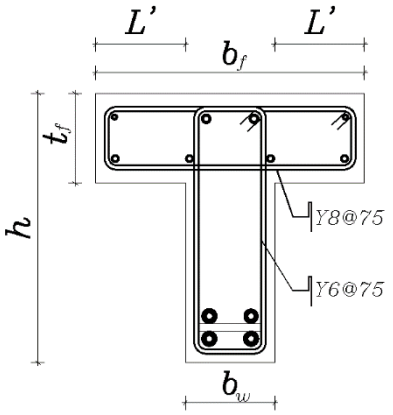

Fig. 6.21 Cross-section

ACI 318M [21]**- Simplified method**

$$V_c = \left[0.17\lambda \sqrt{f_c'}\right] b_w d + \frac{A_v f_y d}{S} \qquad [1]$$

Where λ is the modification factor to reflect the reduced mechanical properties of lightweight concrete relative to normal weight concrete of the same compressive strength, for normal weight concrete = 1

Proposed equation for shear strength of flanged beam ($V_{p,\ proposed}$)

$$V_{p,\ proposed} = V_c + V_{s\text{-}w} + V_{s\text{-}f}$$

$$V_{p,\ proposed} = \left[0.17\lambda \sqrt{f_c'}\ \right][b_w d + 2L' t_f\ ] + \left[\frac{A_v f_y d}{s}\right]_w + \left[\frac{A_v f_y d}{s}\right]_f \qquad [2]$$

V_c: nominal shear strength provided by concrete

$V_{s\text{-}w}$: nominal shear strength provided by web shear reinforcement

$V_{s\text{-}f}$: nominal shear strength provided by flange shear reinforcement

A three-dimensional finite element "F.E" program 'ANSYS' was used for the numerical analysis of all specimens without reinforcement in flange "G1", and additional specimens with different depth ratio "ρ_t" to verify the proposed method (Equation 2). Table 6.4 shows good "conservative" agreement between the results of the proposed equation, which assumes that the total area of the cross section is effective- and experimental as well as finite element results. This is true for T-beams when the flange is subjected to compressive stresses, and the limits given above. The limits are width ratio: ($\rho_b = b_f / b_w$) ≤ 5; depth ratio: ($\rho_t = t_f / h$) of up to 1; and flange protrusion length $L' \leq 2b_w$ on each side.

Table 6.4 Verification of proposed equation with F.E results& ACI

Specimen	f_c Mpa	f_{yt} Mpa	Dimensions [mm]					A_v (mm^2)		Exper.	F.E. method	ACI	Proposed method (kN)				V_P/V_{ACI}	$V_P/V_{F.E.}$
			b_w	d_w	L'	t_f	d_f	$A_{v.w}$	$A_{v.f}$	$V_{Exper.}$ (kN)	$V_{F.E}$ (kN)	V_{ACI} (kN)	V_c	V_{s-w}	V_{s-f}	V_P		
C0	28.8	240	100	280	0	0	0	0	0	53	56.7	25.54	25.54	0.00	0.00	25.54	1.00	0.45
G1-0.15-3					100	45	25	0.00	0.00	------	76.5	25.54	33.76			33.76	1.32	0.44
G1-0.30-3						90	70			141	142.4		41.97			41.97	1.64	0.29
G1-0.40-3						120	100			181.5	181.0		47.44			47.44	1.86	0.26
G1-0.50-3						150	130			215.5	217.5		52.91			52.91	2.07	0.24
G1-0.65-3						195	175			------	220.1		61.13			61.13	2.39	0.28
G1-0.80-3						240	220			------	250.8		69.34			69.34	2.71	0.28
G1-0.90-3						270	250			------	247.3		74.81			74.81	2.93	0.30
G1-1-3						300	280			------	256.0	76.63	76.63			76.63	1.00	0.30
G1-0.15-5					200	45	25	0.00	0.00	------	96.4	25.54	41.97			41.97	1.64	0.44
G1-0.30-5						90	70			149.5	150.9		58.39			58.39	2.29	0.39
G1-0.40-5						120	100			196.0	200.6		69.34			69.34	2.71	0.35
G1-0.50-5						150	130			216.0	226.0		80.28			80.28	3.14	0.36
G1-0.65-5						195	175			------	245.5		96.71			96.71	3.79	0.39
G1-0.80-5						240	220			------	274.0		113.13			113.13	4.43	0.41
G1-0.90-5						270	250			------	301.4		124.07			124.07	4.86	0.41
G1-1-5						300	280			------	307.2	127.72	127.72			127.72	1.00	0.42
C0-S	28.8	240	100	280	0	0	0	56.6	0	------	116.50	76.26	25.54	50.71	0.00	76.26	1.00	0.65
G3-0.15-3				235	100	45	25	56.6	201.2	------	184.28	76.26	33.76	42.56	16.10	92.41	1.21	0.50
G3-0.30-3				190		90	70			179	237.50		41.97	34.41	45.07	121.45	1.59	0.51
G3-0.40-3				160		120	100			192	256.30		47.44	28.98	64.38	140.80	1.85	0.55
G3-0.50-3				130		150	130			227	270.20		52.91	23.55	83.70	160.16	2.10	0.59
G3-0.65-3				85		195	175			------	311.12		61.13	15.40	112.67	189.19	2.48	0.61
G3-0.80-3				40		240	220			------	319.25		69.34	7.24	141.64	218.23	2.86	0.68
G3-0.90-3				10		270	250			------	317.78		74.81	1.81	160.96	237.58	3.12	0.75
G3-1-3				0		300	280			------	350.56	256.91	76.63	0.00	180.28	256.91	1.00	0.73
G3-0.15-5				235	200	45	25	56.6	301.8	------	205.95	76.26	41.97	42.56	24.14	108.67	1.43	0.53
G3-0.30-5				190		90	70			214.5	264.80		58.39	34.41	67.60	160.40	2.10	0.61
G3-0.40-5				160		120	100			218.5	267.80		69.34	28.98	96.58	194.89	2.56	0.73
G3-0.50-5				130		150	130			237.0	271.20		80.28	23.55	125.55	229.38	3.01	0.85
G3-0.65-5				85		195	175			------	356.74		96.71	15.40	169.01	281.11	3.69	0.79
G3-0.80-5				40		240	220			------	369.52		113.13	7.24	212.47	332.84	4.36	0.90
G3-0.90-5				10		270	250			------	392.70		124.07	1.81	241.44	367.33	4.82	0.94
G3-1-5				0		300	280			------	411.71	398.14	127.72	0.00	270.41	398.14	1.00	0.97

Where:

$A_{v,w}$: area of web stirrups

$A_{v,f}$: area of flange stirrups

The proposed method is compared to the code formulation and F.E. Table 6.5& 6.6 present statistical analysis for comparison of the proposed method with the code formulation and F.E. results. It can be observed, the proposed equation 2 correlates better with F.E. results than of the code formulations studied, as it has the lowest coefficient of variation (0.08 to 0.24 for specimens without shear reinforcement and 0.15 to 0.20 for specimens with shear reinforcement) at compared with F.E. results that indicates a good conservative result. On the other hand, the code gives a high coefficient (0.38: 0.47), which leads to an increase in the cost of this concrete sections due to neglect the flange effects.

Table 6.5 Statistics of the ratio of proposed to calculate and analysis.

[specimens without shear reinforcement]

Specimens	ACI	Proposed	V_P/V_{ACI}	$V_P/V_{F.E.}$
	V_{ACI} (kN)	V_P (kN)		
C0	25.54	25.54	1.00	0.45
G1-0.15-3		33.76	1.32	0.44
G1-0.30-3		41.97	1.64	0.29
G1-0.40-3		47.44	1.86	0.26
G1-0.50-3	25.54	52.91	2.07	0.24
G1-0.65-3		61.13	2.39	0.28
G1-0.80-3		69.34	2.71	0.28
G1-0.90-3		74.81	2.93	0.30
G1-1-3	76.63	76.63	1.00	0.30
mean			1.88	0.32
standard deviation			0.71	0.08
coeffecient of var.			0.38	0.24
G1-0.15-5		41.97	1.64	0.44
G1-0.30-5		58.39	2.29	0.39
G1-0.40-5		69.34	2.71	0.35
G1-0.50-5	25.54	80.28	3.14	0.36
G1-0.65-5		96.71	3.79	0.39
G1-0.80-5		113.13	4.43	0.41
G1-0.90-5		124.07	4.86	0.41
G1-1-5	127.72	127.72	1.00	0.42
mean			2.98	0.39
standard deviation			1.34	0.03
coeffecient of var.			0.45	0.08

Table 6.6 Statistics of the ratio of proposed to calculate and analysis.

[specimens with shear reinforcement]

Specimens	ACI	Proposed	V_P/V_{ACI}	$V_P/V_{F.E.}$
	V_{ACI} (kN)	V_P (kN)		
C0-S	76.26	76.26	1.00	0.65
G3-0.15-3		92.41	1.21	0.50
G3-0.30-3		121.45	1.59	0.51
G3-0.40-3		140.80	1.85	0.55
G3-0.50-3	76.26	160.16	2.10	0.59
G3-0.65-3		189.19	2.48	0.61
G3-0.80-3		218.23	2.86	0.68
G3-0.90-3		237.58	3.12	0.75
G3-1-3	256.91	256.91	1.00	0.73
mean			1.91	0.62
standard deviation			0.79	0.09
coeffecient of var.			0.41	0.15
G3-0.15-5		108.67	1.43	0.53
G3-0.30-5		160.40	2.10	0.61
G3-0.40-5		194.89	2.56	0.73
G3-0.50-5	76.26	229.38	3.01	0.85
G3-0.65-5		281.11	3.69	0.79
G3-0.80-5		332.84	4.36	0.90
G3-0.90-5		367.33	4.82	0.94
G3-1-5	398.14	398.14	1.00	0.97
mean			2.87	0.79
standard deviation			1.36	0.16
coeffecient of var.			0.47	0.20

Besides, Figure 6.22 shows that the results of the proposed equation are safe enough compared to the experimental and F.E. results.

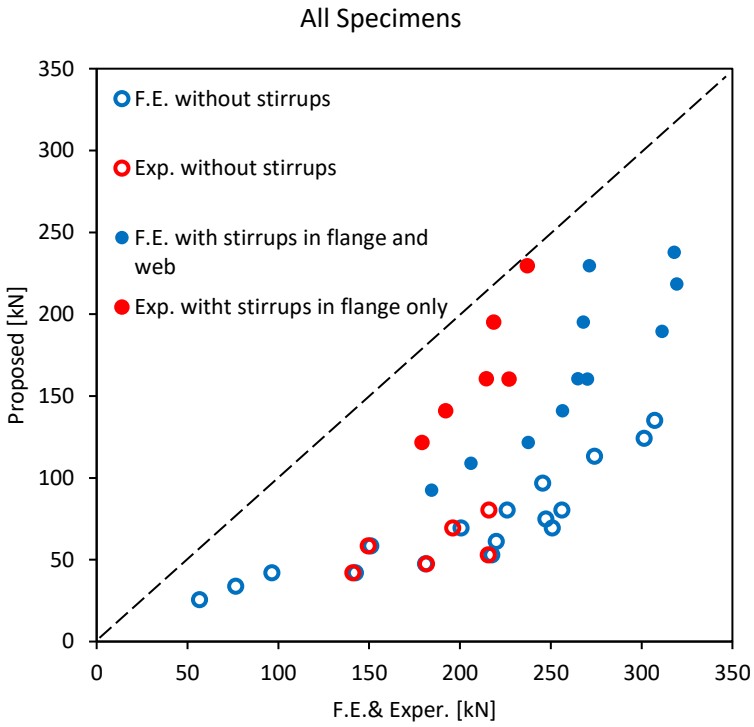

Fig. 6.22 Correlation between the proposal, F.E. and the experimental results

Table 6.4 Verification of proposed equation with F.E results& ACI

Specimen	f_c' Mpa	f_w Mpa	Dimensions [mm]					A_v (mm^2)		Exper.	F.E. method	ACI	Proposed method (kN)				V_P/V_{ACI}	$V_P/V_{F.E.}$
			b_w	d_w	L'	t_f	d_f	$A_{v,w}$	$A_{w,f}$	$V_{Exper.}$ (kN)	$V_{F.E}$ (kN)	V_{ACI} (kN)	V_c	V_{s-w}	V_{s-f}	V_P		
C0					0	0	0	0	0	53	56.7	25.54	25.54			25.54	1.00	0.45
G1-0.15-3						45	25			------	76.5		33.76			33.76	1.32	0.44
G1-0.30-3						90	70			141	142.4		41.97			41.97	1.64	0.29
G1-0.40-3						120	100			181.5	181.0		47.44			47.44	1.86	0.26
G1-0.50-3					100	150	130		0.00	215.5	217.5	25.54	52.91			52.91	2.07	0.24
G1-0.65-3						195	175			------	220.1		61.13			61.13	2.39	0.28
G1-0.80-3						240	220			------	250.8		69.34			69.34	2.71	0.28
G1-0.90-3						270	250			------	247.3		74.81			74.81	2.93	0.30
G1-1-3				280		300	280	0.00		------	256.0	76.63	76.63	0.00	0.00	76.63	1.00	0.30
G1-0.15-5						45	25			------	96.4		41.97			41.97	1.64	0.44
G1-0.30-5						90	70			149.5	150.9		58.39			58.39	2.29	0.39
G1-0.40-5						120	100			196.0	200.6		69.34			69.34	2.71	0.35
G1-0.50-5					200	150	130		0.00	216.0	226.0	25.54	80.28			80.28	3.14	0.36
G1-0.65-5						195	175			------	245.5		96.71			96.71	3.79	0.39
G1-0.80-5						240	220			------	274.0		113.13			113.13	4.43	0.41
G1-0.90-5						270	250			------	301.4		124.07			124.07	4.86	0.41
G1-1-5	28.8	240	100			300	280			------	307.2	127.72	127.72			127.72	1.00	0.42
C0-S				280	0	0	0	56.6	0	------	116.50	76.26	25.54	50.71	0.00	76.26	1.00	0.65
G3-0.15-3				235		45	25			------	184.28		33.76	42.56	16.10	92.41	1.21	0.50
G3-0.30-3				190		90	70			179	237.50		41.97	34.41	45.07	121.45	1.59	0.51
G3-0.40-3				160		120	100			192	256.30		47.44	28.98	64.38	140.80	1.85	0.55
G3-0.50-3				130	100	150	130		201.2	227	270.20	76.26	52.91	23.55	83.70	160.16	2.10	0.59
G3-0.65-3				85		195	175			------	311.12		61.13	15.40	112.67	189.19	2.48	0.61
G3-0.80-3				40		240	220			------	319.25		69.34	7.24	141.64	218.23	2.86	0.68
G3-0.90-3				10		270	250			------	317.78		74.81	1.81	160.96	237.58	3.12	0.75
G3-1-3				0		300	280	56.6		------	350.56	256.91	76.63	0.00	180.28	256.91	1.00	0.73
G3-0.15-5				235		45	25			------	205.95		41.97	42.56	24.14	108.67	1.43	0.53
G3-0.30-5				190		90	70			214.5	264.80		58.39	34.41	67.60	160.40	2.10	0.61
G3-0.40-5				160		120	100			218.5	267.80		69.34	28.98	96.58	194.89	2.56	0.73
G3-0.50-5				130	200	150	130		301.8	237.0	271.20	76.26	80.28	23.55	125.55	229.38	3.01	0.85
G3-0.65-5				85		195	175			------	356.74		96.71	15.40	169.01	281.11	3.69	0.79
G3-0.80-5				40		240	220			------	369.52		113.13	7.24	212.47	332.84	4.36	0.90
G3-0.90-5				10		270	250			------	392.70		124.07	1.81	241.44	367.33	4.82	0.94
G3-1-5				0		300	280			------	411.71	398.14	127.72	0.00	270.41	398.14	1.00	0.97

CHAPTER (7)

CONCLUSIONS AND FUTURE RECOMMENDATIONS

Conclusions and future recommendations

7.1 Conclusions

Based on the analysis of test results presented above, the following conclusions were drawn (limited to the indicated size, arrangement, and reinforcement of tested specimens):

(1) The shear capacity of T-beams was notably higher than that of rectangular beams with the same web size. Presence of flanges increased the shear capacity by 160% to 330% of the web alone (rectangular beam without transverse reinforcement). The actual increase depended on the flange dimensions and the amount of reinforcement in the flange. Moreover, the cracking load of T-beams was slightly higher than that of beams without flange. The results obtained are computed based on the absence of web stirrups, and it is acceptable for ρ_t= 0.3, 0.4 and for ρ_t= 0.5 can be reduced by 0.87.

(2) The flange thickness was most effective for increasing the shear capacity especially for T-beams without reinforcement in flange. Increasing the ratio of the flange thickness to total depth (ρ_t) from 0.3 to 0.5 increased the shear capacity by 53.7%, 34.5% and 26.7%, for G1, G2 and G3 respectively. All refer to flange reinforcement while the web had no shear reinforcement.

(3) Increasing the width of flange had less effect on the shear capacity of T-beams compared to increasing its thickness. For instance, increasing the ratio of the flange width to web width (ρ_b) from 3 to 5 increased the shear capacity by 6% to 19%.

(4) Use of longitudinal reinforcement in flange increased its shear strength and this increase was more pronounced for thinner flanges. In particular, flange reinforcement increased the shear strength by 14% to 43%; 4% to 12%; and 2% to 10%; at flange thickness to total depth ratios, ρ_t, of 0.3, 0.4, and 0.5, respectively.

(5) Presence of flanges delayed crack propagation especially for flanges with longitudinal reinforcement.

(6) The simple model published in [2] for predicting the shear capacity of T-beams gave results that were in good agreement with the experimental results in terms of the mean value and standard deviation. For the 19 tested beams "without web's transverse reinforcement", statistical analysis of the ratio of experimental to theoretical strength values yielded a mean of 1.06 and a standard deviation of 21%.

(7) To sum up from the validation and parametric studies of the finite element computer program ANSYS, the following conclusive points are derived:

(8) A good harmonization in the ending results was achieved by all reached cases of validity, the detected load-deflection response, the points of cracks, and the failure modes which applied the nonlinear FE program (ANSYS). At the final level, the total average value for $[P_{u(FE)} / P_{u(EXP)}]$ ratio and $[\Delta_{u(FE)} / \Delta_{u(EXP)}]$ ratio for the experimented specimens were 1.03 and 0.87 respectively. This result led us to the use of FE programs.

(9) The most important parameters in this research were acted by The effectiveness of the ratio of flange width to web width (b_f/b_w) and

the ratio of flange depth to web depth (t/h) on the shear strength of a point-loaded reinforced concrete T-beam .To consider the geometric ratios discussed in this theoretical study, it was suggested that the rise in the ratio (b_f/b_w) caused a rise in shear resistance from 12:260%.

(10) The push of longitudinal steel reinforcement ratio (ρ) in the flange from 0.5: 2% of the flange concrete area has helped to enhancement in shear capacity by 14:18% for a/h =0.5, 5:9 % for a/h =1 and 37:40% for a/h = 2.

(11) The decrease of shear span-to-depth ratio (a/d) resulted to an observed increase in the shear capacity of flanged beam by a range of 83:260 %, where the increasing (a/h) lowered slightly the toughness (I). As expressed in the load-deflection curves, the toughness was reduced on specimens S8& S12 when they were compared with S4 by 28% and 49% respectively.

(12) The shear capacity (V_u) and the toughness (I) are affected by the rise of concrete compressive strength (fc'). The use of concrete with fc' =60 MPa drove to an enhancement in shear capacity by 55:99% for a/h =0.5, 55:97% for a/h=1 and 27:88% for a/h=2. compared to concrete with fc' = 30 MPa.

(13) Based on obtained experimental and F.E. results, and within the considered limits of section geometry, a simple method is proposed for predicting the shear strength of reinforced concrete T-beams with the flange in compression. This simple method utilizes the full area of T- sections in lieu of the area of web alone specified by design codes. It is shown that the shear strength calculated using the

proposed method is conservative, i.e. less than that obtained by tests and/or F.E. analyses.

(14) The results of this study help in saving construction costs by utilizing the flange's contribution to shear strength for flanged beams with thick flanges in the compression side such as the case of double-cantilevered cap beams with inverted T sections.

7.2 Recommendations and suggestions for future studies

This research confirmed the significant contribution of thick flanges of beams with T-shaped sections with flanges in the compression side to the beam shear strength, within the stated geometric limitations. Based on the findings, the following recommendations and suggestions for future research are made:

(1) More theoretical work is needed to develop a more rigorous method for the calculation of shear strength of flanged beams with flanges in compression.

(2) Cases of flanged sections with flanges in tension need to be considered experimentally and/or theoretically.

(3) Effects of heavy longitudinal reinforcement in flange and web as well as level of web reinforcement in web and flange require further investigations.

(4) More “larger” values of the shear span to depth ratios shall be studied.

(5) Committees of design codes both nationally and internationally are encouraged to modify their shear strength calculation formulas for flanged beams to include the contribution of flanges. Such modification shall include the effect of relative flange dimensions and position of neutral axis.

REFERENCES

References

1. Thamrin, R., Tanjung, J., Aryanti, R., Nur, O. F., & Devinus, A. (2016). Shear strength of reinforced concrete T-beams without stirrups. *Journal of Engineering Science and technology*, *11*(4), 548-562.
2. Cladera, A., Marí, A., Ribas, C., Bairán, J., & Oller, E. (2015). Predicting the shear–flexural strength of slender reinforced concrete T and I shaped beams. *Engineering Structures*, *101*, 386-398.
3. Elgohary, A., Abdelhafiez, A., & Asran, A. (2019). EFFECT OF FLANGEWIDTH ON SHEAR STRENGTH OF RC T-BEAMS. *Journal of Al-Azhar University Engineering Sector*, *14*(52), 875-882.
4. Deifalla, A., & Ghobarah, A. J. E. S. (2014). Behavior and analysis of inverted T-shaped RC beams under shear and torsion. *Engineering structures*, *68*, 57-70.
5. Etman, E. (2011). External bonded shear reinforcement for T-section beams. *Structural Concrete*, *12*(3), 198-209.
6. Amna, H. A., & Monstaser, W. M. (2019). Shear behavior of reinforced lightweight concrete T-beams. *Life Science J*, *16*(8), 11-31.
7. Ayensa, A., Oller, E., Beltrán, B., Ibarz, E., Marí, A., & Gracia, L. (2019). Influence of the flanges width and thickness on the shear strength of reinforced concrete beams with T-shaped cross section. *Engineering Structures*, *188*, 506-518.
8. Eswaramoorthi, P., Prabhu, P. S., & Magudeaswaran, P. (2017). EXPERIMENTAL STUDY CONCRETE CONTINUO AND FLANGED BEAMS A. *International Journal of Civil Engineering*, *8*(7).

9. Samad, A. A. A., Mohamad, N., Al-Qershi, M. A. H., Jayaprakash, J., & Mendis, P. (2016). Shear Mechanism and Shear Strength Prediction of Reinforced Concrete T-Beams. *Jurnal Teknologi*, *78*(5).

10. Yehia, N. A., & Wahab, N. M. (2007). Fracture mechanics of flanged reinforced concrete sections. *Engineering structures*, *29*(9), 2334-2343.

11. Zararis, I. P., Karaveziroglou, M. K., & Zararis, P. D. (2006). Shear strength of reinforced concrete T-beams. *ACI structural journal*, *103*(5), 693.

12. Pansuk, W., & Sato, Y. (2007). Shear mechanism of reinforced concrete T-beams with stirrups. *Journal of Advanced Concrete Technology*, *5*(3), 395-408.

13. Enterprise, A. M. A finite element computer software and user manual for nonlinear structural analysis. *Mechanical APDL Release*, *19*.

14. Hesham, A. A. & Wael, M. M. (2019). Shear behavior of reinforced lightweight concrete T-beams, beams. *Life Science J*, *16*(8), 11-31.

15. Balamuralikrishnan, R., & Saravanan, J. (2019). Finite element modelling of rc T-beams reinforced internally with gfrp reinforcements. *Civil Engineering Journal*, *5*(3), 563-575.

16. El-din, H. K. S., Husain, M. M., Khater, M. A., & Zaghlal, M. Y. A. (2017). Finite Element Analysis on the behavior of Strengthened RC Shallow T- Beams with Large Openings at Shear Zone Using CFRP and BFRP sheets. International Journal of Scientific Engineering and Applied Science (IJSEAS), 3(11), 86–97.

17. Biscaia, H. C., Chastre, C., & Silva, M. A. (2013). A smeared crack analysis of reinforced concrete T-beams strengthened with GFRP composites. Engineering Structures, 56, 1346-1361.

18. Pansuk, W., & Sato, Y. (2007). Shear mechanism of reinforced concrete T-beams with stirrups. Journal of Advanced Concrete Technology, 5(3), 395-408.

19. Pansuk, W., Sato, Y., Takahashi, R., & Ueda, T. (2004). Influence of Top Flange to Shear Capacity of Reinforced Concrete T Beams. Proceedings of JCI, 26, 991-996.

20. Giaccio, C., Al-Mahaidi, R., & Taplin, G. (2002). Experimental study on the effect of flange geometry on the shear strength of reinforced concrete T-beams subjected to concentrated loads. Canadian Journal of Civil Engineering, 29(6), 911-918.

21. ACI Committee. (2008). Building code requirements for structural concrete (ACI 318-08) and commentary. American Concrete Institute.

22. CSA Committee A23.3. Design of concrete structure. Canadian Standards Association Mississauga. Ontario. Canada 2004.

23. Code, P. (2005). Eurocode 2: design of concrete structures-part 1–1: general rules and rules for buildings. British Standard Institution, London.

24. ECP-203 Permanent Committee. (2007). ECP-203: 2007-Egyptian Code for design and construction of concrete structures. *HBRC, Giza*.

25. Marí, A., Cladera, A., Bairán, J., Oller, E., & Ribas, C. (2014). Shear-flexural strength mechanical model for the design and assessment of reinforced concrete beams subjected to point or distributed loads. *Frontiers of Structural and Civil Engineering*, *8*(4), 337-353.

26. Sarsam, K., Khalel, R., & Mohammed, N. (2018). Influence of flange on the shear capacity of reinforced concrete beams. In *MATEC Web of Conferences* (Vol. 162, p. 04003). EDP Sciences.

27. Sahoo, D. R., Bhagat, S., & Reddy, T. (2016). Experimental study on shear-span to effective-depth ratio of steel fiber reinforced concrete T-beams. *Materials and Structures*, *49*(9), 3815-3830.

28. Gonzalez Ribas, C. R., & Fernández Ruiz, M. (2017). Influence of flanges on the shear-carrying capacity of reinforced concrete beams without web reinforcement. *Structural concrete*, *18*(5), 720-732.

29. Placas, A., & Regan, P. E. (1971, October). Shear failure of reinforced concrete beams. In *Journal Proceedings* (Vol. 68, No. 10, pp. 763-773).

30. Zsutty, T. C. (1968, November). Beam shear strength prediction by analysis of existing data. In *Journal Proceedings* (Vol. 65, No. 11, pp. 943-951).

31. Paulay, T., Loeber, P. J., Mattock, A. H., Taylor, H. P. J., Scordelis, A. C., Ngo, D., ... & Regan, P. E. (1974). Shear in reinforced concrete, Volumes 1 and 2. *Shear Reinf Concr, Am Concr Inst (Publ SP-42)*.

32. Wolf, T. S., & Frosch, R. J. (2007). Shear design of prestressed concrete: A unified approach. *Journal of structural Engineering*, *133*(11), 1512-1519.

33. Kachlakev, D. I., Miller, T. H., Potisuk, T., Yim, S. C., & Chansawat, K. (2001). *Finite element modeling of reinforced concrete structures strengthened with FRP laminates* (No. FHWA-OR-RD-01-XX). Oregon. Dept. of Transportation. Research Group.

34. Musmar, M. A., Rjoub, M. I., & Hadi, M. A. (2006). Nonlinear finite element analysis of shallow reinforced concrete beams using SOLID65 element. *elastic*, *25743*, 0-3.

35. Tjitradi, D., Eliatun, E., & Taufik, S. (2017). Plagiat Checker: 3D ANSYS Numerical Modeling of Reinforced Concrete Beam Behavior under Different Collapsed Mechanisms.

36. Shah, S. P., Swartz, S. E., & Ouyang, C. (1995). *Fracture mechanics of concrete: applications of fracture mechanics to concrete, rock and other quasi-brittle materials*. John Wiley & Sons.

37. Bangash, M. Y. H. (1989). Concrete and concrete structures: Numerical modelling and applications.

38. Gere, J. M., & Timoshenko, S. P. (1997). Mechanics of materials, 1997. *PWS-KENT Publishing Company, ISBN 0, 534*(92174), 4.

39. ACI committee 318. (2014). Building Code Requirements for Structural Concrete (ACI 318-14): An ACI Standard; Commentary on Building Code Requirements for Structural Concrete (ACI 318R-14). American Concrete Institute.

40. Kachlakev, D. I., & McCurry Jr, D. (2000). Simulated full scale testing of reinforced concrete beams strengthened with FRP composites: Experimental results and design model verification. *Oregon Department of Transportation, Salem, Oregon*.

41. Tureyen, A. K., Wolf, T. S., & Frosch, R. J. (2006). Shear strength of reinforced concrete T-beams without transverse reinforcement. *ACI structural journal, 103*(5), 656.

بسم الله الرحمن الرحيم

ملخص الرسالة

سلوك الكمرات الخرسانية المسلحة ذات الشفة والمعرضة لقوى القص

مقدمة :-

تعتبر الكمرات ذات قطاع حرف T شائعة الاستخدام في العديد من المنشآت وخاصة في الكباري الخرسانية حيث تستخدم كدعامات للكمرات الثانوية سابقة الصب. وهذه الكمرات تختلف في سلوكها الإنشائي عن الكمرات بدون الشفة المحملة من أعلي حيث تعمل الشفة علي زيادة قدرة تحمل الكمرات وخاصة ما اذا كانت هذه الشفة معرضة لإجهادات ضغط .

ويتضح من معظم الدراسات التجريبية والنظرية السابقة التي تم الإطلاع عليها بشأن هذا الموضوع على هذا النوع من الكمرات المسلحة المعرضة لقوي القص، أننا في حاجة الي بعض الدراسات والتجارب علي هذا النوع من الكمرات " ذات الشفة السميكة والمعرضة لاجهادات الضغط". ولذلك كان الهدف الرئيسي من هذا البحث هو عمل بعض التجارب العملية والنظرية لدراسة سلوك الكمرات المسلحة ذات القطاعات علي حرف T المعرضة الي قوى القص و التركيز على تأثير ابعاد الشفة في مساهمتها لمقاومة قوي القص. قدم البحث اقتراحا لحساب مقاومة القص للكمرات ذات الشفة التى تقع شفتها ناحية إجهادات الضغط وذلك باعتبار كامل مساحة القطاع (بدلا من استخدام مساحة الجذع وحده كما فى الكودات الحالية). وقد بينت النتائج أن هذا الاقتراح ينتج عنه مقاومة قص متحفظة بالمقارنة بنتائج النموذج النظري (Ansys) ونتائج الاختبارات.

أهمية البحث:

تستخدم الكمرات ذات شكل حرف T على نطاق واسع في هياكل الكباري وتكون فيها النسبة بين سمك شفة وعمق العصب كبيره مما هو عليه في المنشآت العادية. ولذلك لايجب أن نتجاهل مساهمة الشفة في مقاومة قوي القص كما هو الحالي في كثير من الأكواد التصميمية المختلفة وخاصة

الكود المصري ECP-203 حيث أنه لا يضع أي مساهمة للشفة في مقاومة القص. ولذلك، يجب عمل دراسات نظريه وتجريبيه حول هذا الموضوع والذي ينعكس بالفائدة الكبيرة علي المهندسين الانشائيين، وشركات البناء، والهيئات المعنية الأخرى.

الهدف من البحث

- تحيد مساهمة او مشاركة الشفه (ذات حرف T) في مقاومة قوي القص.
- التحقق من صحة النموذج النظري (العنصر المحدود) من خلال اجراء بعض الاختبارات العملية.

المتغيرات الأساسية محل الدراسة

في هذا البحث سيتم دراسة بعض المتغيرات ومنها أبعاد الشفة (عمق وعرض القطاع لها)، النسبة بين أبعاد الشفة والعصب، وجود الكانات في الشفة و أخيرا التسليح الطولي بالشفة .

وقد اشتملت الدراسة علي الأبواب التالية:

الباب الأول:

يحتوي هذا الباب علي مقدمة للموضوع مع وصف خطة البحث بالإضافة إلي أهداف البحث محل الدراسة. وفي نهاية هذا الباب تم استعراض ملخص لمحتويات البواب البحث.

الباب الثاني:

يتضمن خلفية عن الموضوع واستعراض للأبحاث السابقة التي تم الحصول عليها والطرق المختلفة لتحليل الكمرات الخرسانية المسلحة ذات الشفة تحت تأثير قوي القص.

الباب الثالث:

يحتوي علي شرح تفصلي للجزء العملي من الدراسة من حيث تحديد خواص المواد وأجهزة القياس المستخدمة في تجهيز العينات، كما أنه يوجد توضيح مفصل لأبعاد وتسليح جميع العينات وأسلوب الاختبار والمتغيرات التي تم دراستها.

الباب الرابع:

يحتوي على تحليل ومناقشة نتائج الإختبار المعملية من حيث تأثير أبعاد الشفة المختلفه والتسليح الطولي بها ووجود الكانات في الشفة والتي لها تأثيرعلي كلا من سهم الترخيم والمقاومة القصوي للعينة و أخيرا الإنفعال لكلا من الحديد والخرسانة.

الباب الخامس:

يشتمل هذا الجزء علي التحليل العددي للعينات المختبرة بواسطة نموذج من احد الأبحاث المرجعية المشار اليها في البحث . وطبقا لتقييم النتائج والمقارنات بين النتائج المعمليه والنظرية التي تم الحصول عليها من النموذج المستخدم، اظهرت المقارنات توافق جيد بين النتائج العملية والنموذج المستخدم.

الباب السادس:

يتضمن الباب الجزء الخاص بالتحليل النظري لبعض العينات باستخدام التحليل بواسطة نظرية العنصر المحدود من خلال استخدام برنامج " ANSYS " وكذلك دراسة متغيرات جديده بعد التحقق من النموذج النظري للكمرات الخرسانية المسلحة ذات الشفة وتأثير تأثير الشفة في مقاومة قوي القص، كما أنه تم دراسة متغيرات جديدة بواسطة النموذج المشار له، ومن هذه المتغيرات دراسة مقاومة الخرسانة، نسبة أبعاد الشفة الخرسانية من حيث العمق والعرض لها للأبعاد العصب و أخيرا نسبة الحديد الطولي بالشفة.

وقد اشتمل الباب على تقييم النتائج وعمل المقارنات مابين النتائج المعمليه والنظرية واظهرت المقارنات توافق جيد بين النتائج للنموذج المستخدم والنتائج العملية.

الباب السابع:

يحتوي الباب علي ملخص لأهم ما توصل اليه الباحث في الدراسة من نتائج.

المراجع

جامعـــة بنهـــا
كليـــة الهندسة ببنها
قسم الهندسة المدنية

سلوك الكمرات الخرسانية المسلحة ذات الشفة والمعرضة لقوى القص

رسالة مقدمة كجزء من متطلبات الحصول علي درجة

دكتوراه الفلسفة في العلوم الهندسية في الهندسة المدنية

إعداد

إبراهيم على ابراهيم العزب

مدرس مساعد بقسم الهندسة المدنية

ماجستير الهندسة والتكنولوجيا في تكنولوجيا الهندسة المدنية

جامعة بنها 2013

تحت إشراف

أ.د/ عثمان محمد عثمان رمضان

استاذ ميكانيكا الانشاءات - كلية الهندسة - جامعة القاهرة - وعميد المعهد التكنولوجي العالي بالعاشر من رمضان

أ.د/ أحمد حسن عبد الكريم

استاذ الخرسانة المسلحة بقسم الهندسة المدنية - وكيل كلية الهندسة ببنها لخدمة المجتمع وشئون البيئة - جامعة بنها

أ.م.د/ هاله محمد رفعت

استاذ مساعد بقسم الهندسة المدنية كلية الهندسة ببنها - جامعة بنها

2022